공학박사 학위논문

Dynamics of Recovering Sheath and Presheath in a Collisionless Plasma

비충돌 플라즈마내 회복 쉬스와 프리쉬스의
동특성 연구

2013년 2월

서울대학교 대학원
에너지 시스템 공학부
최 재 명

Abstract

Dynamics of Recovering Sheath and Presheath in a Plasma

Jae-Myung Choe

Department of Energy Systems Engineering

The Graduate School

Seoul National University

Plasma and sheath evolutions are studied at pulse fall time. By modifying the pulse shape, parameters to govern the sheath and presheath recovery are investigated and their dependency is revealed. The experiments are performed in a collisionless Ar plasma and Langmuir sheath trace the motion of sheath and presheath with time. Pulse fall time and ion inertia in front of the target determine recovery motion.

Sheath motion is investigated with fall time which is faster and slower than ion flight time. The analytical model including charging and discharging property of the system impedance, sheath and plasma current are presented and compared with the experimental result. In fast fall, ion matrix-like sheath recovery proceeds during the early stage. Electrons at the sheath boundary respond immediately and the recovery speed of sheath is faster than Bohm speed. The plasma keeps the distribution of Child-Langmuir sheath formed at pulse plateau time. For the slow fall time, the sheath recovery is satisfied with the well-known Child-Langmuir sheath model because the ions have enough time to be rearranged for the slowly varying electrode voltage. Therefore, the plasma density profile follows the distribution before applying the pulse and Bohm current is flown to the electrode while presheath consistently persists at the boundary.

Recovery motion of presheath with pulse fall time is studied and it is revealed that sheath speed and ion inertia determine the recovery motion of presheath. When the sheath speed is over Bohm speed, presheath-sheath boundary in plateau time recovers with Bohm speed regardless of sheath speed. When sheath speed decreases under Bohm speed, presheath is restricted to the sheath speed but presheath region expands with time because of ambiploar diffusion lower than sheath speed at the bulk plasma. After sheath speed becomes lower than diffusion speed at the bulk, presheath recovers satisfying the presheath profile of Child-Langmuir sheath.

Plasma recovery process is analyzed by varying plateau time. Initial recovery speed of presheath decreases as decreased plateau time because plasma does not form the presheath. After electric field is evacuated at fast fall time, however, rarefaction wave forces the ions to increase the speed and the ions at the presheath recover up to Bohm speed.

Based on the previous results, ion energy distribution is predicted using the fluid code. At slow fall time, induced electric field governs the distribution. Quantity of injected ions is inverse-proportional with ions' energy. At fast fall time, ion inertia determines the high energy of ion energy distribution. Since no electric field exists, residual energetic ions are injected to the target after pulse-off. Spatial distribution of ion inertia and density gradient of the plasma profile give ions an additional energy. Distortion of initial plasma property by short plateau time changes ion energy distribution at fast fall time. Maximum energy of ions decreases but quantity of energetic ions increases as plateau time becomes short.

Keywords: plasma, sheath, presheath, pulse bias operation, Bohm speed, pulse fall time

Student Number: 2004-23437

Table of Contents

List of Tables

List of Figures

Chapter 1. Introduction

1.1 Pulse Bias Operation

Bias operation on the target is a fundamental method to make energetic ions. Many practical plasma systems for various purposes such as modification of surface, metal bonding, beam extraction use bias system to generate adequate ions for plasma processing.[1-4] Diagnostic systems such as Langmuir probe[5] and retarding field energy analyzer (RFEA)[6] also use bias voltage to obtain information. By scanning target voltage, ions or electron with specific energy can be measured.

Bias operation, however, has some limits on operation such as sensitive plasma current with the variation of bias voltage, arc damage by charging, and consolidation of residual gas in the hole on the surface. Especially, currently used large-scaled systems with high density plasma increase the risk drastically.

Pulse bias operation is a technique to overcome the limits of bias operation. [7] By applying negatively biased pulse to the target that is immersed in plasma, physical properties on the surface can be modified or binding between material and plasma particle is formed.[3, 8] Energetic ions are usually injected during the pulse-on time and low energy diffuses at the pulse-off time. Here are some advantages on the pulse bias operation.

- Ions with a high energy and dose are generated with a supply of low power.
- Arc damage by electron charging can be reduced by controlling pulse-on time.
- Evolution of high ion flux at pulse rise time can be maximized using rapid repetition operation.
- Two types of plasma, high energy ion at pulse-on time and low energy ions of steady-state plasma at pulse-off time, can be supplied in one process.
- Electron and head emission and sputtering on the target can be controlled by the adjustment of pulse shape.
- By adjusting repetition rate, duty ratio, and rise and fall time, ion energy distribution is modified for the specific process.
- Locally induced electric field at pulse-on time can generate additional ionization around the target, which accomplishes high ion flux.
- Synchronous pulsed DC bias operation can improve the mono-energy characteristics of ions.[9, 10]

Using these advantages, various applications exist. Some of representative applications are introduced in next section.

1.2 Applications in Pulse Bias Operation

There are widely varied plasma applications to control ion energy. In this section, some representative applications using pulse bias operation are

introduced.

- **Plasma Source Ion Implantation (PSII)**

Plasma source ion implantation (PSII), which is also called as plasma immersion ion implantation (PIII) is a typical method to use the pulse bias operation in the process.[8, 11] Conrad et al invented PSII process In order to overcome the line-of-sight restriction in conventional beam-line ion implantation and improve the cost-effectiveness of the processing.[3]

PSII is purposed to generate high electric field on the surface for injected ions to gain energy. By applying high pulse voltage on the surface, ions of a material can be implanted into another solid to change the physical properties of solid.[12] Ion implantation provides when the ion energy is typically tens to hundreds of kilo-electron volts and pulse operation with high voltage is capable in the system. Pulse bias operation also prevents damages from heat or charge build-up on the surface by controlling the pulse shape and repetition rate.

- **Synchronous Pulsed DC Bias Operation**

Almost previous applications are mainly focused on the pulsed bias operation in steady-state plasma to control ion energy distribution.[13, 14] Since the plasma can be changed drastically during the time when plasma is generated or afterglow, synchronous pulsed DC bias operation is one of the methods to make use of pulse operation effectively.[9, 10, 15] In process device such as an etcher, broadening of ion energy distribution is an important

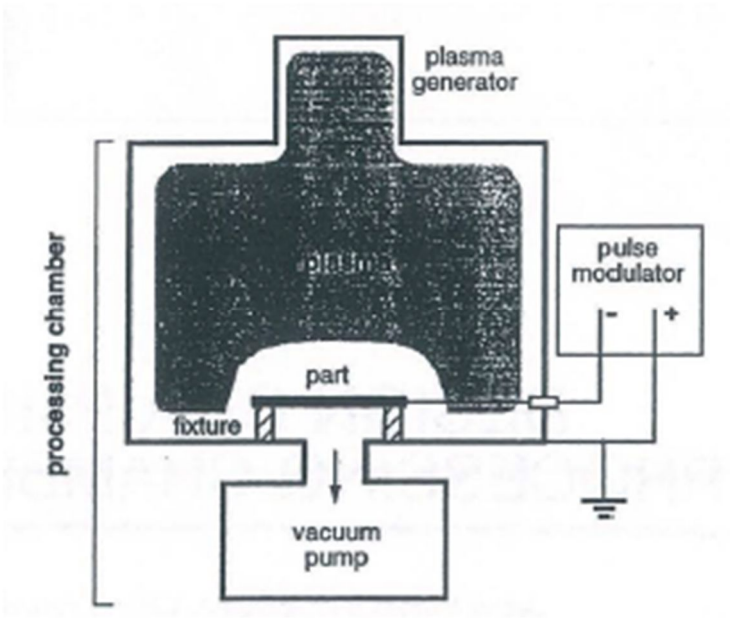

Figure 1.1 Schematic diagram of plasma source ion implantation (PSII) device

limiting factor, which is in turn proportional to the electron temperature.[16] To minimize the ion energy spread, afterglow plasma is employed using two synchronized pulse sources, pulsed RF and DC bias source. Pulse DC bias operation is processed after RF pulse, which generates the bulk plasma, is turned off. Since electron temperature drastically decreases comparing with the plasma density, the full width at half maximum (FWHM) can make thinner during the afterglow duration. By adjusting pulse phase, duty ratio, and repetition rate of the synchronous dc bias at later times in the afterglow,

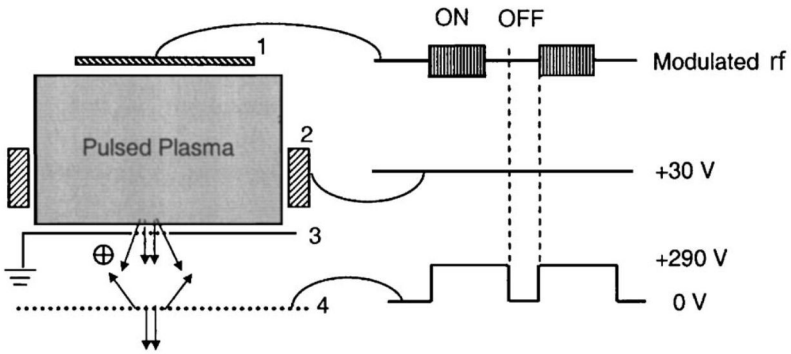

Figure 1.2 Schematic diagram and operating scenario in the system for synchronized pulsed DC bias operation.

sharpness is improved and production rate increases.

1.3 Importance of sheath and presheath motion at pulse fall time

Goal on pulse bias operation is to gain the controlled energy and flux of ions which are injected to the wall. With a different energy band that ions impose on, different surface modification such as sputtering, deposition, or implantation occurs. High flux is one of mandatory requirements for improvement of efficiency and rapid processing time in the plasma processing.

Ion energy is determined in the sheath. Located between the target and

plasma, sheath is the region where charges with single polarity exist. By the polarity, induced electric field from the target voltage is distributed in the sheath. Ions entering from the plasma gain their energy across the sheath and energetic ions are injected to the target.

As being recognized and proved by Langmuir [11] and Bohm [17], presheath is known for the area where ion gains a Bohm speed in the bulk plasma.[18, 19] Presheath is a region where ions supply to the sheath and take a role to connect between bulk plasma and sheath. Injected number of charges is determined from the presheath property.

Pulse bias operation consists of three motions, pulse rise, plateau, and fall. Contrary to the DC bias operation, therefore, accurate prediction of the ion dose and energy is quite difficult. Drastic change of the target voltage, which is based on the time-varying voltage at pulse rise and fall, causes the evolution and shrinkage of induced electric field that in the sheath. Sheath size is also a function of target voltage thus presheath moves responding to the target voltage.

Difference of ion and electron mobility enhances the variation of sheath and presheath. Ion performs a delayed action responding to the electric field comparing with the electrons, which dominates non-linearity of plasma motion and determines the sheath type such as ion-matrix or Child-Langmuir sheath. [3, 20, 21] These parameters are the challenging point for control of ion energy and flux on pulse bias operation.

Previous studies have been mainly focused on the motion of sheath at pulse rise time. After sheath expansion is first analyzed by Conrad[3], many

works are revealed that transition from ion matrix to Child-Langmuir sheath occurs after pulse rise and delayed saturation of sheath motion after pulse rise are measured. [22, 23] Its speed is proportional to the square root of the pulse rise rate and insensitive to ion mass.[24] As the study at pulse rise time is progressed, plasma effect at presheath has been studied. Many studies showed that rarefaction wave expands and presheath is formed after sheath becomes stable. [25-28] Other studies shows the non-uniformity of plasma density and drift speed of ions by diffusion suppress the expanding speed of the rarefaction wave and sheath size when plasma become stable.[29, 30]

Studies at pulse fall time have been insufficient comparing with that at pulse rise time, expecting similar parameters at the pulse rise govern the motion at the pulse fall. Almost studies at pulse fall time have assumed that fall time is zero. Instead of sheath and presheath motion, they are focused on the motion of bulk plasma which recovers into the depletion region in front of target after floating sheath is formed. En et al [31] suggested that electric field supporting the sheath no longer exists so plasma recovers with Bohm speed. Briehl et al[32] extends the theory that current from the refilling plasma to the target delay the plasma recovery in a plasma recovery. Chung et al [33] revealed that plasma recovery are accompanied by a compression wave. Calculation of ion energy distribution was also performed at limited cases. Stewart and Lieberman [34, 35] calculate the ion energy distribution in the assumption of zero flight time during the pulse fall.

Contrary to the generalized notion, sheath and presheath motion at pulse fall have their own characteristics. Here are some characteristics on the

motion.

- **Initial plasma property that is starting from plateau time**

Plasma at pulse rise starts from the initial condition that target voltage is floated or zero in steady-state plasma. The initial condition at pulse fall time, however, is formed at pulse plateau time, which says high electric field is induced in the expanded sheath and accelerated ions already exist in the sheath. In front of the target, drastically non-uniform ion profile is distributed that was formed at the plateau time, which can modify sheath and ion energy distribution during the pulse fall time. Moreover, initial sheath and presheath property can be changed unstably by variation of rise and plateau time.

- **Same direction of sheath and ion motion**

Contrary to the direction at the rise time, ion and sheath moves same direction. In result, the difference of speed between them becomes one of main parameter to determine ion motion and energy distribution. Due to the non-uniformity of plasma profile and presheath, ions have a non-uniform profile of speed and it is expected that sheath and presheath motion can be affected by sheath speed.

- **Large-scale variation of finite fall time**

When pulse-on starts, charging process is progressed on the target through the capacitor bank. In order to maintain the voltage at plateau time and increase repetition rate, the capacitor's capacity is large comparing with the capacity at the target and pulse rise is rapidly saturated. In result, electric field by target voltage is a main force for sheath and presheath motion and sustained until the plateau time. At pulse fall, however, it is easy to control the target voltage. By adjusting the neutralizing speed by external system, fall time can be sensitively varied with system impedance. In result, various plasma effects such as ion inertia, plasma density profile, and ambipolar diffusion from the bulk plasma, can be evaluated by adjusting the pulse fall time. In addition, ion energy distribution during pulse-on time can be varied with the fall time.

Due to these characteristics, it is important to investigate the sheath and presheath motion at pulse fall time and it is required to reveal the effect of control parameters on the motion.

1.4 Objective and Scope of This Study

This study is purposed to reveal the sheath and presheath recovery at pulse fall time. Motion of sheath and presheath is investigated and their dependency on pulse fall time is analyzed. Since the recovery starts from the plateau time contrary to the case at pulse rise time, effect of initial plasma condition is also considered. Based on the analysis, ion energy distribution is

predicted.

This thesis is composed of 8 chapters. First, motivation and objective of this study are announced in this chapter. Chapter 2 reviews static sheaths and introduces previous works of sheath and presheath motion at pulse rise and fall time. Chapter 3 describes plasma sources and diagnostic tools for the experiments. In Chapter 4, analytic model describing sheath motion is derived and is compared with experiment results. Recovery of presheath with the variation of pulse fall time is investigated in chapter 5 and dependency of presheath recovery on ion initial property at pulse fall time is studied by adjusting plateau time in Chapter 6. Based on previous results, ion energy distribution is predicted using fluid code in Chapter 7. Finally, conclusion of dynamic sheath and presheath motion at pulse fall time is described in Chapter 8.

Chapter 2. Theoretical Backgrounds

In this chapter, fundamentals of sheath and plasma motion are presented. Typical models explaining a high voltage sheath are reviewed and their characteristics are described. Previous studies to analyze sheath and presheath motion at pulse rise and fall time are reviewed and current issues are introduced.

2.1 High Voltage Sheath and Presheath

Plasma is a collection of ions and electrons being satisfied with quasi-neutrality.[16] Since ions and electrons are charged particles, particles' motion can be controlled by electric field that is induced from the target voltage. When a negatively biased voltage is applied to the target, electrons are evacuated and ions are located in front of the target, which is called a sheath.

Sheath boundary, in general, is determined from the combination of induced potential profile and thermal diffusion of electrons. When sheath voltage, however, is driven to be large compared to the electron temperature.

Potential in the sheath is highly negative with respect to the sheath boundary and only ions exit in the sheath. [16] In result, ion motion becomes a governing factor to develop sheath and two types of typical sheath model exists by that as presented in Figure 2.1.

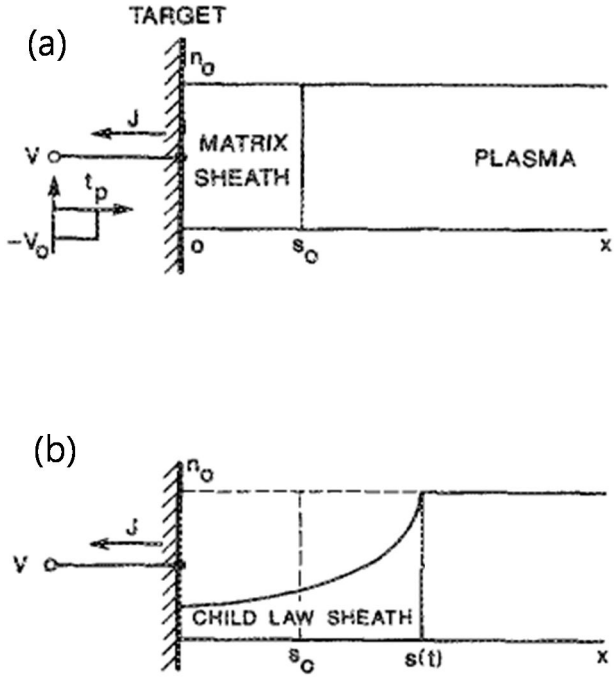

Figure 2.1 Geometry of (a) ion matrix sheath and (b) Child-Langmuir sheath

2.1.1 Ion matrix sheath

Ion matrix sheath is the simplest sheath model to explain a high voltage sheath. It is assumed that ions in front of the target have a uniform density profile and do not move responding to the variation of target voltage. Since electrons do not exists in the sheath, Poisson equation can be driven as

$$\frac{dE}{dx} = \frac{en_s}{\varepsilon_0} \tag{2.1}$$

From the equation above, electric field is calculated by an integration with a boundary condition that plasma-sheath boundary is located at ***x=0***

$$E = \frac{en_s}{\varepsilon_0} x \tag{2.2}$$

Potential profile is given by integrating with *x*.

$$\Phi = -\frac{en_s}{\varepsilon_0} \frac{x^2}{2} \tag{2.3}$$

With a boundary condition ϕ=-V_0 at ***x=s***, s is sheath size, thickness of ion matrix sheath is obtained.

$$s = \left(\frac{2\varepsilon_0 V_0}{en_s} \right)^{1/2} \tag{2.4}$$

Since ion matrix sheath assumes that ions do not move by the induced potential, the model can be applied in a limited condition such as sheath motion within a time shorter than inverse of ion plasma frequency and ions do not have enough time to respond to the electric field.

2.1.2 Child-Langmuir sheath

Ion matrix sheath assumes that ion is fixed regardless of induced potential profile. Ions, however, have a non-uniform profile responding to the electric field and it also manipulates electric field in the sheath, which is a basic assumption of Child-Langmuir sheath.

Ions in the sheath is satisfied with the energy conservation law and is driven as below

$$\frac{1}{2}Mu_1^2 + e\Phi_1 = \frac{1}{2}Mu_2^2 + e\Phi_2 \tag{2.5}$$

Since potential in the sheath is large compared to ion energy injected from the plasma, the equation reduces to

$$\frac{1}{2}Mu^2(x) = -e\Phi(x) \tag{2.6}$$

Ion current can be defined due to the flux conservation

$$J = en(x)u(x) \tag{2.7}$$

Using (2,6) and (2.7), plasma density, *n(x)*, is obtained.

$$n(x) = \frac{J_0}{e}\left(-\frac{2e\Phi}{M}\right)^{-1/2} \tag{2.8}$$

The equation is inserted into Poisson equation with a condition of no electrons and the 2nd order differential equation is obtained.

$$\frac{d^2\Phi}{dx^2} = -\frac{J}{\varepsilon_0}\left(-\frac{2e\Phi}{M}\right)^{-1/2} \tag{2.9}$$

By integrating with boundary condition of zero electric field and zero potential at sheath-plasma boundary (x=0), current is calculated with a boundary condition of $\phi(s) = -V_0$, where s is a sheath size.

$$J = \frac{4}{9}\varepsilon_0\left(\frac{2e}{M}\right)^{1/2}\frac{V_0^{3/2}}{s^2} \tag{2.10}$$

J is balanced with the current that is injected from the bulk plasma,

$$J = en_s u_B \tag{2.11}$$

In result, Child-Langmuir sheath is obtained as below.

$$s = \frac{2}{3}\sqrt{\frac{2\varepsilon_0}{n_s u_B M}}V_0^{3/4} \tag{2.12}$$

Comparing to the ion matrix sheath, Child-Langmuir sheath is larger by a factor of $\sqrt{2}/3(eV/kT_e)^{1/4}$ because Child-Langmuir sheath assumes that ions are rearranged responding to the target potential thus density of plasma profile in Child-Langmuir sheath is lower than that in ion matrix sheath.

2.1.3 Presheath

Presheath is a region that is located between sheath and bulk plasma. In this region, ions flown from the bulk plasma are injected into the sheath and

electric field from the sheath is shielded. To describe the ion motion at the presheath, it is assumed that ion temperature is zero and electrons have a Maxwellian distribution with a temperature, T_e. From the energy conservation equation, ion speed is given as below

$$\frac{1}{2}Mu^2(x) = \frac{1}{2}Mu_s^2 - e\Phi(x) \tag{2.13}$$

With a flux conservation of $n_i(x)u(x) = n_{is}u_s$, where $n_i(x)$ and $u(x)$ is an ion density and speed at the position of x, respectively, ion density can be calculated with a function of potential and ion density at the sheath boundary. By inserting $n_i(x)$ and electron density, which is satisfied with Boltzmann relation, into Poisson's equation, the equation is obtained.

$$\frac{d^2\Phi}{dx^2} = \frac{en_s}{\varepsilon_0}\left[e^{-\Phi/T_e} - \left(1 - \frac{\Phi}{\varepsilon_s}\right)^{-1/2}\right] \tag{2.14}$$

where $\varepsilon_s = 1/2Mu_s^2$ is the initial ion energy. By integrating the equation, we obtain square of 1st derivative of plasma potential.

$$\frac{1}{2}\left(\frac{d\Phi}{dx}\right)^2 = \frac{en_s}{\varepsilon_0}\left[T_e(e^{\Phi/T_e} - 1) + 2\varepsilon_s\left\{\left(1 - \frac{\Phi}{\varepsilon_s}\right)^{1/2} - 1\right\}\right] \tag{2.15}$$

Since left side is not a negative value, right hand side of the equation should be positive and ion speed at sheath boundary has a relation with electron temperature like this

$$\frac{1}{2}\frac{\Phi^2}{T_e} - \frac{1}{4}\frac{\Phi^2}{\varepsilon_s} \geq 0 \tag{2.16}$$

This relation is well known as Bohm sheath criterion and $\boldsymbol{u_B(=(kT_e/M)^{1/2})}$ is defined as Bohm speed.

$$u_s \geq u_B = \left(\frac{eT_e}{M}\right)^{1/2} \tag{2.17}$$

In order to obtain condition of ion speed at sheath-plasma boundary, Boltzmann relation, ion conservation and momentum conservation equations are used with a condition of quasi-neutrality, $\boldsymbol{n_i=n_e=n}$.

$$n\frac{du_i}{dx} + u_i\frac{dn}{dx} = G \tag{2.18}$$

$$Mnu_i\frac{du_i}{dx} = enE + f_c \tag{2.19}$$

$$enE + kT_e\frac{dn}{dx} = 0 \tag{2.20}$$

Combining above equations, 1st derivatives of density and ion speed with $\boldsymbol{x}$ are given.

$$\frac{dn}{dx} = \frac{f_c / M - Gu_i}{u_B^2 - u_i^2} \tag{2.21}$$

$$\frac{du_i}{dx} = \frac{Gu_B^2 - u_i f_c / M}{u_B^2 - u_i^2} \tag{2.22}$$

Because collision force on the ions, $\boldsymbol{f_c}$, is negative, both derivatives become

singular when ion speed is Bohm speed. In result, the region where quasi-neutrality is satisfied and potential exists in front of sheath is called a presheath. Since quasi-neutrality breaks in the sheath, ions boundary between presheath and sheath have Bohm speed.

2.2 Previous Works on Dynamics of Sheath and Presheath

In dynamics of sheath and presheath motion with potential variation, two types of motion, expanding and collapsing sheath, can be categorized with a difference of ion and sheath direction. Expanding sheath occurs while pulse-on starts and target voltage negatively increases. As induced electric field in front of the target becomes stronger, plasma is evacuated toward the bulk plasma. While positive ions move toward the target due to a negatively biased potential, sheath moves with an opposite direction.

Collapsing sheath is generated when pulse off starts and target voltage returns to zero. As the potential decreases, electric field that was induced in the sheath is diminished and sheath is collapsed. Direction of sheath and ion motion is same, back to the target. As the sheath is collapsed, plasma which is recovering from the bulk plasma fills the depletion region.

This section reviews basic theories of sheath expansion and collapse. To simplify the analysis, expanding and collapsing sheath are described at the case of pulse rise and fall time, respectively.

2.2.1 Sheath Expansion responding to the target voltage

When a voltage is applied to the target within the time scale of the inverse of ion plasma frequency, electrons in front of the target is evacuated and only ions exists. Except for the condition that sheath is moving, therefore, expanding sheath can be described like the analysis of static sheath. Lieberman and Scheuer built an analytical model based on the Child-Langmuir sheath. [36, 37] The model starts from five assumptions

- The ion motion in the sheath is collisionless (low pressure).
- The electrons react instantaneously ($\omega_{pe} >> \omega_{pi}$)
- The applied voltage is large compared to the electron temperature ($e|U_0| >> kT_e$)
- Sheath evolution can be described by quasi-static Child-Langmuir law.
- During the motion of an ion across the sheath, the electric field within the sheath is frozen at its initial value.

Scheuer et al built an analytical model considering these assumptions. He assumed that ions are not injected from the bulk plasma to the sheath since ion does not enough time to move at the early time of pulse-on within the scale of inverse of ion plasma frequency. Based on the assumptions, time variation of sheath is calculated.

$$\frac{ds}{dt} = \frac{2}{9}\frac{s_0^2 u_0}{s^2} \tag{2.23}$$

where s_0 is the static matrix sheath size and ω_{pi} is an ion plasma frequency.

After time passes over the scale of the inverse of ion plasma frequency, ions start moving to the target and the sheath evolves toward Child-Langmuir sheath. Lieberman derived the equation of sheath motion based on these assumptions. Since Child-Langmuir sheath is formed, ions at the sheath boundary have Bohm speed and it changes sheath expansion speed as below

$$\frac{ds}{dt} = \frac{2}{9}\frac{s_0^2 u_0}{s^2} - u_B \tag{2.24}$$

where u_B is the Bohm speed. Sheath speed at Lieberman's model is slower than that at Scheuer's prediction and the deviation is Bohm speed.

Rieman approached the sheath expansion based on the ion matrix sheath.[23] He presented an analytical model combining cold fluid equations for the ions, an electron step model, and Poisson equation. His model dose not use any artificial assumptions that were noted from Lieberman and Schuer's model. He described two different mode of sheath expansion, the matrix extraction phase and the sheath expansion phase.

The matrix extraction occurs within the scale of $3/\omega_{pi}$ after initial expansion occurs, as described in Figure 2.2. The evolution consists of two processes, homogenous part in front of the target and inhomogeneous one

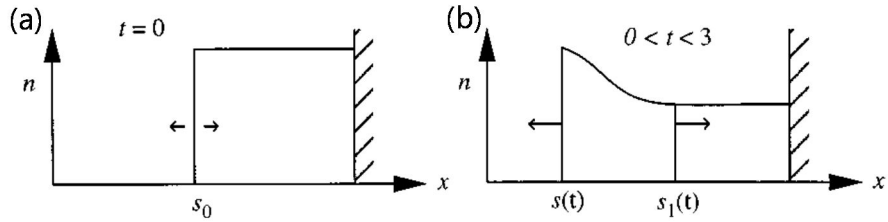

Figure 2.2 Sheath expansion at (a) when pulse starts and (b) during matrix extraction phase

faced to the bulk plasma. When pulse-on starts, the original (***t=0***) boundary $s_1=s_0$ of the homogeneous part of the ion matrix moves with the ion flow velocity to the wall. As time passes, plasma density decreases but its uniformity is sustained. The inhomogeneous part expands to the bulk plasma with time building the non-uniformed density profile. Length of each part can be obtained from the fluid equations.

$$s_1(t)=\frac{5s_0}{6}+\frac{t}{2}+\frac{2+t^2}{2}\left[\frac{1}{\sqrt{2}}atn\frac{t}{\sqrt{2}}+\frac{s_0}{6}\left(1+\ln\frac{2}{2+t^2}\right)\right] \tag{2.25}$$

$$s(t)=t+\frac{3s_0}{2}+\frac{s_0-2s_1(t)}{2+t^2} \tag{2.26}$$

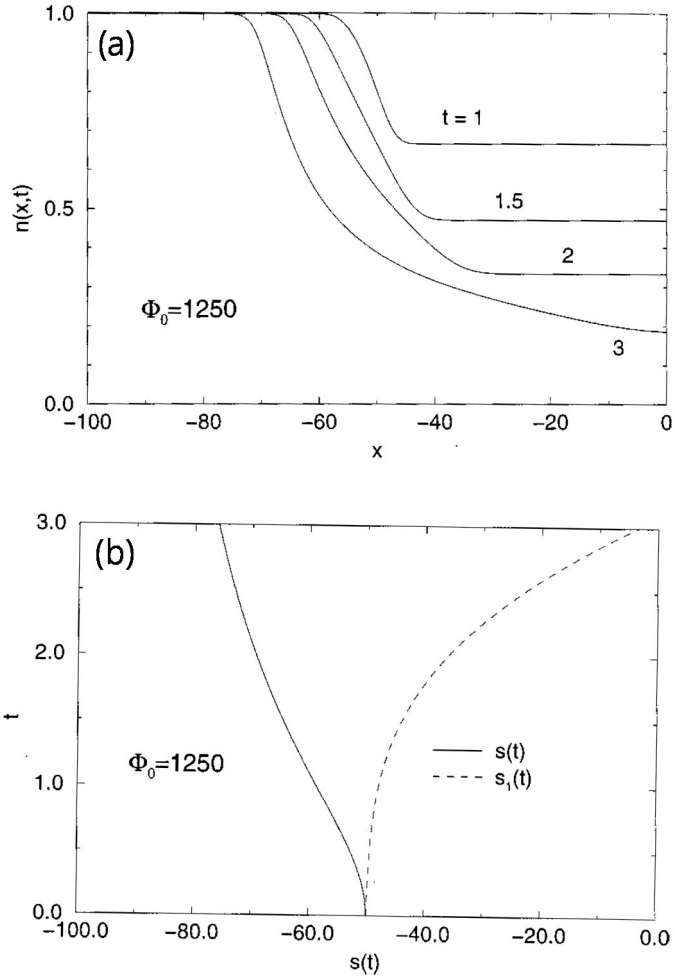

Figure 2.3 (a) ion density variation in the sheath and (b) sheath boundaries of $s_1(t)$ and $s(t)$.

Time transient motion of $s_1(t)$ and $s(t)$ is depicted in Figure 2.3. When s_1 becomes zero and homogeneous part is removed, the matrix extraction phase ends and sheath expansion phase starts. Sheath expands making non-uniform ion profile in the sheath by induced electric field. He noted that it is assumed that Child-Langmuir sheath is formed during the sheath expansion phase and are stabilized.

2.2.2 Propagation of Rarefaction wave

In plasma related operation, rarefaction wave is generated in two types of plasma motion. At first, plasma expansion into a vacuum causes the rarefaction wave as presented in Figure 2.4. By the electron pressure, free streaming of ions into the vacuum is proceeded and depletion of plasma occurs in return, which is the rarefaction wave. Both ions in the leading edge and rare faction wave have a Bohm speed and it is verified using theoretical, numerical, and experimental methods. [1, 2, 38, 39]

The other is generation of rarefaction wave by pulse rise and is presented in Figure 2.5. When sudden pulse is applied to the target, sheath expands with supersonic speed over a Bohm speed. Sheath speed decreases as time passes after pulse rise ends. When sheath propagation drops below the Bohm speed, rarefaction wave is launched and propagates into the bulk plasma regardless of sheath motion. This motion is explained numerically and experimentally by Widner el al and is verified by many studies with experimental result, analytical model or numerical code such as PIC simulation. [29, 40-45]

Rarefaction wave sets up a non-uniformed plasma spatial distribution, which is called as presheath, between sheath and bulk plasma to give ions Bohm speed. Rarefaction wave persists after sheath is stabilized then stabilized after the voltage drop in the presheath forces the ion speed to increase up to the ion acoustic speed. [27]

2.2.3 Effect of non-uniform plasma profile

Non-uniformity also takes a major role to control sheath expansion and formation of presheath. Many previous studies assume that the plasma spatial distribution in front of the target has a uniform profile for simplicity. In real system, however, plasma has a non-uniform density profile by the cases such as diffusion from bulk plasma or additional generation.

Sheath is a region to shield target voltage and potential decreases along the sheath by the residual ions. Accumulated number of ion in the sheath determines the sheath size and the non-uniformity causes a variation of sheath size compared to the expected one from the model. Previous study verified this phenomenon which occurs the plateau time of pulse. [30] It showed that Child-Langmuir sheath is formed when pulse applied but it does not follow $V^{3/4}$ due to the non-uniformity of the plasma profile.

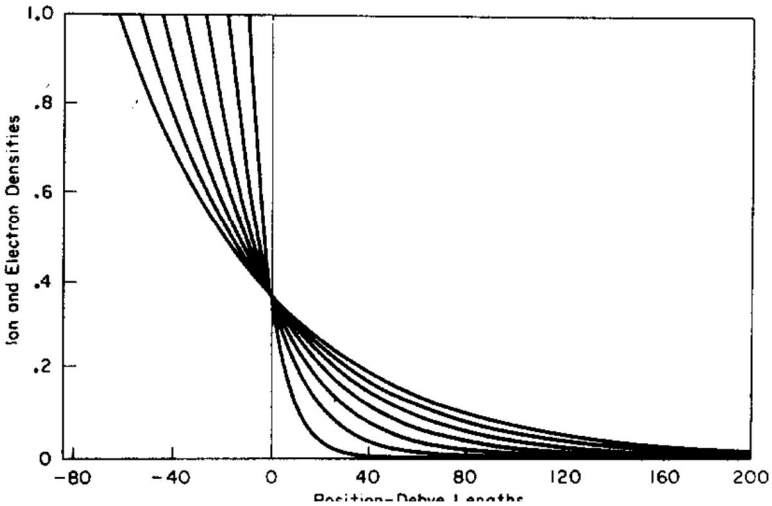

Figure 2.4 Plasma streaming into a vacuum and propagation of rarefaction wave.

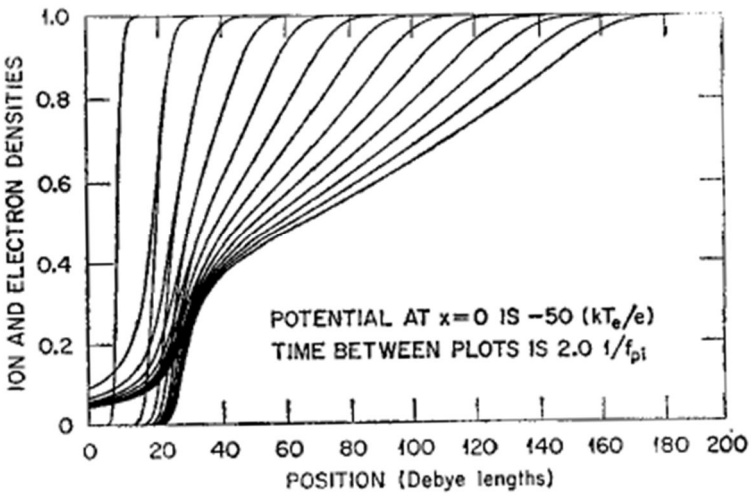

Figure 2.5 Drop of sheath expansion and launch of rarefaction wave.

Another effect on non-uniformity of plasma potential is the suppression of sheath expansion due to the ion drift speed.[29] Ion drift has the opposite direction of sheath expansion. In result, thickness of the expanding sheath edge is reduced by the ion drift velocity when compared to the thickness without ion drift. Since the ion drift also prevents the propagation of the rarefaction wave, the expansion speed of the wave is observed to be less than the Bohm speed, which is depicted in Figure 2.6.

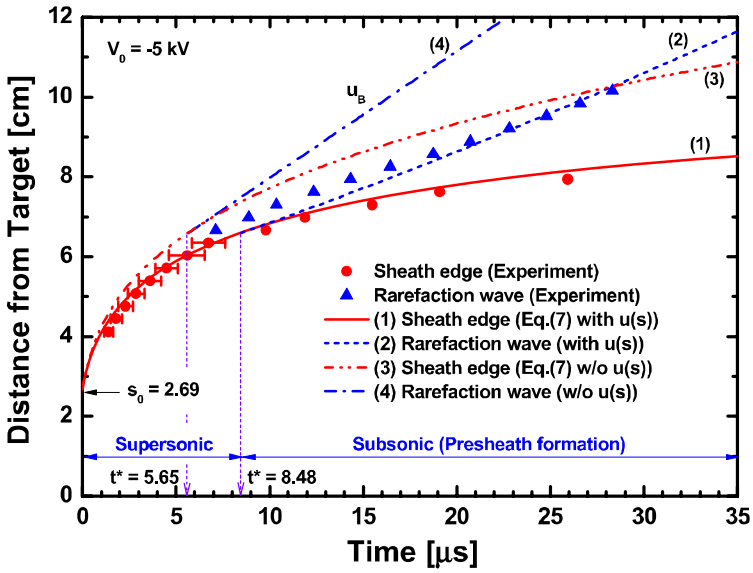

Figure 2.6 Temporal evolutions of the sheath edge (error bars and circles) and the rarefaction wave (error bars and triangles).

2.3 Plasma Recovery at Pulse Fall Time

Plasma recovery occurs when pulse-off starts and target voltage returns to zero. Sheath is collapsed responding to the target voltage and plasma at the presheath start injecting to the depletion region that was formed at pulse plateau time.

Wood first observed plasma recovery and developed the model based on ambipolar diffusion, which is called a depleted region fill-in model as presented in Figure 2.7.[46] He assumed that sheath is immediately collapsed when pulse-off starts and plasma fills the depletion region by ambipolar diffusion. Fill-in time is determined from the balance of the diffusion from the bulk plasma (Γ_1) and to the bulk plasma (Γ_2). In result, plasma density at the depletion region can be obtained.

$$n_s(t) = n\left[1-\left(1-\frac{n_{s0}}{n}\right)e^{-\gamma t}\right], \quad \gamma = \frac{T_e}{T_i}\frac{1}{s}\left(\frac{eT_i}{2\pi}\right)^{1/2} \tag{2.27}$$

where $\boldsymbol{n}$ is a plasma density at the bulk, $\boldsymbol{n_{s0}}$ is a plasma density at the depletion region when **t=0**, and γ is a fill-in rate.

After the Wood's model, various models are proposed and these can be categorized with two types, which is referred as ion inertia model and plasma expansion model.

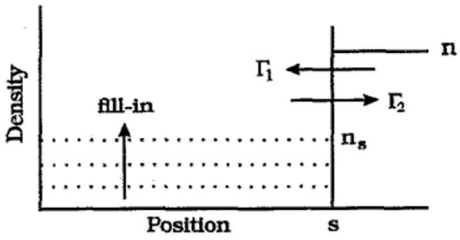

Figure 2.7 Depleted region fill-in model

2.3.1 Ion Inertia Model

Ion inertia model is based on the theory that plasma recovers with ion speed that was given. En et al first develop the model.[31, 47] Current to the target is due to the uncovering of ions by moving sheath and ambipolar diffusion of ions toward the sheath boundary. Since the presheath is stably formed before the pulse-off starts, Bohm speed is derived as the diffusion speed and the balance equation is obtained.

$$qn_0\left(\frac{ds}{dt}+u_B\right)=J_{target} \tag{2.28}$$

During the pulse fall time, target current (J_{target}) becomes negligible. In result,

$$\frac{ds}{dt}=-u_B \tag{2.29}$$

Plasma recovery during the pulse fall time is shown in Figure 2.8.

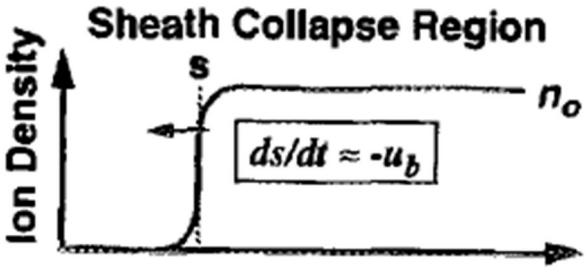

Figure 2.8 Plasma recovery with an uniform Bohm speed.

Briehl et al extends En's model adding the plasma current to the target.[32] The recovering plasma at the depletion region is also injected to the target voltage with a Bohm speed and the time variation of fill-in plasma density is calculated as below.

$$n_s(t) = n\left(1 - e^{-u_B t / s_0}\right) \tag{2.29}$$

where s_0 is a sheath size before pulse-off.

Briehl's model has a longer recovery time than both En's model and Wood's model. He noted that En's model neglected the slow process occurring during ambipolar diffusion after plasma ions hit the wall. He also noted that the strength of the ambipolar diffusion current at Wood's model is reduced considerably by the floating potential repelling electrons from the wall.

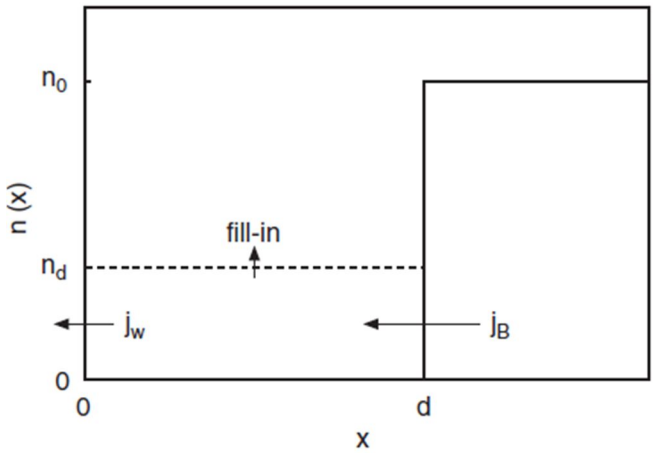

Figure 2.9 Plasma recovery and absorption with a uniform Bohm speed

2.3.2 Plasma Expansion Model

Another model is based on the plasma expansion into a vacuum. It is also an ion's motion by ambipolar diffusion but it generates the density gradient at the boundary of sheath and bulk plasma.

Based on the plasma expansion model from Gurevich et al, Chung et al developed the plasma recovery model.[12] Since the drastic density gradient at the boundary exists in front of the depletion region when pulse-off starts, plasma recovery follows like the plasma expansion into a vacuum. In addition, ions at the boundary have a speed that was formed at the plateau time enhancing the plasma recovery. Combining these effects, the fill-in density can be obtained.

$$n_s(t) = \exp\left(-1 + \frac{u_0}{u_B}\right) n_0 \frac{u_B t}{s_0}\left(1 - \exp\left(-\frac{s_0}{u_B t}\right)\right) \tag{2.30}$$

where $\boldsymbol{u_0}$ is an ion speed and $\boldsymbol{s_0}$ is a sheath size before pulse-off starts. Time-transient recovery motion is shown in Figure 2.10.

Daube et al investigated plasma recovery process using PIC and fluid code.[45] In his study, compression wave runs into the plasma and shifts the presheath corresponding to the small extension of the final sheath. In result, the compression wave makes the depletion region fill the plasma as presented in Figure 2.11.

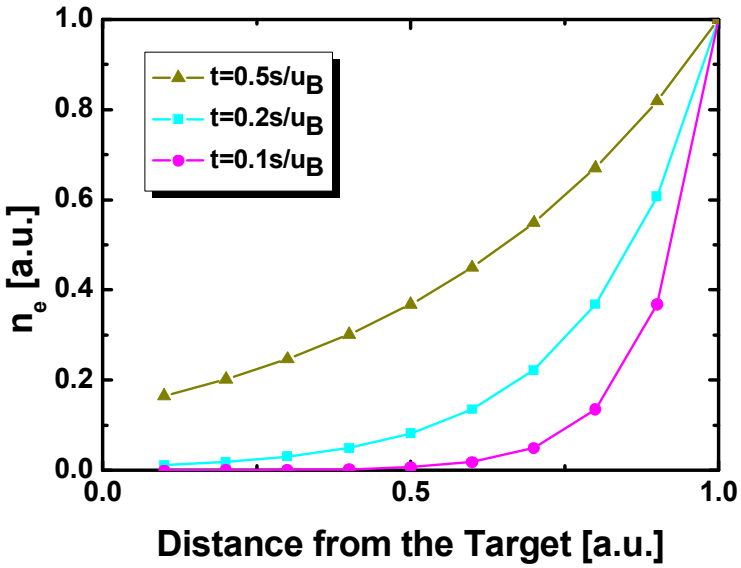

Figure 2.10 Plasma recovery by plasma expansion

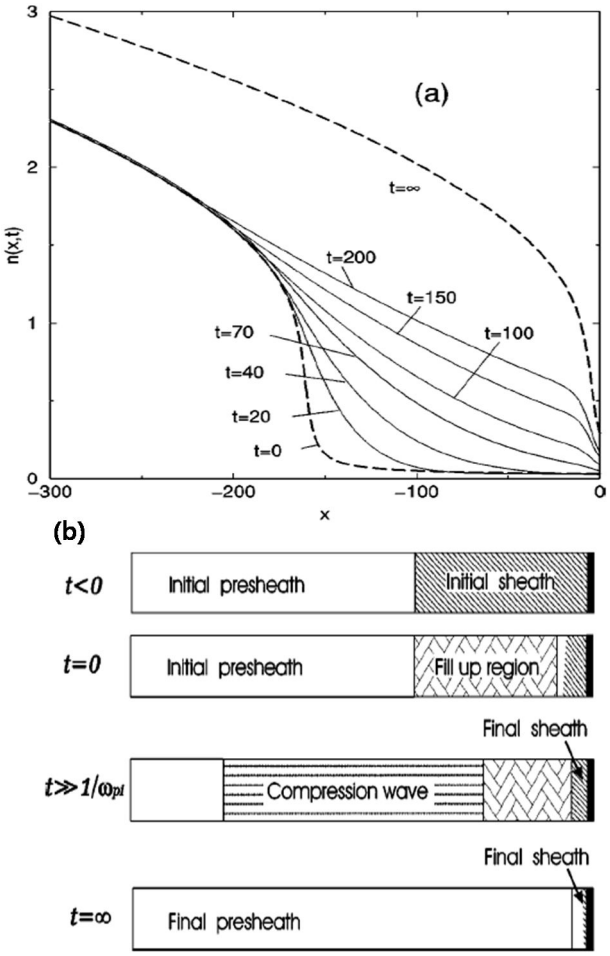

Figure 2.11 (a) variation of plasma density and (b) its schematic diagram after pulse-off

Chung et al also investigated plasma recovery process using fluid code. [33] He noted that the compression wave is generated in front of the target and rarefaction wave that goes forward the bulk plasma is progressed when pulse-off starts. From the simulation result, recovery time is calculated and its value is proportional with $5s_0 / u_B$.

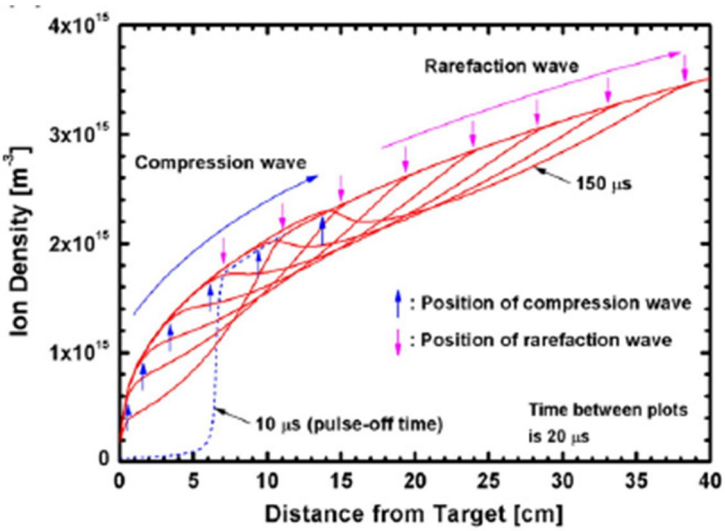

Figure 2.12 motion of compression and rarefaction wave during plasma recovery process

2.4 Current Issues on Plasma Recovery at Pulse Fall

In previous section, previous studies at pulse rise and fall time is reviewed and historic progress is presented. Many studies are progressed and a lot of issues have been solved theoretically, experimentally, or numerically but unsolved issues exist. Especially, generally accepted models exist at the analysis of expanding sheath and presheath motion at pulse rise. At pulse fall time, however, accomplishment of sheath and presheath recovery analysis is not yet sufficient. Here are some issues to be solved.

- **Absence of presheath recovery study**

In general, recovery process is carried out at the voltage falls after voltage is sustained such as pulse fall time after pulse plateau time or decreased voltage shape after maximum voltage at Sinusoidal voltage shape. Therefore presheath that was formed at the previous phase react to the variation of the target voltage. In addition, the presheath is located after the sheath, which affects the sheath motion. In result, analysis of presheath recovery has a dominant role for plasma recovery. Previous studies explains the formation of presheath but modification of presheath profile and motion during the pulse fall time is not investigated sufficiently.

- **Insufficient studies of effect of sheath and presheath recovery on duration of pulse fall**

As noted earlier, previous studies are progressed with the assumption that pulse fall time is within the inverse of ion plasma frequency. In real system, however, pulse fall time is determined by plasma load and system impedance and its value can be from sub-us to several ms, which less or more than an inverse of ion plasma frequency. In result, previous studies have its limit to explain the recovery motion.

Stewart et al analyzed sheath motion and current variation with a finite fall time. [34] The model, however, is based on the assumption that quasi-static Child-Langmuir sheath is consistently formed during the time and variation of ion's mobility with time is not considered. Thus, the result has a limit to explain the effect of plasma property on pulse fall time.

- **Overlapping of sheath expansion and recovery**

High repetitive pulse operation is one of the most effective tools to maximize the capabilities of pulse operation and to reduce processing time. In order to archive a high repetition, there are several ways to control, such as increase of frequency, short of pulse-off time, and short of pulse-on time. Previous studies focused on the high frequency and short pulse-off effect and the variation of plasma and target current. [32, 46, 48-50] Control of plateau time, however, also is a significant factor for the recovery. When pulse-off starts after plateau time passes and sheath and rarefaction wave is saturated, presheath recovery starts at the initial condition that Child-Langmuir sheath is

formed and ions flows with a Bohm speed. As the plateau time decreases under the sheath saturation time or between sheath and rarefaction wave saturation time, initial condition at presheath and ions at the boundary is distorted because of unsaturated Child-Langmuir sheath, which affects the recovery process.

Chapter 3. Experimental Setup

This chapter presents experimental arrangements to employ for the study. Chambers and pulse system for the experiment are announced and diagnostic system to measure time-transient plasma profile is described.

3.1 Plasma Sources

Three plasma sources, inductively coupled plasma, remote inductively coupled plasma, and DC filament plasma, are arranged for the study. To achieve a correct diagnosis of sheath and presheath motion, operating parameters at all chambers are precisely adjusted. Ar plasma is generated and its pressure is controlled to generate collisionless plasma. Target is located out of skin depth and plasma generated so that no plasma generation occurs around. Additional apparatuses are installed to suppress RF fluctuation. Pulse voltage is adjusted to prevent addition ionization by electric field during pulse bias operation.

3.1.1 Inductively coupled plasma chamber

Chamber at Figure 3.1 is operated for the diagnosis of sheath at slow fall

time. Inductively coupled plasma is generated in the left side of the chamber, which has a cylindrical shape with a length of 600mm and diameter of 500mm. The stainless-steel target is located at the center of right side in the chamber with a diameter of 100mm. Its position is in an opposite and the furthest side from the plasma generation region to maximize the diffusion of plasmas to the target. Quartz tube with a height of 100mm guides the target to prevent plasma flown at the edge. The position and quartz tube, moreover, have a role to suppress plasma fluctuation within a value of 4.2V, which is much smaller than target voltage. Operating pressure is 1mTorr and additional ionization was not observed during the pulse operation.

3.1.2 Remote inductively coupled plasma chamber

Figure 3.2 shows a schematic diagram of the remote ICP chamber. Chamber at the top generates inductively coupled plasma which diffuses into the main chamber. The generation chamber has a cylindrical shape with a diameter of 60mm and height of 200mm and the main chamber has a cylindrical shape with a diameter of 420 mm and height of 370mm. To minimize the fluctuation of the plasma, Faraday shield is located between the generation and main chamber. The stainless-steel target with a diameter of 100mm is located at the center and bottom of the main chamber and sheath motion is performed in front of the target. Collisionless plasma is generated at the pressure of 1mTorr and local ionization by pulse operation was not generated.

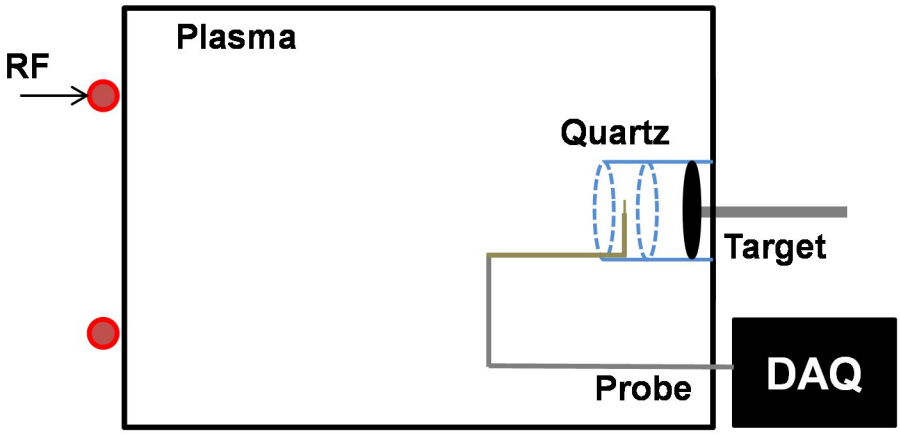

Figure 3.1 Schematic diagram of ICP chamber.

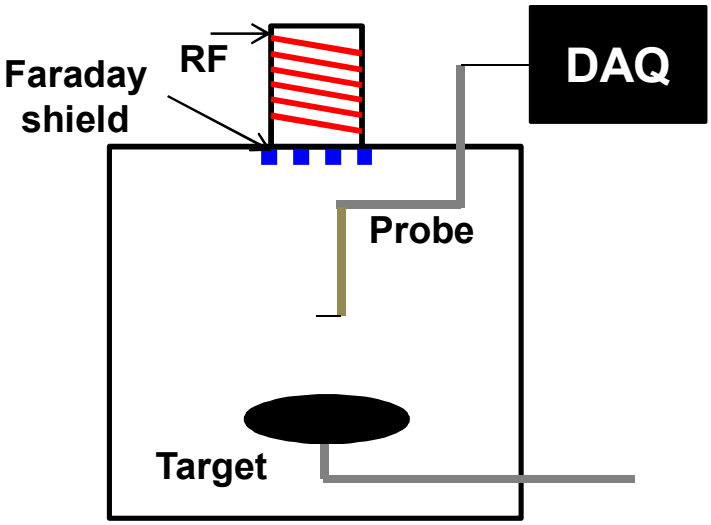

Figure 3.2 Schematic diagram of remote ICP chamber.

3.1.3 DC filament chamber

A schematic diagram of DC filaments chamber is presented in Figure 3.3. The plasma is generated in a cylindrical chamber with an inner diameter of 380mm and a length of 330mm. Hot tungsten filament emits electrons to ionize Ar gas in a pressure of 0.4mTorr. Filament is biased at V_{bias} = - 60V with respect to the ground wall and emission current ($I_{filament}$) is 42A. The outer surface of chamber is surrounded by multi-dipole array of permanent magnets to confine the plasma and improve the density and uniformity.[51] Magnetic field is about 0.683G around the target so acceleration of ions by magnetic force is negligible comparing to the electric field induced by target voltage.

Stainless steel target is located at the right side of the chamber with a diameter of 100mm. Quartz tube with a height of 142mm guides the target and distance from the target and end of the quartz is 75mm. Like the previous experiments, pulse voltage is adjusted so that maximum sheath boundary is within the quartz tube and distortion of plasma profile at the bulk plasma out of quartz tube is minimized. In result, it is assumed that bulk plasma is injected to the plasma in the quartz tube regardless of pulse operation. Cylindrical probe with diameter of 0.2mm and length of 14mm is located at the opposite side of the target and scan time-transient plasma density in the quartz tube.

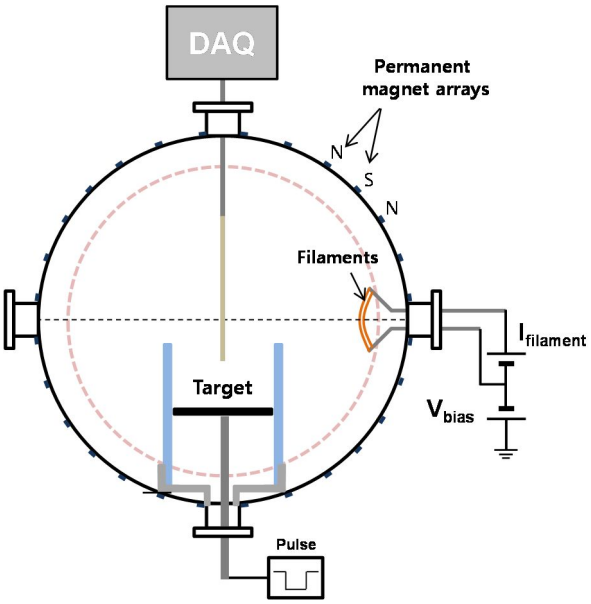

Figure 3.3 Schematic diagram of filament chamber

3.1.4 Plasma density and temperature

Spatial distribution of plasma density and electron temperature at three chambers is depicted in Figure 3.4. Plasma has a non-uniform profile from the target to the bulk plasma. Since plasma generation does not occur and plasma diffuses to the target, linear plasma profile is formed in front of the target. Plasma density is varied from 3.5×10^{7} cm^{-3} and 4.0×10^{9} cm^{-3} for the adequate measurement of sheath and presheath. Electron temperature at three chambers can be assumed to be a constant in operating range. Plasma property may be

different at each experiment but linearity of plasma density and uniform electron temperature are maintained in all experiments

3.2 Pulse System

Schematic diagram of the pulse system is presented in Figure 3.5 and detailed specification of the pulse system is arranged in table 5. The system consists of DC power system and switch parts. DC power system consists of high voltage DC power supply and energy storage capacitor to supply charges to the target and sustain target voltage. Switch part consists of two MOSFET switches to modify pulse shape. 1st switch is connected between energy-storage capacitor and the target, which supply voltage to the target when pulse starts. 2nd switch is located between the target and the grounds with a resistor.

Pulse-on and -off are controlled by operation of 1st and 2nd switch. When pulse-on starts, 1st switch is on and 2nd switch is off. Target voltage is sustained by the DC power supply and charges are supplied from the energy-storage capacitor. When pulse-off starts, the 1st switch turns off and 2nd switch turns on.

The target that was charged at pulse-on time is neutralized by the current in the 2nd switch. Switches have a natural capacitor (C_C) and coupling capacitances (C_N) in and between ports and its values are 39pF and 20pF, respectively.

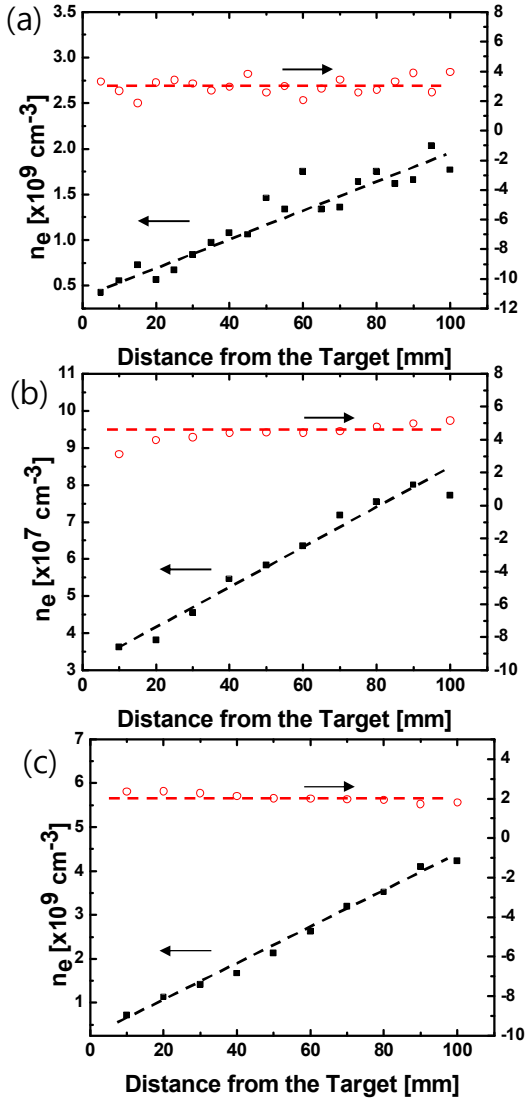

Figure 3.4 Spatial distribution of plasma density and electron temperature at (a) ICP, (b) remote ICP, and (c) filament chamber.

Stray Capacitance (C_{stray}) exists in the system between the system and the target. Previous studies showed that stray capacitance is not negligible in the pulse system.[52] In this study, the stray capacitance is measured using dummy resistor connected to the target and its values are 310pF, 297pF, and 210pF for the chamber of slow and fast fall time operation, respectively. Comparing to other capacitors, the stray capacitor has a major role to hold charges in the target. Small variation of capacitance by changing chamber indicates that almost stray capacitors are included in the pulse system.

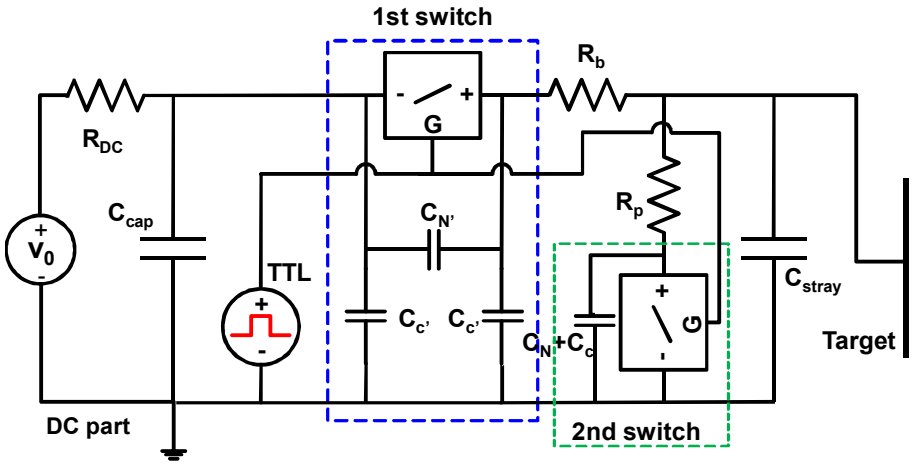

Figure 3.5 Schematic diagram of pulse system.

Table 3.1 Specifications of components in the pulse system.

Component	Specification	Model/Manufacturer
High voltage DC power supply	50kV,6mA	SHV300/Convertech
Energy-storage capacitor	50kV, 0.101uF	37330/Maxwell
1st switch	65kV, 30A	HTS 651-03-LC/Behlke
2nd switch	33kV, 30A	HTS 331-03-LC/Behlke
Trigger pulse generator	2 ch, 250MSa/s, 30MHz	33522a/Agilent

3.3 Langmuir Probe System

Single Langmuir probe is commonly used to measure the variation of plasma motion. In this study, cylindrical and planar type tips, which are made of tungsten or tantalum, are used and its size is adjusted to collect adequate current for measurement and to minimize plasma perturbation.

Figure 3.6 shows a schematic diagram of Langmuir probe and current sensing unit. Since the variation of plasma potential during the pulse operation is not drastically changed, electron saturation current is measured by biasing the probe voltage around plasma potential. It is assumed that the election saturation current is proportional with the electron density.

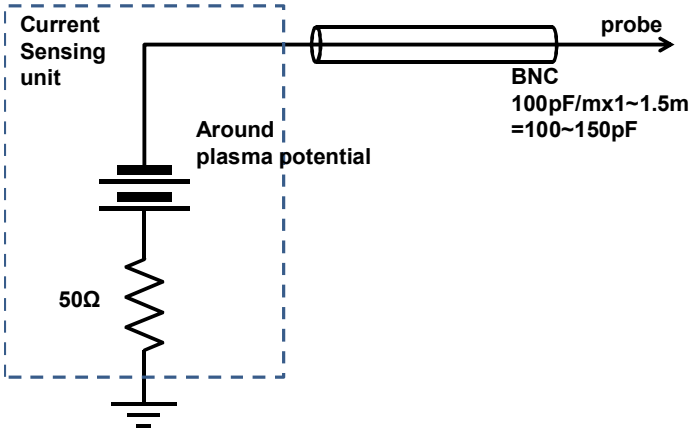

Figure 3.6 Schematic diagram of Langmuir probe system

In order to maintain the stable voltage against the drastic change of plasma property, battery is used as a voltage source to the probe tip. One of limitations when time-transient plasma property is measured is stray capacitance in the diagnosis system. BNC cable to connect the probe and current sensing unit is as short as possible and 5RC time is within 37.5nsec, which is the range that the data are valid enough to respond to the variation of plasma motion. Time-transient current is measured using the current sensing resistor with 50Ω.

Figure 3.7 shows example of time-transient current profile with time. When pulse-on starts and sheath meets probe tip, current is diminished and it recovers after pulse-off and as plasma recovers.

3.4 Numerical Analysis on Plasma Dynamics

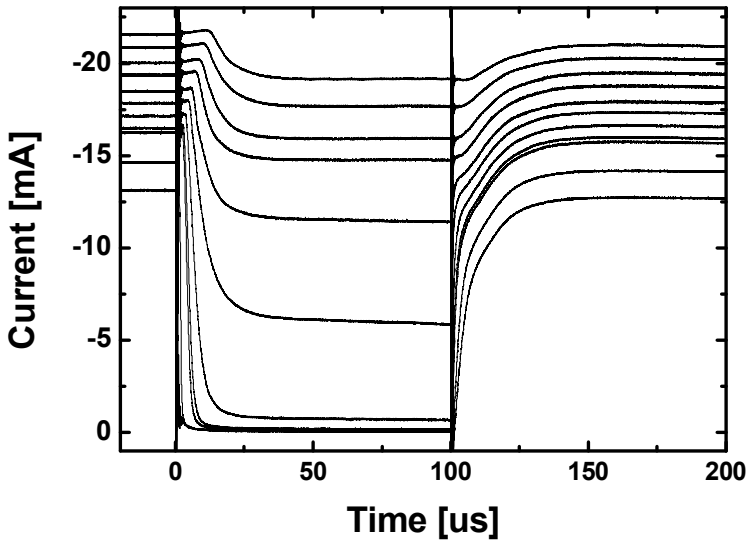

Figure 3.7 Time-transient electron saturation current profile with positions.

Although experimental study is a direct method to reveal plasma dynamics, limitation exists to describe the ion and electron motion separately. Analysis of plasma dynamics that are based on the fluid code is developed to describe the motion of ions and electrons responding to the voltage on the target.

3.4.1 Governing equations

The numerical fluid model for sheath and presheath motion is developed with the assumptions described below.

- Ion motion is collisionless.
- Electrons are instantly respond to the induced electric field due to the time scales of motions longer than the inverse of electron plasma frequency ($1/\omega_{pe}$)
- Electrons obey the Boltzman relation
- Thermal motion of ions is neglected due to the electric field higher than ion temperature.

Based on these assumptions, the governing equations are given as follows.

Continuity equation for ions

$$\frac{\partial n}{\partial t}+\frac{\partial}{\partial x}(nu)=0 \tag{3.1}$$

Equation of motion for ions

$$\frac{\partial u}{\partial t}+u\frac{\partial u}{\partial x}=-\frac{e}{M}\frac{\partial \Phi}{\partial x}+\frac{\partial P}{\partial x} \tag{3.2}$$

Poisson equation

$$\frac{\partial^2 \Phi}{\partial x^2}=-\frac{e}{\varepsilon_0}(n-n_e) \tag{3.3}$$

Boltzmann relation for electrons

$$n_e=n_0\exp\left(\frac{e\Phi}{kT_e}\right) \tag{3.4}$$

where $\boldsymbol{n}$ is the ion density, $\boldsymbol{n_e}$ is the electron density, $\boldsymbol{u}$ is the ion velocity, Φ

is the potential, ***P*** is the pressure gradient, ***x*** is the position, and ***t*** is the time.

The code is carried out in one-dimensional geometry following the previous studies adding the addition of the force density due to the pressure gradient of plasma density.[12, 44] Almost previous studies performed the simulation with an assumption that plasma has a uniform profile in the domain. In the non-uniformed plasma profile, however, variation of plasma diffusion speed by pressure gradient exists. The pressure gradient is adapted separately in the sheath and presheath region. In the presheath region, ambipolar diffusion has a role to describe the motion since quasi-neutrality exists and electrons and ions move responding to electric field. Induced electric field by ambipolar diffusion is represented as below.

$$E = \frac{D_i - D_e}{\mu_i + \mu_e} \frac{\nabla n}{n} \tag{3.5}$$

where $\boldsymbol{D_i}$ and $\boldsymbol{D_e}$ are the diffusion coefficient of ions and electrons and $\boldsymbol{\mu_i}$ and $\boldsymbol{\mu_e}$ are the mobility of ions and electrons. Using Einstein relation and mobility difference of ions and electrons, the electric field can be simplified with a function of electron temperature.

$$E = \frac{\mu_i kT_i / e - \mu_e kT_e / e}{\mu_i + \mu_e} \frac{\nabla n}{n} = -\frac{kT_e}{e} \frac{\nabla n}{n} \tag{3.6}$$

In result, the pressure gradient term can be expressed as below.

$$\frac{\partial P}{\partial x} = qnE = -kT_e \nabla n \tag{3.7}$$

In the sheath, the pressure gradient by ambipolar diffusion is neglected

since only ions exist and electric field controls the distribution. Thermal diffusion of ions can be neglected by the assumption that ion temperature is zero.

3.4.2 Numerical domain and boundary conditions

Numerical simulation is performed in the region as presented in Figure 3.7. The simulation assumes that no variation of plasma property in radial direction and the geometry is constrained in the one-dimensional geometry that is the center in the quartz tube and target. Plasma is supplied from the bulk plasma and only the target is a loss area of plasma in the geometry.

In order to improve the accuracy of the code, the initial condition and boundary condition are taken from the experimental data. Initial plasma density and potential profile are obtained from the non-uniform plasma density when no pulse is applied. The potential and electric field in the domain geometry and the bulk plasma is calculated from the density profile and it is assumed that there is no distortion by the variation of the target voltage.

In the boundary faced on the target, target voltage is obtained from a fitted function based on the experimental data during the operation. Secondary electron emission by injected ions is included in the calculation using the coefficient obtained from the previous studies.[13, 14, 53, 54]

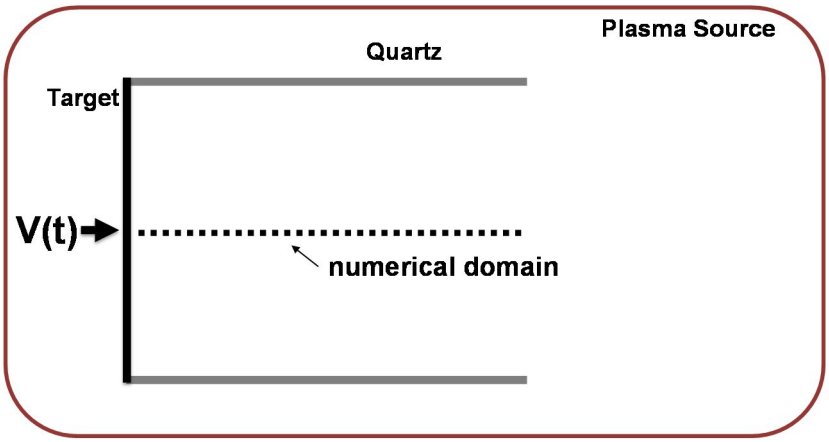

Figure 3.8 Operating scheme of the fluid code

Chapter 4. Dynamics of Sheath Recovery

When pulse off starts, voltage target decreases and sheath and presheath start recovering responding to the voltage. In this chapter, dependence of sheath motion on pulse fall time is investigated. With two extreme cases, slow fall time referring to time longer than ion flight time and fast fall time referring to time around or shorter than ion flight time, sheath motion is compared with the pulse fall time.[23] The models which includes not only plasma motion but also system impedance are developed and sheaths are proposed. By the comparison of model data, experimental result and two typical sheaths (ion matrix and Child-Langmuir sheath), validation of the model is checked and their discrepancy is explained. From the result, discussion is carried out.

4.1 Experiment Setup and Pulse Shape

The experiments are carried out with two extreme fall duration, which is named as fast fall time and slow fall time. The basis is ion flight time, which is a time when ion flights in the sheath. Fast fall time is defined as the fall time is less than flight time so ions do not have enough time to respond to the target voltage and are fixed during the fall time. In contrast, slow fall time is defined as the fall time that is much longer than the ion flight time. Therefore,

ions have enough time to respond to the induced electric field in front of the target and target voltage is fixed during the flight of ions in the sheath

Two chambers are used for the adequate experiments. Inductively coupled plasma chamber is for the analysis of fast fall time and remote inductively coupled plasma is for the slow fall time.

Pulse shapes at the experiment are shown in Fig. 4.1. All pulses have a plateau time of 100 us and it is enough time for expanding sheath at pulse rise time to be stabilized and steady-state plasma is maintained when pulse-off starts.

Fall time is adjusted by controlling resistance of the resistor connected between the target and the 2nd switch. Slow fall time is achieved by disconnecting 2nd switch. To increase the validity of the experiment, plateau voltages of 2kV and 5kV are applied to the target and each pulse fall time is 400us and 550 us. Fast fall time is achieved with resistor of 5kΩ and 20kΩ resulting in a fall time of 5us and 20us, respectively. Plateau voltage is constrained as 1.5kV. Fall time, which is defined as time between 10% and 90% of plateau voltage.

4.2 Sheath Recovery Model

Equivalent circuit of the system at pulse fall time is presented in Fig. 4.2. As mentioned earlier, when pulse-off starts 1st switch is disconnected but energy-storage capacitor is connected to the target by the coupling capacitor in the switch. Therefore the coupling capacitor where plateau voltage is

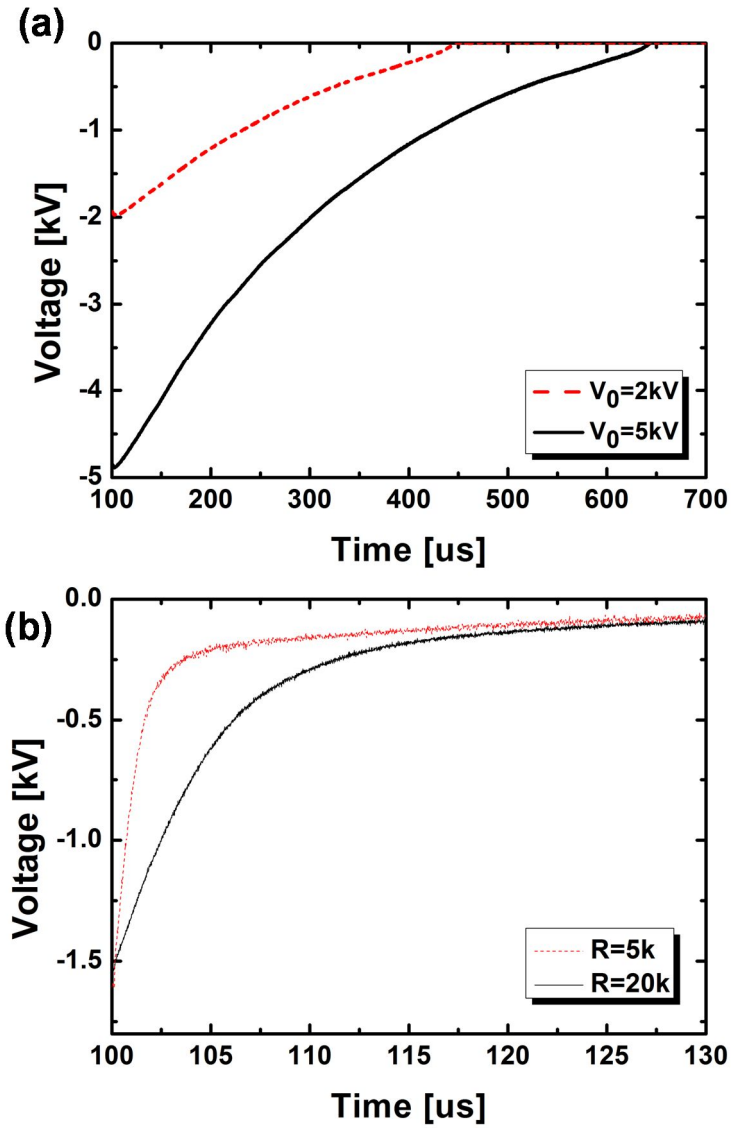

Figure 4.1 Voltage shape at a) slow and b) fast pulse fall time.

sustained by the energy-storage capacitor is connected to the target.

natural capacitor at the output of the 1st switch and stray capacitor as a charge reservoir are also contained in the target. Since the 2nd switch turns on, resistor is connected to the target in parallel and current is flown in addition to plasma current to the target.

Based on the equivalent circuit, governing equation from the equivalent circuit is given by.

$$\frac{dQ_N(t)}{dt}+\frac{dQ_c(t)}{dt}+\frac{dQ_{stray}(t)}{dt}+\frac{dQ_s(t)}{dt}=-I_{target}(=I_{plasma}+I_{see})-\frac{|V(t)|}{R} \qquad (4.1)$$

where $\boldsymbol{Q_N(t)}$, $\boldsymbol{Q_c(t)}$, $\boldsymbol{Q_{stray}(t)}$, and $\boldsymbol{Q_s(t)}$ are a capacitance between input and output of the 1st switch, capacitance at the output of 1st switch, stray capacitance, and charge by sheath in front of the target, respectively. $\boldsymbol{I_{target}}$ is plasma current which flow at the target. The target current consists of plasma current ($\boldsymbol{I_{plasma}}$) and secondary electron emission current ($\boldsymbol{I_{see}}$). $\boldsymbol{V(t)}$ is an target voltage and $\boldsymbol{R}$ is a resistance connected to the 2nd switch. Stray capacitor and switch capacitors keep charges during the plateau time and it has enough plateau time to charge all capacitors in the system. When pulse-off starts, current flown from the 2nd switch, which is defined as $\boldsymbol{|V(t)|/R}$, and plasma current neutralize charges in the system. Secondary electron emission also takes a role to extract charges from the target.

4.2.1 Slow fall time

At slow fall time, variation of target voltage is slow and ions have time enough to respond to the target voltage. Therefore, the governing equation can be simplified with the some assumptions as below.

1) Child-Langmuir sheath are consistently maintained and Bohm current is flown to the target during the pulse fall time
2) Density at the sheath-presheath boundary follows its density that was formed when no pulse applies.
3) Injected ions have much shorter flight time comparing with pulse fall time so that ions at the sheath-presheath boundary is flown to the target immediately and electric field is fixed while ions go through the sheath.
4) No current is flown from the 2nd switch. Only plasma current and secondary electron emission current discharge the capacitor in the system

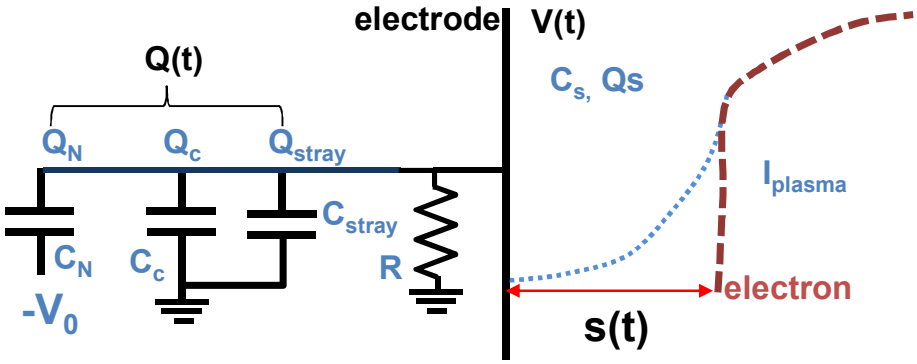

Figure 4.2 Equivalent circuit of the pulse system attached to the plasma.

Based on these assumptions, schematic diagram for the slow falling rate is depicted at Figure 4.3.

From equivalent circuit and its assumption at slow fall time case, charges in the system can be presented as below.

$$Q_N(t) = C_N(V_0 - V(t)),\ Q_C(t) = -C_C(t),$$
$$Q_{stray}(t) = -C_{stray}V(t),\ Q_s(t) = -C_s(t)V(t) \tag{4.2}$$

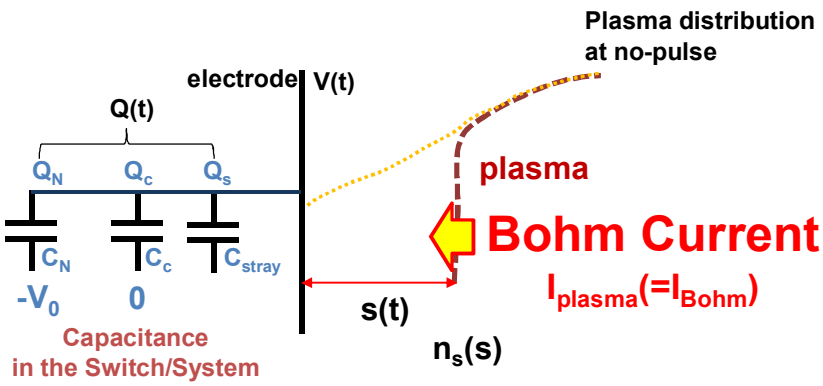

Figure 4.3 Equivalent circuit of the pulse system attached to the plasma for slow fall time case. 2nd switch is disconnected and Bohm current is flown to the target.

Voltage in the sheath is the difference of plasma potential and target voltage but it is assumed that plasma potential can be neglected because target voltage is much larger than that. Capacitance of sheath is defined as $\varepsilon A_{target}/s(t)$ where A_{target} is target area and $s(t)$ is sheath size. Sheath size is determined from Child-Langmuir sheath equation with non-uniform plasma profile. Child-Langmuir sheath is given by

$$s^2 n_s(s) = A^2(-V)^{-3/2} \tag{4.3}$$

where $n_s(s)$ is a plasma density at the plasma-sheath boundary and $A=2/3[\varepsilon_0/e(2e/M)^{1/2}]^{1/2}$ is a coefficient.

At free diffusion plasma in a cylindrical geometry, plasmas diffuse along r-axis and its profile is

$$n(r) - n_0(1 - \left(\frac{r}{r_0}\right)^2) \tag{4.4}$$

where n_0 is a plasma density at the center, r_o is a radius of the target and r is a position of r-axis. We do not consider spatial difference of the property and averaged plasma density, $n_p(s)$, becomes

$$n_p = \frac{2}{3} n_0 \tag{4.5}$$

By integrating with r. Including a linearly increased plasma density, $n_p(s)=as+b$, and presheath, plasma density at the boundary is

$$n_s(s) = \frac{2}{3}\frac{1}{\sqrt{2}}(as+b) \tag{4.6}$$

Inserting Eq. (4.6) into Eq. (4.1) and Differentiating with t, Eq. (4.1) can be a function of sheath and voltage rate as below

$$\frac{2}{3}\frac{1}{\sqrt{2}}(3as^2+2bs)\frac{ds}{dt} = \frac{3}{2}A^2(-V)^{1/2}\frac{dV}{dt} \tag{4.7}$$

Combining of Eq. (4.1), Eq. (4.2), and Eq. (4.7), the governing equation can be a differential equation with sheath size, s, and can be given by

$$\frac{ds}{dt} = \frac{e\left(1+\gamma_{v=20k}\frac{\left\{K^{-1}\sqrt{2}(as^3+bs^2)/3\right\}^{2/3}}{2\times10^4}\right)\sqrt{\frac{kT_e}{M}}A_{target}\frac{\sqrt{2}}{3}(as+b)}{(C_N - C_c - C_{stray} - \frac{\varepsilon_0 A_{target}}{s})\alpha + \varepsilon_0 A_{target}\left\{K^{-1}\sqrt{2}(as^3+bs^2)/3\right\}^{2/3}/s^2} \tag{4.8}$$

For simplicity, assuming that plasma density at target is zero (***b=0***), the dependency of sheath size on the target voltage is presented by combining Eq. (4.6) and (4.3).

$$s = \left(\frac{3}{\sqrt{2}}A^2\right)^{1/3}(-V)^{1/2} \tag{4.9}$$

As shown in the equation, sheath size is proportional to the square root of target voltage.

4.2.2 Fast Fall Time

At fast fall time, ions do not have enough time to respond so ions are

fixed during the time. Based on this motion, assumptions can be set as below

(1) Plasma current ($\boldsymbol{I_{plasma}}$) is zero during the fall time. Only current from the 2nd switch neutralize the target.
(2) Sheath recovers through the ion profile that was formed at plateau time.

Based on the assumptions, schematic diagram of the governing equation is depicted in Figure 4.4. The model assume that sheath follows an electron step model so sheath size is defined as the length between the target and the electron head.[23] Based on the above assumptions, equation of sheath size is derived. Contrary to the case at slow fall time, resistor at the 2nd switch is connected to the target. Inner capacitances at the 1st switch and stray capacitance are as same as that at slow fall time.

At plateau time, Child-Langmuir sheath forms and ions fill in the sheath. Density profile in the sheath is given as

$$n(x) = n_0 \left(\frac{x}{s_0} \right)^{2/3} \tag{4.10}$$

where $\boldsymbol{n_0}$ and $\boldsymbol{s_0}$ are plasma density and sheath size at plateau time, respectively.[55] When pulse fall starts, ions are fixed and ion distribution in the sheath sustains its profile. Combining Poisson equation, sheath size can be derived as

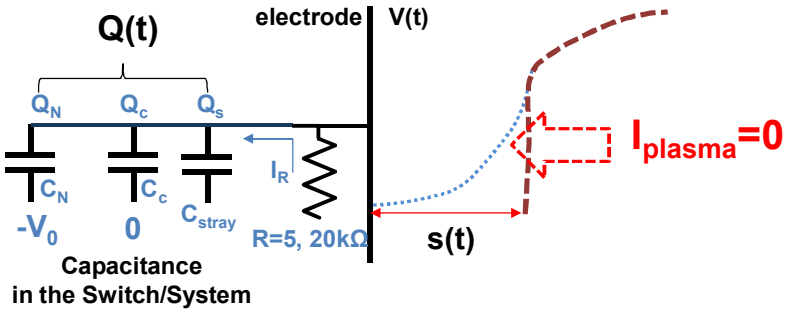

Figure 4.4 Equivalent circuit of the pulse system attached to the plasma for fast fall time case. Current is flown only from 2nd switch.

$$s(t)/s_0 = \left(\frac{4\varepsilon_0}{9}\frac{1}{n_s}\right)^{3/4}(-V(t))^{3/4} \tag{4.11}$$

The equation shows sheath is a function of ***V(t)*** on the order of 3/4, which is the relation of Child-Langmuir sheath with a uniform plasma profile. From the condition, however, derived sheath value is an ion matrix sheath with non-uniform ion profile. With a low-density condition, capacitance at the region between the target and the plasma is low due to a large sheath with voltage and can be neglected. Previous study[52] also said capacitance of the sheath is 2~10pF and its value is negligible as charge reservoir comparing stray capacitance, about 300pF. Following the procedure, governing equation can be modified and its solution is

$$\frac{dQ_N(t)}{dt} + \frac{dQ_c(t)}{dt} + \frac{dQ_{stray}(t)}{dt} + \frac{dQ_s(t)}{dt} = \frac{V(t)}{R} \tag{4.12}$$

$$V(t) = -V_0 e^{-t/R(C_N+C_c+C_{stray})} \tag{4.13}$$

Voltage is exponentially decayed due to the capacitor of the system. Combining the governing equation and the sheath size, analytic solution of sheath size is

$$s(t)/s_0 = \left(\frac{4\varepsilon_0}{9}\frac{1}{n_s}\right)^{3/4} (-V_0)^{3/4} e^{-3t/4R(C_N+C_c+C_{stray})} \tag{4.14}$$

Sheath size is recovered with ***3/4R(C_N+C_C+C_{stray})*** RC time.

4.3 Sheath Recovery with two Extreme Cases

Fig. 4.5 shows the time-resolved profile of a predicted and measured sheath and recovery of plasma profile during slow fall time. In Figure 4.5(a), filled and open dots represent experimental and model data and line represents calculated Child-Langmuir sheath. Round and square dots are data at the plateau voltage of -5kV and -2kV, respectively. Solid and dashed arrows indicate sheath and presheath boundary in Figure 4.5(b). In Fig. 4.5(a), experiment data and the proposed model from Eq. (4.8) are compared with Child-Langmuir sheath calculated by target voltage. It shows sheath is matched with the others. Noting that slow fall time causes both ions and electrons to be rearranged freely by the induced electric field and the electric field to be fixed during the flight, it is reasonable that Child-Langmuir sheath forms responding to the target voltage and Bohm current flows. In Fig. 4.5(b)

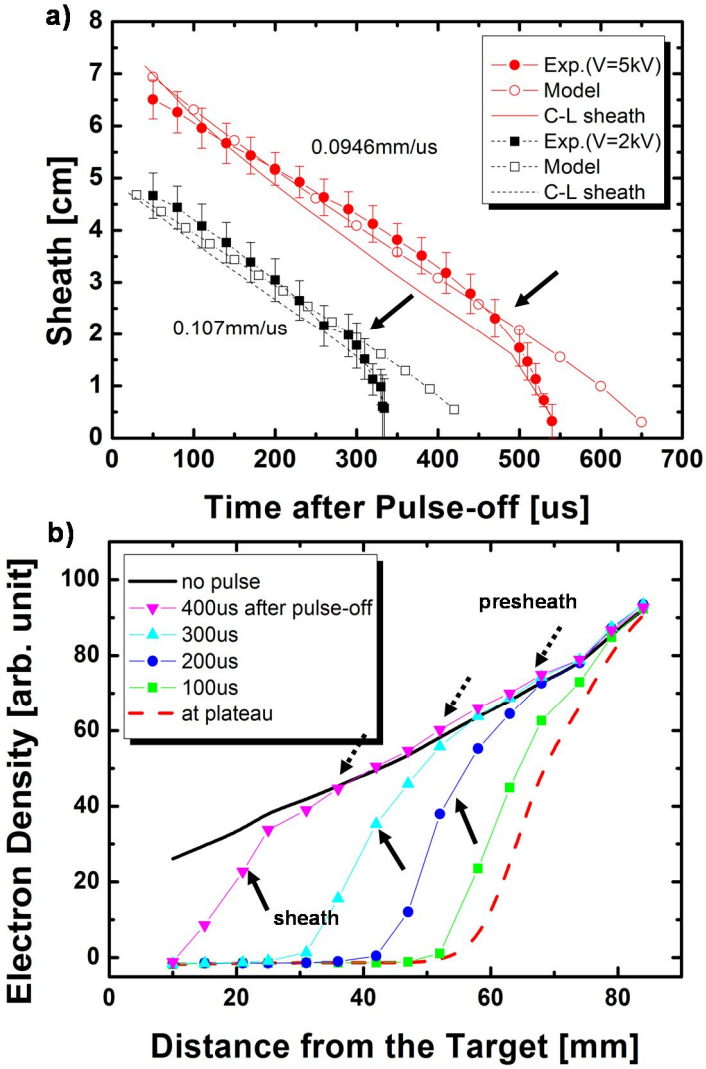

Figure 4.5 (a) Recovery of sheath recovery at slow pulse fall time and (b) variation of plasma profile.

, presheath persists during the fall time so it supports Child-Langmuir sheath is consistently formed responding to the target voltage.

Bulk plasma recovers fully as the sheath is collapsed so that plasma at sheath-presheath boundary has the same density at the sheath edge position at no pulse condition, which is also revealed in Fig. 4.5(b). Sheath speed is much slower than Bohm speed and it says that ions entering from the presheath-sheath boundary have enough to time to flight. In result, the assumption that transit time across the sheath is zero is valid.

As time goes and sheath approaches to the target, however, discrepancy starts between the model and measured sheath around 500us. Sheath is collapsed earlier than expected and calculated Child-Langmuir sheath also follows the experiment one. The model assumes that Child-Langmuir sheath is formed but it is not matched with Child-Langmuir sheath calculated from target voltage and it means the target voltage returns to floating potential earlier than the model expects. The time is matched with when plasma starts attaching the target. Being different from the assumption, slope of plasma profile exist in transition region between sheath and presheath region. Although sheath boundary dose not reach the target, plasma already arrive at the target and the system is neutralized and voltage recovers a floating potential by flooded plasma.

Sheath position at fast fall time and recovery of plasma profile are presented in figure 4.6. Filled and open dots represent experimental and model data and line represents calculated ion matrix sheath using measured electrode voltage. Round and square dots are data at the resistor of 20kΩ and

5kΩ, respectively. Solid arrow indicates sheath boundary. Sheath is compared with the results of proposed model from Eq. (4.13) and ion matrix sheath calculated from the measured target voltage. In Fig. 4.6(a), all data are matched with each other at the onset of pulse fall and they show that sheath is drastically collapsed preserving ion matrix sheath when pulse-off starts. Result also implies that ions sustain Child-Langmuir sheath profile that was formed at plateau time and only electrons move as sheath recovers. Plasma recovery is explained in Fig. 4.6(b). Contrary to the case of slow fall time, plasma profile recovers without refilling the depletion region. Electron head rushes to the target and fill ion depletion region that was formed at pulse plateau time. In result, slope of plasma profile is decreasing while following ion profile as time passes. After time goes, sheath arrives at the target and target voltage returns to floating potential. The region in front of the target starts being filled with plasma, which has been noted from the previous studies.[33, 45]. Sheath is faster than Bohm speed and most ions that entered the sheath at plateau time cannot propagate sheath. Ions over sheath speed by ion inertia[35] exists but its current is small.

As time goes on, the model is drastically laid but measured sheath is collapsed without any change of recovery speed. Calculated ion matrix sheath also follow the proposed model and it says that sheath is collapsed earlier than expected while target voltage is sustained. Fast recovering electrons by electric field form a negatively charged virtual cathode in front of the target.

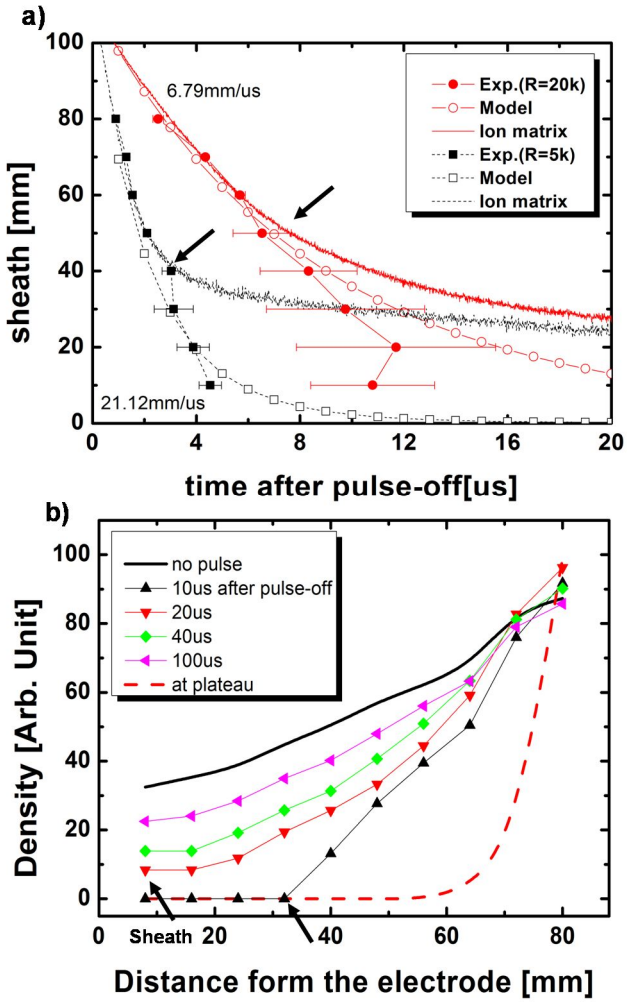

Figure 4.6 (a) Recovery of sheath and (b) variation of plasma profile at fast fall time.

The reason is expected to be inertia of ion motion. During the fall time, ions in front of the target remain their inertia that was gained in the sheath at pulse plateau time. As the target voltage decreases, electrons cover the ions and ambipolar diffusion by accompanying electrons and ions enhances sheath recovery. The target voltage is sustained because the diffusion current is small comparing with charges in the capacitors at the system.

Difference of motions at slow and fast fall is also shown in the fluid code as presented in Figure 4.7. Electron profile at both cases is constrained by ion profile during the operation. Electrons at fast fall time, however, recover along the fixed ion profile that was a sheath before pulse-off. Ions and electrons at slow fall time move together with time.

Fig. 4.8 shows a variation of sheath size with a target voltage. Two types of sheath are grouped by the fall time. At slow fall time, depletion region that was formed at the plateau time fully recovers while sheath is collapsed. At fast fall time, however, depletion region is remained during the fall time. Therefore, longer sheath exists at the fast fall time due to the depleted ion profile. With a combination of sheath characteristics and different ion profile in front of the target, sheath at fast fall time is proportional to $V^{3/4}$, as noted in the model, and that at slow fall time is varied approximately as $V^{1/2}$. In result, it is verified that recovering sheath is transformed from ion matrix sheath to Child-Langmuir sheath as pulse fall time increases.

Two extreme cases, however, have both minimum and maximum limit. At fast fall time, ions are fixed and ion profile is sustained during the process regardless of the variation of fall time. At slow fall time, also, ions fully

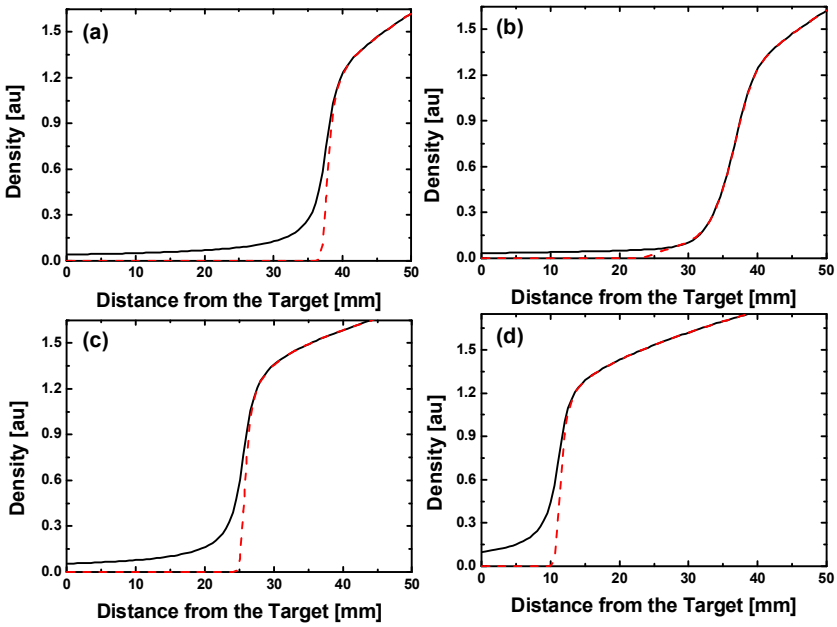

Figure 4.7 Density spatial distribution at (a) 0.1us and (b) 0.9us at fast fall and (c) 30us and (d) 100us at slow fall after pulse-off.

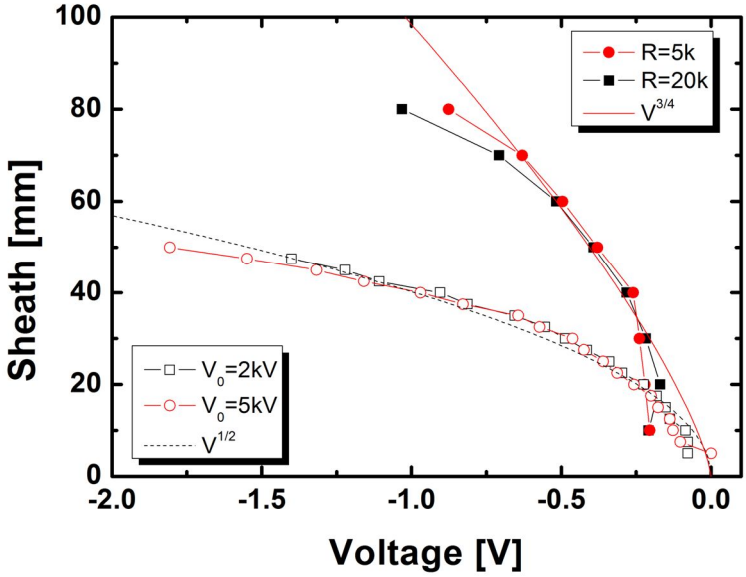

Figure 4.8. Curves of sheath size with target voltage.

respond to the electric field and ion profile is not changed when pulse fall time is over the residence time when ions are fully rearranged. All sheath recovery is expected to move between the two limits.

4.4 Summary

Sheath recovery is investigated at the pulse fall time on the pulsed bias operation. Two different motions are revealed at the two extreme cases, fast and slow fall time. Its basis to divide is a time scale of ion flight time.

Ion's motion responding to the target voltage determines sheath motion. In case that enough time is given for ions to respond with target voltage, which is a case of slow fall time, sheath size is same as that at stead state case, Child-Langmuir sheath. If short time is given to decrease the voltage, however, ion matrix sheath recovers through the profile. In result, Bohm current consistently flows at slow fall time but plasma current is negligible during fast fall time.

Like the case at pulse rise and plateau time, non-uniformity of plasma profile is also a control factor to determine sheath motion. Different distribution by ion motion, however, exists with fall time. At slow fall time, plasma has same profile when no pulse applies but the profile during the fast fall time follows the distribution that was formed at pulse plateau time.

Both case at fall time, sheath is collapsed earlier than expected but its reason is different. At slow fall time, plasma head at the transition region is injected to the target and neutralize it. Enhancement of ambipolar diffusion by ion inertia cause the drastic diminish of the sheath at fast fall time.

Chapter 5. Dynamics of Presheath Recovery

Target current which is injected from the plasma is composed of ion energy and flux. In previous chapter, sheath, which has a key part of an energy provider, recovery is analyzed with pulse fall time. This chapter describes recovery of presheath as a role to determine ion flux. As pulse fall time is varied under or over the scale of inverse of ion plasma frequency, recovery motion of presheath is measured and the dependency of presheath speed on pulse fall time is analyzed. Our interest is mainly focused on ion's recovery speed and presheath motion with pulse fall time.

5.1 Experimental Condition

5.1.1 Pulse Shape

Experiments are performed at the filament chamber, which was introduced in Chapter 3 and operating condition is not changed. Pulse fall time is varied by changing resistor that is connected to the 2nd switch. Pulse shapes at the experiments are given in Figure 5.1. Pulse voltage at plateau time is from 2.0kV to 2.4kV not to overcome sheath out of the quartz tube.

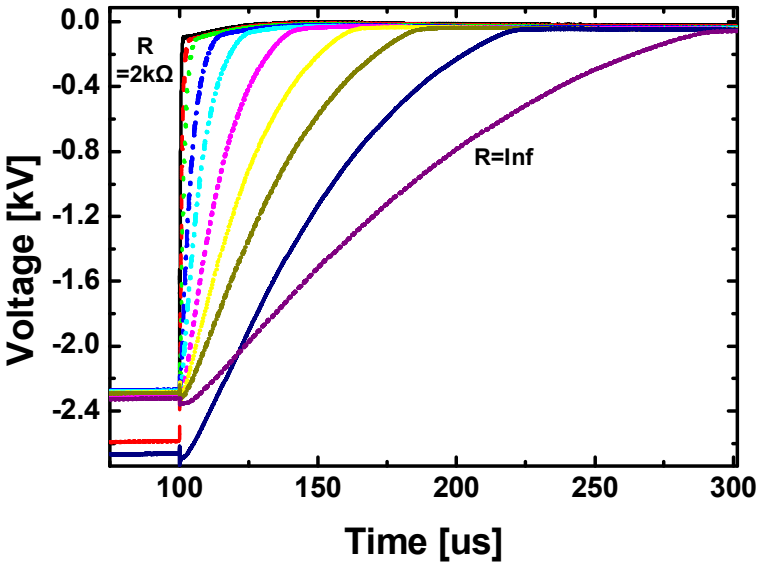

Figure 5.1 Voltage shape during pulse fall

Plateau time is sustained as 100us so that sheath and presehath are stabilized and Child-Langmuir sheath is formed when pulse-off starts. Pulse fall time and falling rate is displayed in Table 5.1. Pulse falling rate is varied from 2.78kV/us to 13.3V/us and fall time is from 0.679us to 158.64us as fall time, respectively. Inverse of ion plasma frequency is about 5us~10us, which is varied due to the non-uniformity of plasma density. In result, ion motion's effect on the presheath recovery is analyzed by varied pulse fall time.

Table 5.1 Pulse falling rate and fall time with resistance at 2nd switch

Resistance	fall time(t_f) [us]	falling rate [V/us]
R=2kΩ	0.679	2.78kV/us
R=5kΩ	1.80	1.16kV/us
R=10kΩ	3.69	0.533kV/us
R=26kΩ	9.65	0.203kV/us
R=52kΩ	17.07	0.116kV/us
R=120kΩ	30.68	66.5V/us
R=250kΩ	48.58	41.8V/us
R=500kΩ	68.54	30.2V/us
R=1MkΩ	96.75	24.9V/us
R=Inf	158.64	13.3V/us

5.1.2 Plasma Spatial Distribution

Spatial distributions of plasma density and diffusion speed are presented in Figure 5.2. As mentioned in the previous chapter, plasma has a typical profile as diffusive plasma. Plasma has a linearly increased profile. Plasma density is adjusted for adequate measurement of presheath but linearity is not changed. Diffusion speed is calculated from the plasma profile. Although density is varied at each data set, diffusion speed has a similar profile.

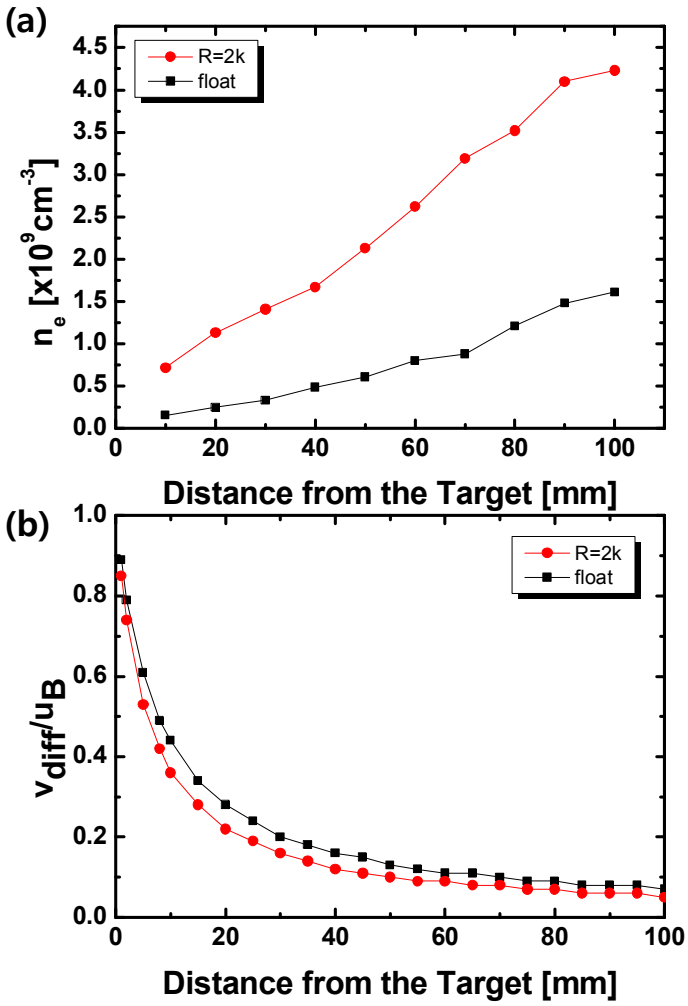

Figure 5.2 spatial distribution of (a) plamsa density and (b) diffusion speed

5.1.3 Definition of Plasma Profile

Plasma profile when pulse is applied to the target is given in Figure 5.3. The square dot indicates the profile just before pulse off starts and the stable plasma is formed by the plateau voltage. Gray line is the plasma profile when no pulse is applied. Since negative voltage is applied to the target just before pulse-off starts, sheath expands responding to the target voltage and presheath and transition region between the presheath and sheath are stably formed. [56] Bulk plasma out of the quartz tube is not changed in spite of pulse voltage, which says ions are consistently injected with a same speed from the bulk plasma.

For the simplicity of the analysis, three edges at the plateau time are defined as heads. Electron head is selected at the boundary between ion sheath and transition region where electron exists. Presheath head is positioned between transition and presheath region, and bulk head is located between presheath and bulk region. From now on, heads are traced with time and variation of position and speed with pulse fall time is analyzed.

5.2 Three types of Recovery Profile

According to the experimental results, three types of plasma recovery can be grouped with motion of each head, which is presented in Figure 5-4. These features are named as fast, intermediate, and slow fall time by pulse fall time.

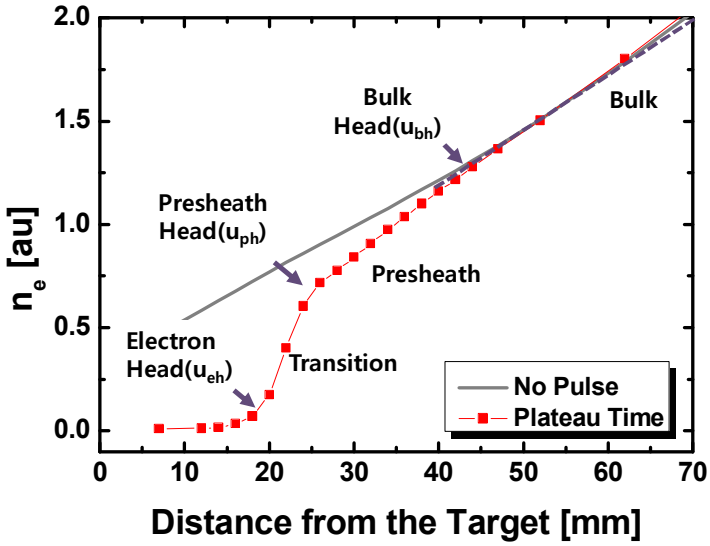

Figure 5.3. Plasma profile and the definition of electron, presheath, and bulk head and transition, presheath, bulk region.

Regime of fast fall time, as indicated in Figure 5-4 (a), occurs at the fall time of 0.679us and 1.80us. At the regime, motion of electron head is dominant and another head are slower than the electron head. In result, only transition region expands with time. As fall time increases, regime of intermediate fall time occurs after the regime of fast fall, which fall time is from 3.69us to 48.58us. At the intermediate regime, not only electron head but also presheath head take a dominant recovery motion as time goes but bulk head has a slower motion. Transition region sustains its length but presheath expands with time.

As fall time increases after the intermediate regime, which is ranged

from 68.54us to 158.64us, motion of presheath head is accompanied with that of the other heads. All head recovers equally and both transition and presheath region holds their length during the pulse fall time.

Motion of heads at each fall time is depicted in Figure 5.5. At fast fall time, only electron head recovers following target voltage. Presheath and bulk heads sustain their motion regardless of target voltage. As fall time increases and approaches to intermediate regime, presheath head accompanies recovering motion responding to the target voltage. At slow fall time, all heads decreases as time goes.

Ion matrix sheath are compared with head motion at fast fall time. The sheath is calculated from the measured target voltage and it is assumed that ion density covering the target follows the profile that was formed at pulse plateau time, which is the same assumption of sheath at the fast fall time in chapter 4. The graph shows that electron head is matched with ion matrix sheath. As mentioned in the previous chapter, at fast fall time when ion does not have enough time to respond, only electrons are recovering and sheath can be defined as the boundary where electrons exist. This data verify that electron motion determine sheath at fast fall time.

Child-Langmuir sheath is plotted in the figure and it is matched with presheath head at intermediate and slow fall time (Figure 5.5(b) and 5.5(c)). Presheath is preserved during the fall time and it is reasonable that Child-Langmuir sheath sustains similar length with the presheath head. At intermediate regime, ions in the sheath are also rearranged it is reasonable presheath head follows Child-Langmuir sheath although bulk head is not yet

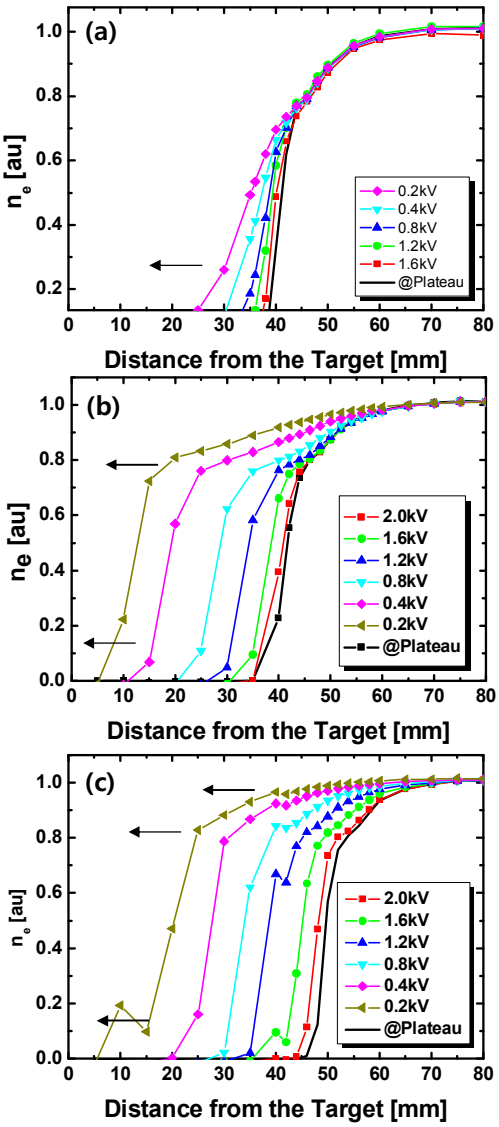

Figure 5.4. Sheath recovery at (a) fast (t_f=1.80us), (b) intermediate (t_f=30.68us), and (c) slow fall time (t_f=158.64us)

prepared. The fact that CL sheath and the experiment data is more matched as time passes confirms presheath head following Child-Langmuir law.

Based on the recovering motion of heads and matched sheath speed, average speed is plotted with recovering sheath speed, as depicted in Figure 5.6. u_{eh} is the speed at electron head, u_{ph} is that at presheath head, and u_{bh} is that at bulk head. At fast fall time, only electrons head follows the sheath recovery speed. Speed of electron head is proportional with the sheath recovery speed and it has supersonic speed, which says sheath recovery speed is faster than Bohm speed. Presheath head, however, has an upper limit of Bohm speed regardless of the sheath recovering speed. Electron head responds to the variation of electric field induced from target voltage but presheath head is not affected because it is located out of the sheath. Although speed at bulk speed is not displayed in the figure, it has a negative value during the pulse fall time, which indicates that bulk head expands instead of collapsing. Similar with the fast rising rate at pulse bias operation, fast sheath recovery over Bohm speed generates rarefaction/compression wave which goes forward the bulk plasma.[33, 45]

At intermediate fall time and sheath has a sub-sonic speed, electron and presheath head are controlled by the fall time. In result, electron and presheath recovers together with same speed. Speed of presheath head does not overcome that of electron head and presheath does not recover ahead of electron head. Bulk head, however, sustains an upper limit although the sheath recovering speed is varied because electric field does not affect bulk region.

Speed limit of bulk head has a value of 0.15 times Bohm speed and it is a

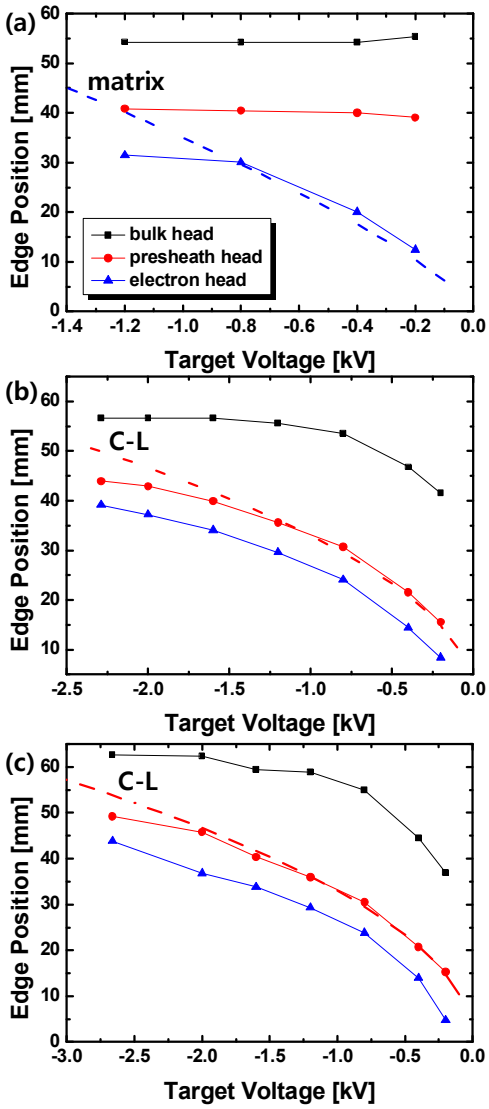

Figure 5.5 Recovering motion of electron, presheath, and bulk head at (a) fast, (b) intermediate, and (c) slow fall time.

diffusion speed at sheath. From the spatial distribution of diffusion at in Figure 5.2(b), sheath starts to recover at the position of 40mm when pulse-off starts. At the point, diffusion speed is about 0.15 times of diffusion speed, which is matched with the limit speed.

As fall time increases approaching to the slow fall time and the sheath recovery speed is lower than around 0.15 times of Bohm speed, all head recovers with a same speed and it starts at the point when recovery speed of electron head have a lower value of maximum speed at bulk head.

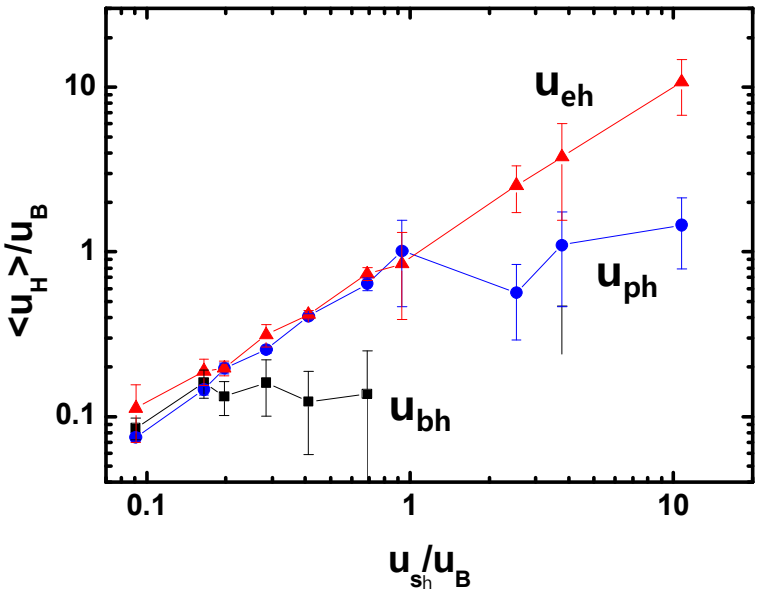

Figure 5.6. Average speed of electron, presheath, and bulk head with sheath recovering speed

5.3 Dependency of Presheath Recovery on Sheath Recovering Speed

From previous section, three groups are categorized with pulse fall time and it reveals the correlation of sheath recovering speed and presheath recovery motion. Variation of fall time and target voltage determined the speed of recovering sheath, which is a key factor to control the presheath recovery. Presheath motion can be categorized with the sheath recovering speed, ion inertia dominant regime, presheath expansion regime, and quasi-Child-Langmuir sheath regime, which are depicted in figure 5.7.

(1) Fast fall time: Ion inertia dominant regime ($u_{sh} = u_{eh} > u_{ph} > u_{bh}$)

At this regime, electron head has a speed over Bohm speed but speed at presheath head maintains Bohm speed. Due to short fall time, ion doesn't have enough time to respond to the variation of the target voltage during the time. When target voltage decreases, only electrons react on the voltage and recovery begins. In result, electron head recovers with time following ion matrix sheath. Sheath recovery speed is over Bohm speed. Presheath head is a position that ions pass with a Bohm speed by Child-Langmuir sheath. When pulse-off starts, electrons shield electric field induced from the target voltage and no additional force is applied to the presheath. Ions sustain their inertia, therefore, and presheath head preserve its Bohm speed regardless of pulse

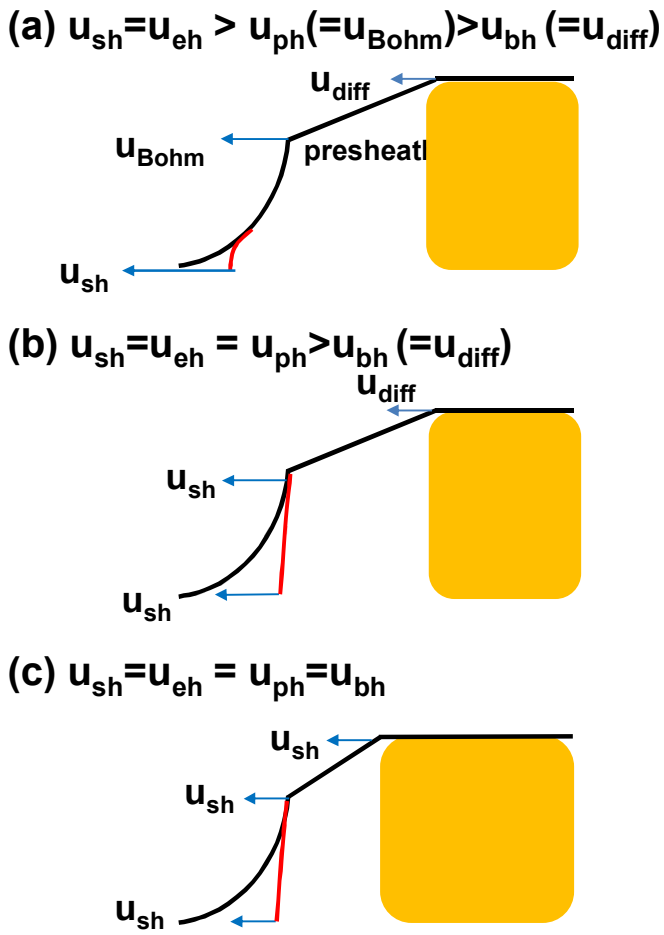

Figure 5.7 Motion of presheath recover with sheath recovering speed at (a) fast, (b) intermediate, and (c) slow fall time.

falling rate. bulk head also preserve its speed which was gained at the plateau time and its value is the same as the diffusion speed by the non-uniform plasma density profile at the bulk plasma. Due to the difference of speed at each head, transition and presheath region is wider as time passes.

(2) Intermediate fall time: Presheath expansion regime ($u_{eh} > u_{sh} = u_{ph} > u_{bh}$)

When sheath speed decreases and becomes below Bohm speed, presheath recovery is accompanied with the electron head. Recovery motion of presheath head is prohibited by target voltage. After ion passes through the presheath head, ions gain their energy by induced electric field. However, bulk plasma motion is prohibited and follows the variation of target voltage.

Although density variation occurs during the time, transition region is conserved due to the same speed of electron and presheath head. The preservation is expected that ions hold their Bohm speed regardless of pulse fall time and sheath boundary hold their position at presheath head, which is different from the definition of sheath at fast fall time.

Sheath speed is lower than Bohm speed but faster than the speed at bulk head. In result, ions at the bulk head do not follow another heads and only diffusion by non-uniformity of bulk plasma density governs the ion speed. Bulk head sustains its diffusion speed regardless of pulse fall time and ions at the bulk head have the same speed with bulk head. Due to the difference of presheath and bulk head, presheath expands with time.

(3) Slow fall time: Quasi-Child-Langmuir sheath regime ($u_{eh} > u_{ph} > u_{sh} = u_{bh}$)

As pulse fall time increases and responding sheath recovery speed is slower than the speed at the bulk head, regime of slow fall time begins. At this regime, all heads suppress their speed by the induced electric field and decreases with pulse fall time. All heads have a same speed and transition and presheath region recovers holding their size. Because recovery process is proceed sustaining plasma profile during the fall time, quasi-Child-Langmuir sheath is consistently formed without distortion. In result, ion at the presheath head moves with a Bohm speed in spite of lower head speed.

5.4 Model of Recovering Volume with Pulse Fall Time

Based on the analysis in above section, presheath recovery model is built up and the schematic diagram is presented in Figure 5.8. While pulse fall time processes, each head recovers with their own speed. It is assumed that electron head has zero plasma density and bulk head has a maximum density. Density at each head is not changed while operation so density of presheath head is located with the value of $1/\sqrt{2}$ times bulk plasma density. Density profile among each head has a linear profile so recovering volume has an

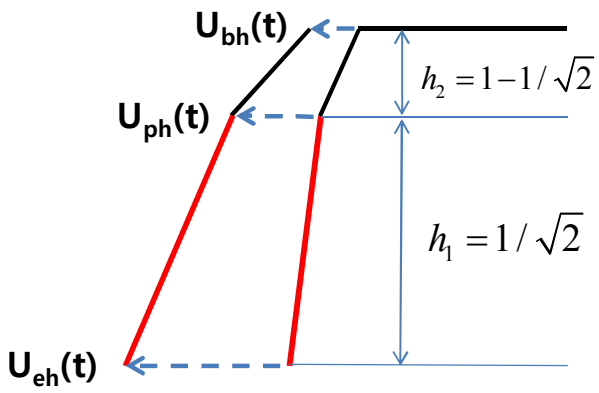

Figure 5.8 Presheath recovery model

Table 5.2 Recovery speed at fast, intermediate, and slow fall time and recovering particle number

fall time	condition	value
Fast	$u_{eh}=u_{sh}$ $u_{ph}=u_{Bohm}$ $u_{bh}=0.1u_{Bohm}$	$= \frac{n_0 A h_1}{2}\int_0^t s(t')dt' + \frac{n_0 A u_B t}{2}(h_1 + 1.1h_2)$
Interme diate	$u_{eh}=u_{sh}$ $u_{ph}=u_{sh}$ $u_{bh}=0.1u_{Bohm}$	$= \frac{n_0 A}{2}(2h_1 + h_2)\int_0^t s(t')dt' + \frac{n_0 A h_2}{2}0.1u_B t$
slow	$u_{eh}=u_{sh}$ $u_{ph}=u_{sh}$ $u_{bh}=u_{sh}$	$= n_0 A\int_0^t s(t')dt'$

accumulated trapezoidal shape. From the shape, recovering volume is calculated and can be presented as Eq. (5.1).

$$N(t) = \frac{n_0 A h_1}{2}\left(\int_0^t u_{eh}(t')dt' + \int_0^t u_{ph}(t')dt'\right) + \frac{n_0 A h_2}{2}\left(\int_0^t u_{ph}(t')dt' + \int_0^t u_{bh}(t')dt'\right) \qquad (5\text{-}1)$$

where $\boldsymbol{A}$ is a target area, $\boldsymbol{h_1}$ is a heigh of presheath edge, $\boldsymbol{h_2}$ is a distance from the maximum density and presheath head. $\boldsymbol{u_{eh}}$, $\boldsymbol{u_{ph}}$, and $\boldsymbol{u_{bh}}$ is a speed at electron, presheath, and bulk head, respectively.

Speed at each head is changed with a pulse fall time and explained in Table (5.1). At fast fall time, only electron head has a sheath speed and speed at another head has its own constant speed, as mentioned earlier. Electron and presheath head has a sheath speed at intermediate fall time and all heads are assumed to have a sheath recovery speed at slow fall time. From these assumptions, calculated recovering volumes with time are presented in the table. Sheath recovery speed is adapted from the measured value in the experiments.

Experimental results and calculated data from the model are compared in Figure (5.9). All cases at the experiment data are matched with the model within error bar. At each fall time the model has a higher recovery volume than the experiment result, which says faster recovery is expected. At early time, ions are still rearranged with target voltage variation so the non-linear

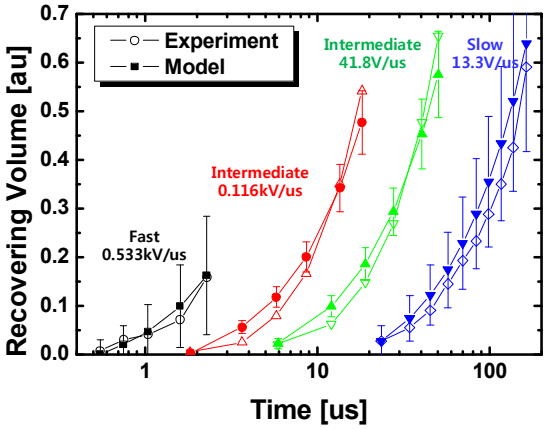

Figure 5.9 Comparison of experiment (open dot) and model data (filled dot) during pulse fall

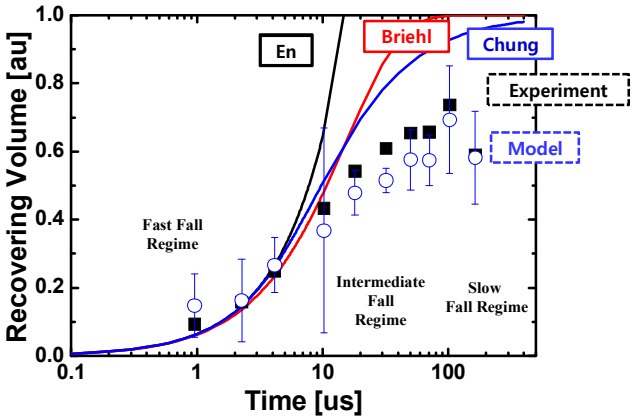

Figure 5.10 Comparison of recovering volume from the model, experiments data, and previous studies.

slope is expected but the model doesn't consider it.

Experimental result and the model are compared with the data from previous studies when the target voltage is 0.1 times of plateau voltage as depicted in Figure 5.9. Two regions can be categorized on the base of inverse of ion plasma frequency. Until 10usec after pulse-off starts, recovering volume follows the previous studies, which says that presheath recovers with a Bohm speed. Matched region is the regime of fast fall time, when presheath head had a Bohm speed. Since transition region between electron and presheath head doesn't take a major role due to the condition of fixed ion distribution at fast fall, presheath motion has a dominant role for plasma recovery and it is reasonable plasma recovers with Bohm speed.

As time pass over inverse of ion plasma frequency, however, presheath motion is at intermediate and slow falling rate regime. Induced electric field by the target voltage controls the recovery speed of presheath which is lower than Bohm speed. In result, recovering volume is lower than that at En and Briehl' model.

Figure 5.11 shows recovering volume with time at ion inertia dominant regime (fast fall time), presheath expansion regime (intermediate fall time), and quasi-Child-Langmuir sheath regime (slow fall time) as time passes over pulse fall. At ion inertia dominant regime, recovering volume follows En's model but after time passes over inverse of ion plasma frequency, it follows Chung's model. At early time, presheath recovers with Bohm speed sustaining speed that ions at the presheath were gained. As time passes and ions start responding, ions diffuse by drastic gradient of plasma density at the transition

region. Chung's model is based on the assumption that plasma expands by the density gradient, which is matched with the result. Chung's model, however, has no rarefaction wave due to the initial drift velocity of Bohm speed at all position but the experiment data shows that rare faction wave exits at the ion inertia dominant regime. In result, recovering volume at the experiment data has a lower value than Chung's model. At other regimes, target voltage controls the presheath motion and both no diffusion and ion inertia exist in the recovery. In result, recovering volume has a linear increase with the target voltage until the target voltage exists. When the voltage returns floating potential, recovering volume is saturated. Recovery time and ratio of recovering volume when recovering motion is saturated are presented at Table 5.2. According to the data, recovering time, which is defined as the time when the speed of recovering volume is saturated, is the fastest when the shortest fall time is given to the target but the ratio is the lowest due to the depletion by rarefaction wave generated by collapsing sheath.

5.5 Summary

In this chapter, presheath recovery with pulse fall time is investigated. Sheath recovery speed responding to the variation of target voltage and ion inertia at the presheath determine presheath recovery.

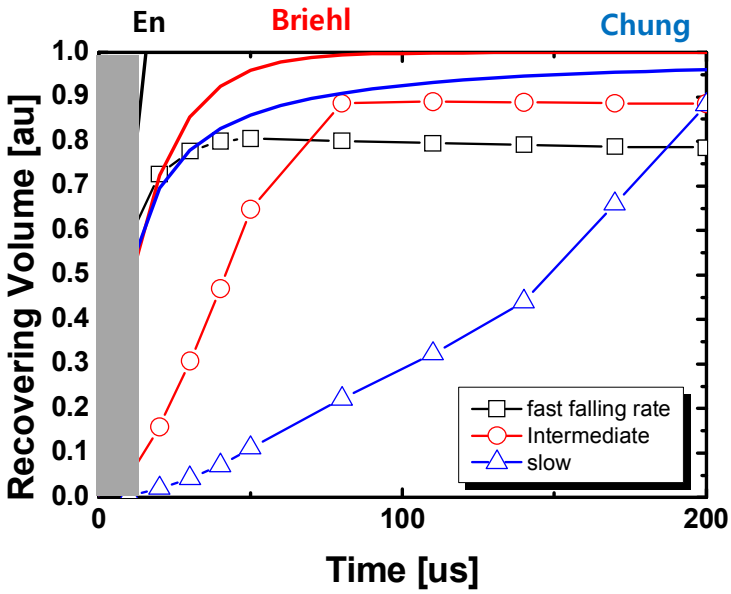

Figure 5.11 time-transient recovering volume as time passes after pulse-off. Gray zone is time within the inverse of ion plasma frequency.

Table 5.3 Recovering time at the recovering volume is 50% (time@50%), 86% (time@86%), and saturated (time@sat) and volume ratio when volume is saturated (volume@sat)

t_{fall}[us]	9.650	17.07	30.68	48.58	68.54	96.75	158.64
time@50%	11.67	17.12	27.63	41.07	58.85	79.13	149.6
time@86%	39.262	41.02	49.83	76.85	100.93	125.02	196.67
time@sat.	43.15	49.96	63.16	81.33	110	140	200
volume@sat.	0.876	0.883	0.890	0.890	0.893	0.905	0.882

Three regimes, ion inertia dominant (fast fall time), presheath expansion (intermediate fall time), and quasi-Child-Langmuir sheath regime (slow fall time), are categorized from the head speed and sheath recovering speed. Head speed under sheath speed sustains its speed that was formed at the plateau time and head speed over sheath speed is suppressed to the sheath speed by the induced electric field in the sheath. Therefore, when the sheath is collapsed with supersonic speed, presheath recovers maintain Bohm speed which was formed in the former sheath. As fall time increases and sheath recovering speed decreases under the subsonic speed, head speed over the sheath speed is adjusted to the sheath speed due to the induced electric field in the sheath which is satisfied with quasi-Child-Langmuir law.

Sheath recovering speed also determines the overall recovering motion of presheath after ion inertia removes. Sheath controls presheath recovery, when the sheath speed is lower than Bohm speed at presheath expansion and quasi-Chlid-Langmuir sheath regime and presheath speed is matched with the sheath speed during the recovery process. At ion inertia dominant regime, however, plasma recovering speed is distorted by the plasma density gradient at the presheath head after the time scale of inverse ion plasma frequency, which tells ion inertia at the presheath head breaks by the ion response to the plasma profile.

Chapter 6. Effect of Plateau Time Variation

Plasma recovery motion at pulse fall time starts from the plasma property at the plateau time. In previous chapters, it is assumed that stable plasma that Child-Langmuir sheath makes is prepared when pulse-off starts and presheath recovers with Bohm speed when no induced electric field control the plasma by the supersonic recovery of sheath. Pulse operation, however, is usually performed at high repetition rate in order to take advantage of characteristics of plasma motion at pulse rise times, which causes the distortion of initial plasma property at the fall time. In this chapter, sheath and plasma recovery are investigated with a variation of plasma property at the end of plateau time. By changing the plateau time, effect of plasma motion at pulse rise time on plasma recovery and parameters to control the recovery are revealed.

6.1 Experimental Set-up

Experiments are performed at the filament chamber with the same apparatus in the previous chapter. Only pulse voltage is changed for the purpose of this study.

6.1.1 Voltage shape

Related operating parameter and voltage waveforms are presented in Table 6.1 and Figure 6.1, respectively. Two types of experiments are carried

out with two extreme cases of fall time, fast fall time of 1.23us and slow fall time of 39.8us, following the case of sheath size analysis in the previous chapter. At each case, rise time and plateau voltage are fixed with 0.0676us and 1.1kV. Only plateau time is changed from 2us to 100us, which covers under/over the scale of inverse of ion plasma frequency. Target voltage and time after pulse-off is matched and is shown in Table (6.2).

Table 6.1 Operating parameter at slow and fast fall time

	Fast fall	**Slow fall**
Fall time[us]	1.23	39.8
Falling rate[V/us]	713	22.4
Resistance	500k	10k
Plateau voltage [kV]	-1.12	
Rising rate [kV/us]	19.9kV/us	
Rise time [us]	0.045	
Plateau time [us]	3,6,12,25,50,100	2,7,13,25,50,100

Table 6.2 Time after pulse-off starts at target voltage.

% of V_{plat}	**0.9**	**0.8**	**0.7**	**0.6**	**0.5**	**0.4**	**0.3**	**0.2**	**0.1**
Slow[us]	9.03	13.2	17.4	21.7	26.3	31.2	36.7	42.4	49.4
Fast[us]	-	-	0.498	-	0.753	0.743	0.953	1.24	1.72

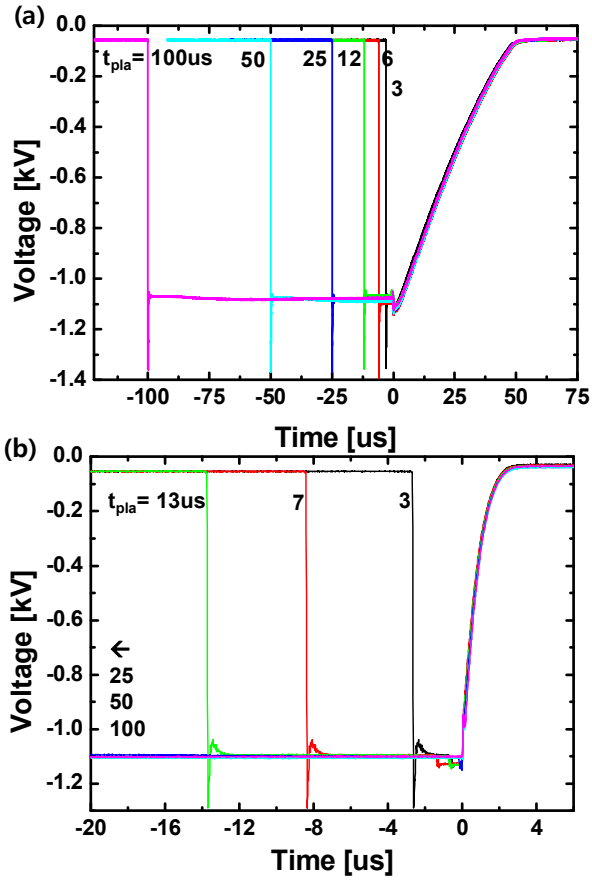

Figure 6.1 Voltage shape at (a) fast falling rate and (b) slow falling rate.

6.1.2 Plasma expansion at pulse rise time

Since the plateau time at the operation is the time range when plasma expansion at rise time and collapse at fall time can be overlapped, analysis of plasma expansion is required. Figure 6.2 shows the plasma profile at the pulse rise. When pulse-on starts, sheath expands responding to the target voltage and plasma in front of the target are evacuated. It also shown that presheath is created as rarefaction wave expands, which was already shown in previous studies.[26-29, 57]

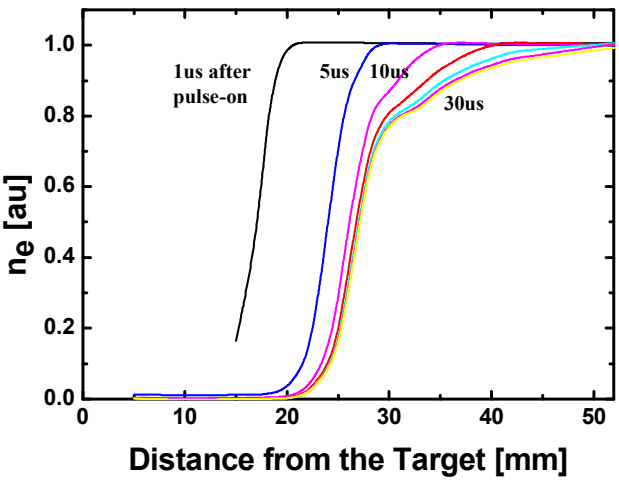

Figure 6.2 Plasma density profile at pulse rise from t=1us to 30us after pulse-on.

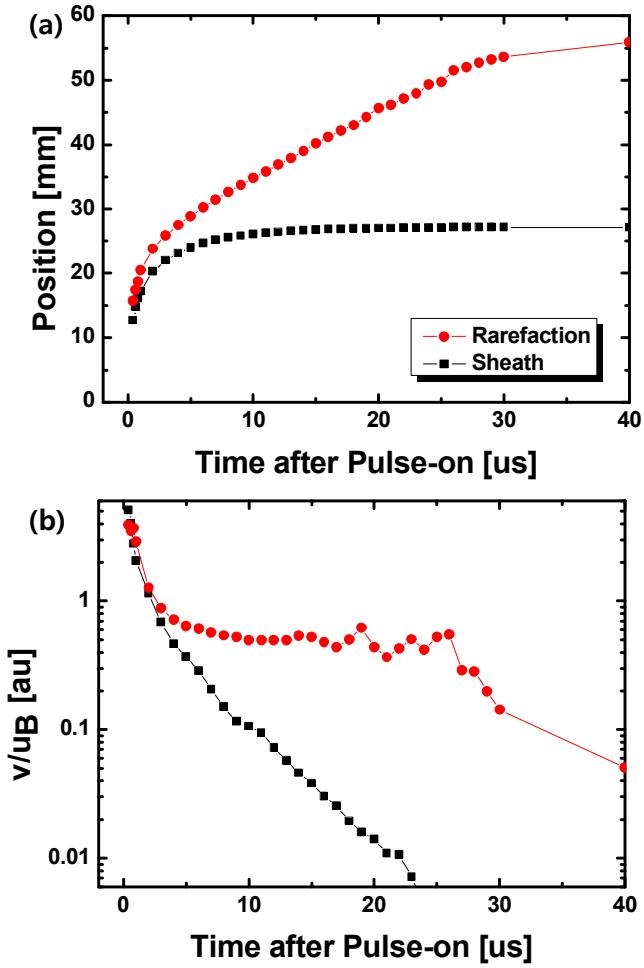

Figure 6.3 Variation of position and speed at sheath and rarefaction wave.

Position and moving speed of sheath and rarefaction wave are presented in Figure 6.3. In the early time of pulse rise, sheath and rarefaction wave expands with same supersonic speed. After speed passes under Bohm speed, sheath and rarefaction wave separated. Sheath speed decreases with time but rarefaction wave sustains its speed under a Bohm speed due to an ion drift from the bulk plasma.[12, 29] If it is defined the saturation as the speed is 0.05 times of Bohm speed, sheath is saturated at t=15us and rarefaction is at t=30us after pulse starts. From the result, plasma is saturated after about 30us and unstable plasma property becomes an initial condition of plasma recovery in the case that the plateau time is under 30us. This study investigates sheath and presheath motion with conditions that pulse fall starts when sheath is not saturated, sheath is saturated but rarefaction wave expands, and sheath and rarefaction wave stop, which is referred as unsaturated, intermediate, and saturated regime, respectively.

6.2 Plasma Recovery at Slow Pulse Fall Time

Plasma recovery with plateau time interval at slow fall time is presented in Figure 6.4. $t_{sat\text{-}sh}$ is a saturation time of sheath, and $t_{sat\text{-}rare}$ is a saturation time of rarefaction wave. Three types of plasma profile have different motions on the recovery process at each regime. When pulse fall starts before sheath and presheath are not stable, unsaturated regime, sheath expands although target voltage decreases. Rarefaction wave are also separated and expands regardless

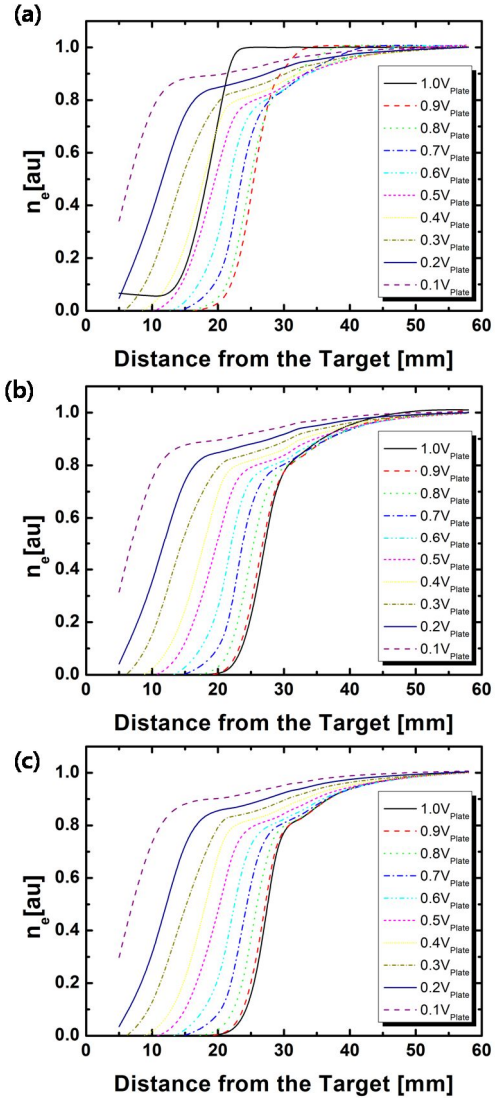

Figure 6.4 Variation of plasma profile at pulse fall time at (a) t_{plat}=3us < $t_{sat\text{-}sh}$,$t_{sat\text{-}rare}$, (b) $t_{sat\text{-}sh}$,<t_{plat}=25us<$t_{sat\text{-}rare}$, (c) $t_{sat\text{-}sh}$,$t_{sat\text{-}rare}$,< t_{plat}=100us

of the voltage. As time passes, sheath speed decreases and starts collapsing. After rarefaction wave stops and presheath is formed, presheath also recovers sustaining its profile.

At the intermediate regime, sheath is collapsed responding to the decreased target voltage but rarefaction wave sustaining its motion to the bulk plasma. Recovery at the presheath region is the same motion at the case of unsaturated regime and presheath also recovers sustaining its profile after presheath is formed,

At the saturated regime, stable sheath and presheath recovery are performed during the fall time. Since the plasma starts responding to the target voltage with an initial plasma property with a steady-state condition, plasma recovers with no distortion.

Figure 6.5 shows the comparison of plasma spatial distribution at the same target voltage. In the early time of pulse fall, sheath position and plasma profile are different in spite of the same target voltage. Ions dose not respond to the target voltage at unsaturated regime, short sheath exists compared to the other cases. As the time passes and voltage decreases, the profile is saturated to the specific profile by expansion of unsaturated sheath and collapsing sheath. Time interval of saturation of sheath and presheath exists but its profile converges in the end.

From the plasma spatial distribution, electron, presheath, and bulk head are selected and the motions are traced with time, which is depicted in Figure 6.6. Electron and bulk head are the same positions which were defined in Chapter 5. Presheath does not exist in the condition of short plateau time, so

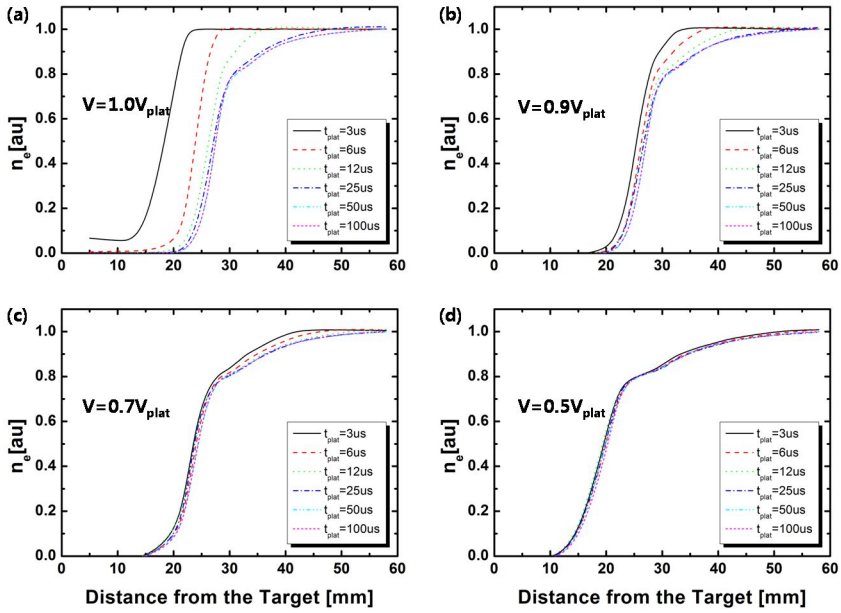

Figure 6.5. Plasma profile at target voltage of (a) $1.0V_{plat}$ (b) $0.9V_{plat}$ (c) $0.7V_{plat}$, and (d) $0.5V_{plat}$, where V_{plat} is a saturated voltage at the plateau time.

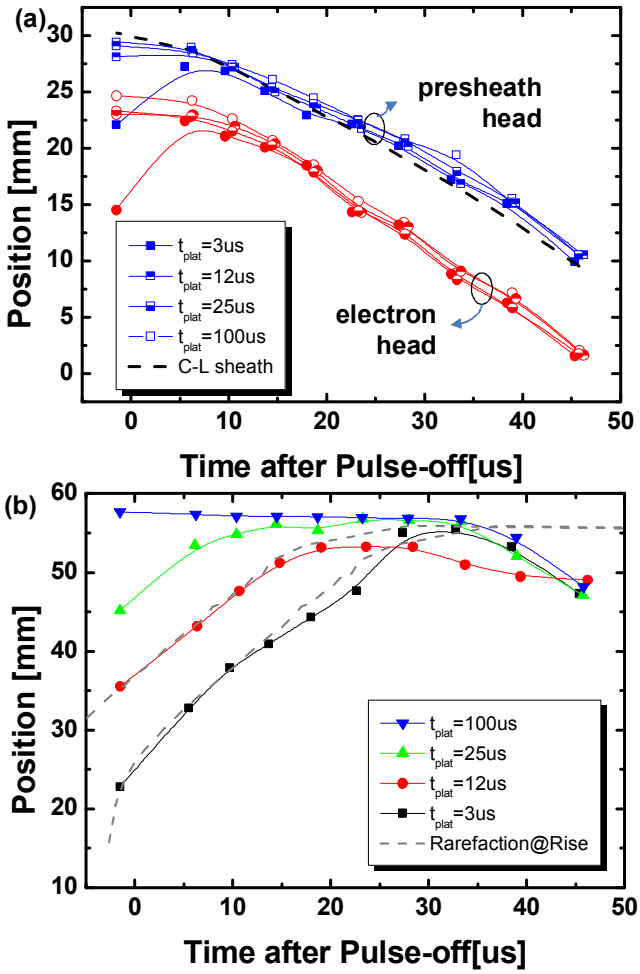

Figure 6.6. Recovering motion of (a) electron, presheath, and (b) bulk head with time.

the presheath head is defined as the position where the density is same as that at presheath point when plateau time is 100us.

At saturated regime, which is the case at the plateau time of 100us, the heads are collapsed with time. The plasma at the transition region recovers responding to the target voltage. Although recovery speed is faster than diffusion speed from the bulk, quasi-Child-Langmuir sheath is consistently formed during the fall time due to the ions that have enough time to be rearranged.

As plateau time decreases and when pulse-off start at the unsaturated regime, initial head position moves backward to the target and expands although target voltage decreases. The expansion continues until presheath head is matched with quasi-Child-Langmuir sheath then moves back. Since ions in the sheath are grouped and its density is higher due to the delayed ion motion, induced electric field by target voltage continuously forces the ions to be rearranged until the ion profile in the sheath is matched with at in Child-Langmuir sheath.

Comparing to the matched time at presheath and electron head, the saturated time of bulk head is longer but bulk head also perform the same expansion at unsaturated and intermediate regime. Its position is matched with the position of rarefaction wave that was generated at pulse rise time (gray line), which says that induced electric field does not influence the expansion of rarefaction wave.

6.3 Plasma Recovery at Fast Fall Time

Time-transient spatial distribution of plasma recovery at fast fall time is depicted in Figure 6.7. When pulse-off start at unsaturated regime, rarefaction wave and sheath is not separated and presheath is not yet developed, which is the same initial condition at the profile at slow fall time. As time passes, however, sheath does not expand anymore and the front of the transition region (electron head) is collapsed instantly responding to the target voltage. Rarefaction wave still expands regardless of the target voltage. As the regime pass from unsaturated regime to saturated regime, stable presheath becomes an initial plasma profile and only electron heads are collapsed.

Figure 6.8 shows the plasma spatial distribution with same target voltages. Contrary to the motion at slow fall time, presheath head does not expand at unsaturated regime. Instead, the head moves back as soon as the pulse-off starts. Presheath head also does not converge as time passes and deviation between electron heads decreases as time passes.

Electron, presheath, bulk head are also traced during the fall time as presented in Figure 6.9. Electron heads approach to the target as time pass and converge with supersonic speed. In previous chapter, it was noted that sheath is determined as the electron head and follow the ion matrix sheath. In result, electron head are collapsed instantly responding to the target voltage variation with a supersonic speed due to the fast falling rate. Collapsing speed is different, 3.5uB at t_{plat}=2us(unsaturated regime) and increased up to 4.0uB at t_{plat}=100us(saturated regime). It can be explained the ion profile in the sheath

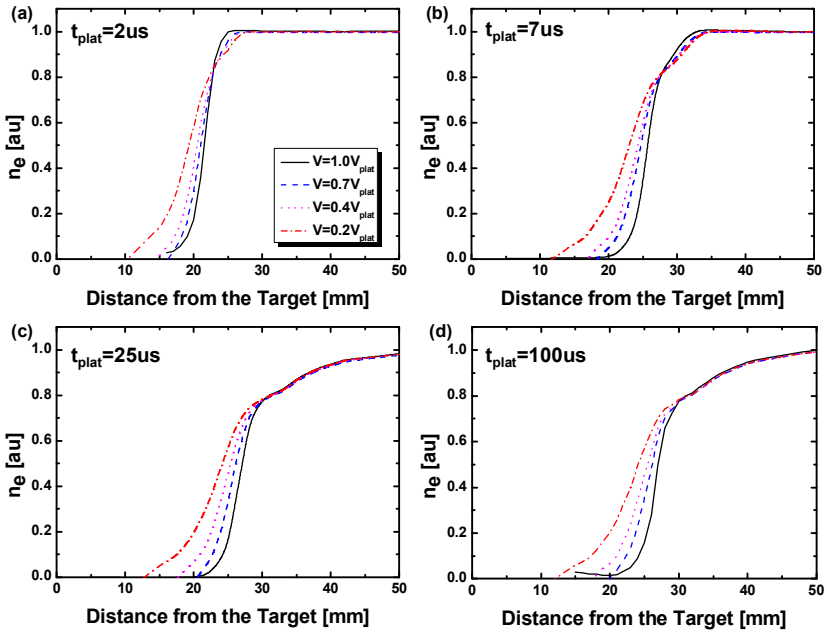

Figure 6.7 Variation of plasma profile at fast pulse fall

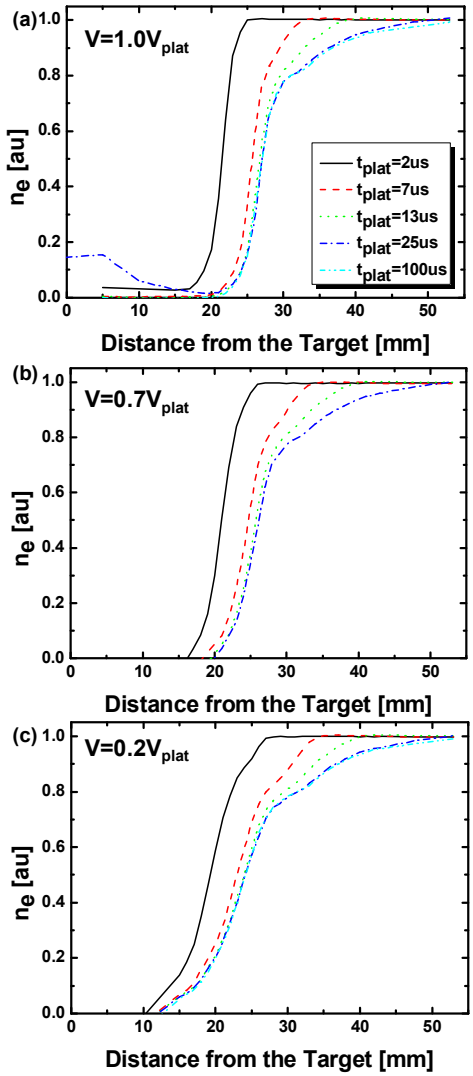

Figure 6.8 plasma spatial distribution at the target voltage of (a) 1.0V_{plat}, (b) 0.7V_{plat}, and (c) 0.2V_{plat}.

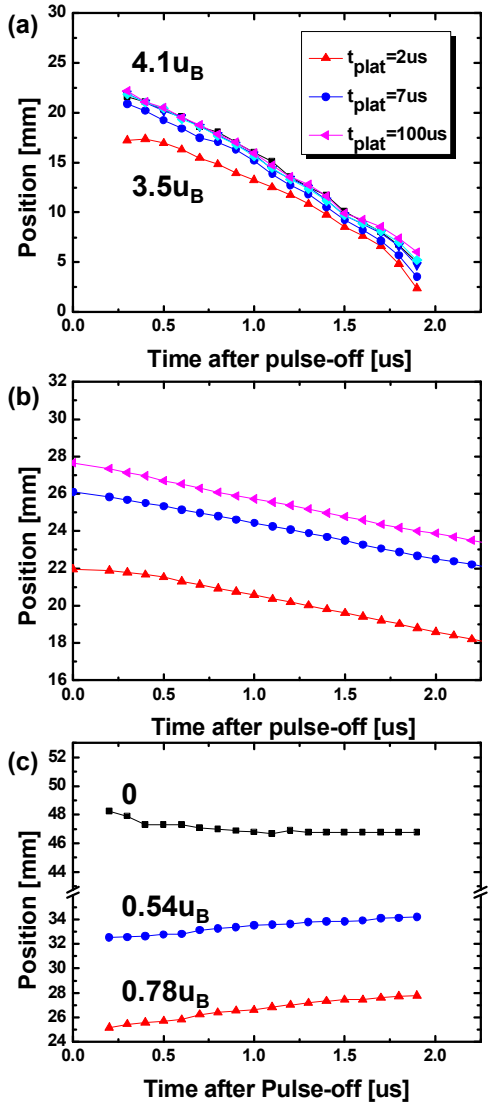

Figure 6.9 time transient motion of (a) electron head, (b) presheath head, and (c) bulk head during the pulse fall time.

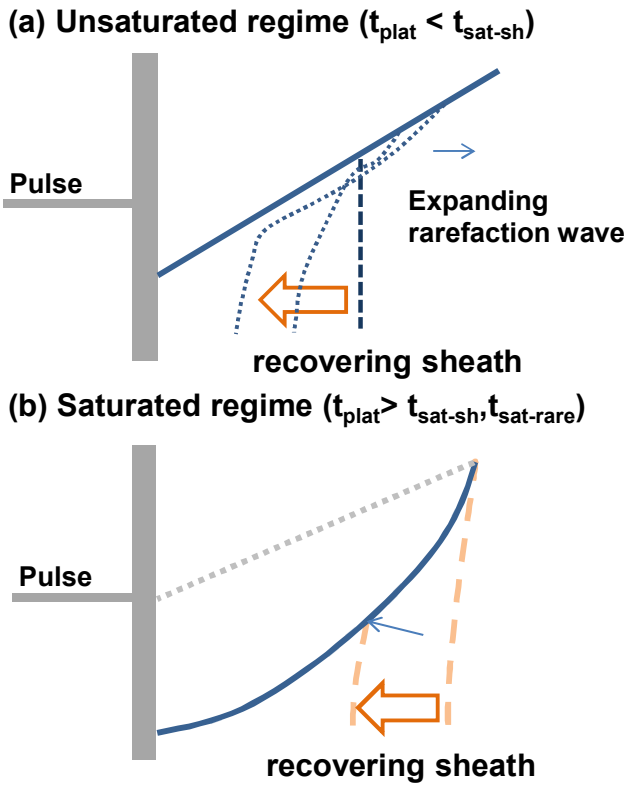

Figure 6.10 motion of collapsing electron head at (a) unsaturated regime and (b) saturated regime.

during the operation, as presented in Figure 6.10. At unsaturated regime, ion profile in the sheath is not rearranged until pulse-off starts due to the expanding sheath. Ions are not evacuated and high density is sustained comparing to the ion profile at saturated regime. When pulse-off starts, therefore, electron head's position is close to the target. Its collapsing speed is determined from the ion density accumulated between the target and electron head and smaller than that at saturated regime. As time passes, ions in the sheath starts being rearranged and the sheaths converge to that at saturated regime.

Rarefaction wave expands regardless of sheath collapse and speed of bulk heads is around $0.78u_B$, $0.54u_B$ and 0 at t_{plat}=2us, 7us, and 100us, respectively. Their value is matched with expanding speed of rarefaction wave speed when pulse-off starts and it shows target voltage does not control rarefaction wave. At saturated regime(t_{plat}=100us), it is expected that recovering speed by diffused plasma from the bulk exists since rarefaction wave stops, although it is calculated around zero due to the short pulse fall time.

Presheath head also progresses a recovering motion without additional expansion. Since the induced electric field is shielded at electron head and no external forces control the motion of presheath heads, its inertia is sustained. Deviation between the heads at unsaturated and saturated regime is maintained during the operation.

Recovering speed of presheath head with time is depicted in Figure 6.11.

At saturated regime (t_{plat}=100us), presheath head move maintaining its own speed that is similar with Bohm speed, which is matched with the previous result. At unsaturated region, however, and as plateau time decreases, initial speed decreases and its value is similar with the diffusion speed from the bulk plasma when no pulse is applied. When plateau time is short and the rarefaction wave is not revealed, ions are absorbed in the sheath with a drift speed that is diffused from the bulk plasma. When pulse-off starts and induced electric field is removed, presheath head recovers sustaining its diffusion

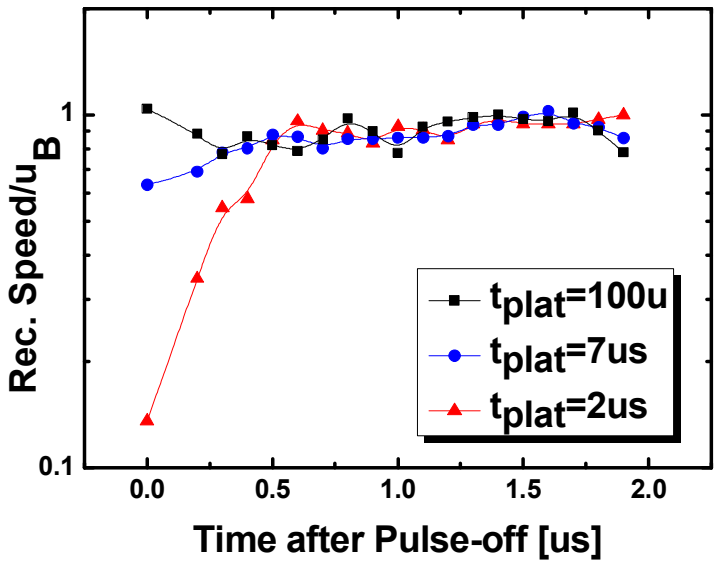

Figure 6.11 Recovering speed of presheath head at the plateau time of 2us, 7us, and 100us.

speed that is under Bohm speed. The speed increases as time passes and saturated around Bohm speed. Saturation time is about 0.5us, which is under the saturation time scale of both sheath and rarefaction wave and the inverse of ion plasma frequency. As rarefaction expands to the opposite direction of sheath recovery during the fall time, ions at the presheath head are accelerated by drastic gradient of plasma density around the presheath head like the motion of plasma expansion into a vacuum. [38, 39, 58] Rarefaction wave performs a stable expansion during the fall time and presheath head speed is saturated.

6.4 Summary

Plasma recovery process at pulse fall time is investigated with the variation of initial plasma property. By changing the plateau time of the pulse, effect of initial property which is formed at pulse rise and plateau time on plasma recovery is studied.

At slow fall time, induced electric field governs sheath and presheath motion. Sheath follows quasi-Child-Langmuir law. Unsaturated sheath by the lack of plateau time expands until sheath is matched with Child-Langmuir sheath then collapsed responding to the target voltage.

At fast fall time, ion profile in front of the target governs the plasma recovery. As plateau time decreases, ions are remained in the sheath and high density profiled is formed. In result, recovering speed of sheath is

proportional to the plateau time. Motion of presheath head follows initial motion of ions when pulse-off starts. As the plateau time decreases and plasma is unsaturated, presheath does not have an initial speed of Bohm speed. Instead, ambipolar diffusion by the non-uniformity of plasma distribution becomes an initial recovery speed at presheath. As time passes and rarefaction wave that was generated at the pulse rise time expands, speed increases up to Bohm speed.

Chapter 7. Prediction of Ion Energy Distribution

Sheath and presheath motions which were described in previous chapters are revealed as a flux and energy of ions that is injected to the target. In this chapter, ion flux and energy that are injected to the target are investigated. Variation of ion energy distribution and current are analyzed using the fluid code and dominant factor to control energy are described.

7.1 Governing parameter to control ion energy distribution function at pulse Fall Time

Energy distribution of ions (IED) which are injected to the target is determined from the parameter as being shown below

$$IED = f(u_{init}, E, n_{boundary}) \tag{7-1}$$

where u_{init} is an initial speed at plasma-sheath boundary, $n_{boundary}$ is a density at the boundary, and E is an energy gained during the flight until ions meets target.

Ions are ejected from the bulk plasma to the sheath boundary by diffusion. At the boundary, particle density is also determined by the sheath size and bulk plasma density. In steady-state uniform plasma, initial speed of ions are Bohm speed due to presheath and density is $1/\sqrt{2}n_p$, where n_p is a density at the bulk plasma. Ion gains energy when ions pass through the

sheath. Induced electric field by target voltage supplies energy to the ion.

During the pulse fall time, sheath motion is added to the conventional energy gaining process, which can be a dominant factor to change the ion energy distribution. Experiments are carried out using fluid code that was introduced in table 5.1. Voltage waveform is a modified shape from the experiment data with a plateau voltage of 2kV for the improved comparison. Rise and fall is linearly fitted shape which rate is the same as that in experiments data at chapter 5. Fall time operations of 0.679us, 9.65us, 48.58us, and 96.75us are selected for the analysis. Plasma density spatial distribution and other plasma property are applied from the data in the experiment. Data in ion energy distribution are particle number with ion energy and is normalized in order to compare the count of energetic ions among operating conditions.

7.2 Time-transient flux of injected ions with fall time

With a time-varied condition, ions gain different energy and flux with time. In this section, time-transient energy and particle number is analyzed.

7.2.1 Variation with pulse fall duration

Figure 7.1 shows a time-transient energy of ions that is injected to the target with pulse fall time. Plateau time is fixed as 100us. Since slow fall time is an electric-field dominant regime, induced electric field control the sheath

and ion motion. Since sheath speed is much slower than Bohm speed, which of ions injected from the bulk plasma to the sheath-plasma boundary, ions gain full energy during the flight in the sheath. Ion energy is proportional to the target voltage and decreases following the voltage as time passes. As fall time duration decreases, energetic ions are injected in the early time of the recovery. Although maximum energy is not changed and the energy decreases like that at slow fall duration, energetic ions are gained by electric field rapidly decreases due to the fast shrinkage of target voltage. After target voltage becomes zero, energetic ions under 750eV are still injected to the target.

Amount of injected ions follow a similar shape with fall time duration, presented in Figure 7.2. As time passes at slow fall duration, ions at sheath-plasma boundary decrease due to the non-uniformity of plasma density and it is expected that injected ions decrease. By flux conservation, however, ions' energy decreases faster and the ions increase with time. At fast fall time, density decreases during the target voltage exists and increases. When pulse-off starts, remained energetic ions in the sheath are absorbed to the target and depletion region is created. Sine electric field does not exist after initial absorption, bulk plasma diffuses to the depletion region and density increases with time.

7.3 Prediction of ion energy distribution

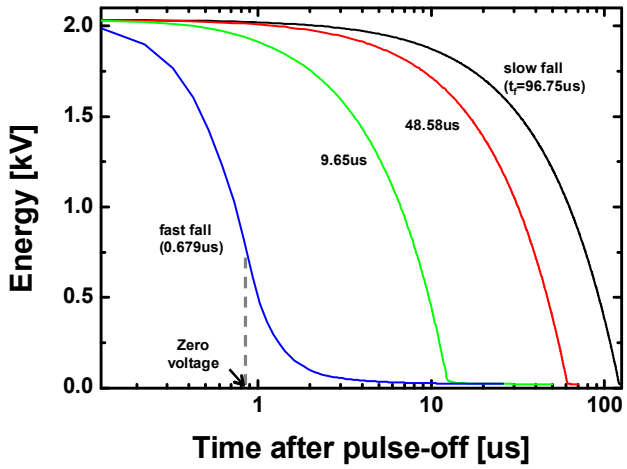

Figure 7.1 Time-transient energy distribution of injected ions at the target after pulse-off

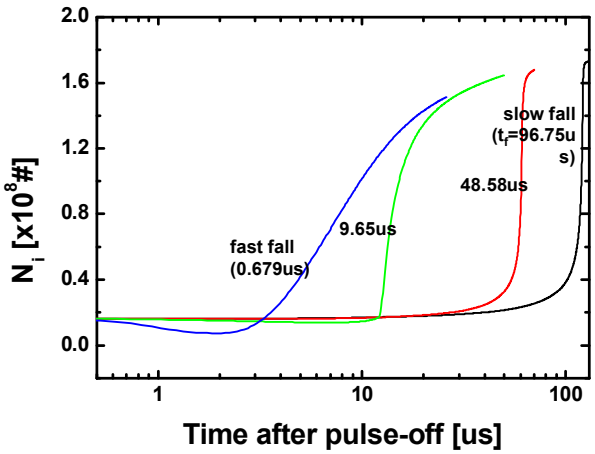

Figure 7.2 Time-transient ions injected at the target with pulse fall duration

Governing factor to determine ion energy is a speed of sheath during the recovery. Different from the case of stead-state sheath, ions partially gain energy with the deviation of sheath and ion speed. Process to gain energy in the sheath is presented in Figure 7.3 and governing equation is as below

$$W_{ion}(x_{target}) = W_{ion}(x_{boundary}) + q\int_{x_{boundary}}^{x_{sheath}} E(x)\,dx \qquad (7\text{-}2)$$

where $\boldsymbol{x_{target}}$, $\boldsymbol{x_{boundary}}$ and $\boldsymbol{x_{sheath}}$ are the position where that target and sheath-plasma boundary and sheath are located. *E(x)* is an electric field at the position of ions. Ion with an energy of $\boldsymbol{W_{ion}(x_{boundary})}$ is accelerated by the electric field that is induced at ion's position. Because of the finite speed of sheath, ion does not flight in the induced electric field fully and does not gain maximum energy. Also, since electric field is a function of decreased potential drop and collapsed sheath during the pulse fall, ion energy is not always proportional with target voltage. In next section, ion energy distribution is investigated in the two extreme cases, slow and fast fall.

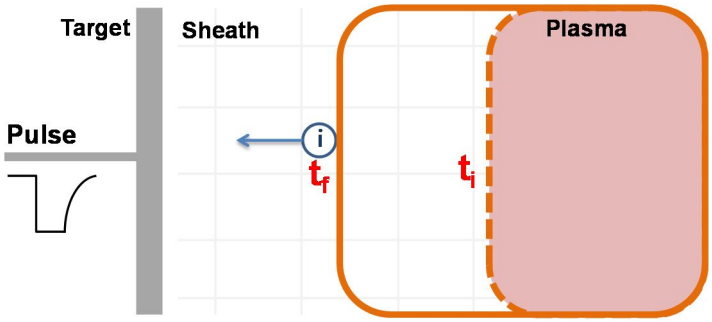

Figure 7.3 process to gain ion energy during the flight of sheath

7.3.1 Slow fall time ($u_{sh} << u_{ion}$)

At slow fall time, two types of ions exists, injected ions and pre-accelerated ions in the sheath

- **Injected ions in the sheath**

With a condition that sheath speed is much slower than ion one, ions pass the sheath-plasma boundary and gain energy until they reach the target. It can be assumed that voltage is not changed during the flight across the sheath and ions gain full energy with a potential when ion enters into the sheath. Ion energy is obtained from the energy conservation law.

$$W_{ion}(t_{target}) = W_{ion}(t_{boundary}) + eV(t_{boundary}) \tag{7-3}$$

where $t_{target} = t_{boundary}$ from the assumption.

Density at the region at the sheath-plasma boundary is expressed from the slow fall time case in previous chapter.

$$n(x_{boundary}) = n_{grad}x_{boundary} + n_0 = n_{grad}\alpha V(x_{boundary})^{1/2} + n_0 \tag{7-4}$$

where linearly increased density profile is expressed as $n(x) = n_{grad}x + n_0$ and α is a coefficient of the relation of sheath and target voltage at slow fall time. Inserting Eq. (7.3) and eq. (7.4) into flux conservation law, IED can be expressed as

$$n(W) = u_B \sqrt{\frac{M}{2}} \left\{ \frac{n_{grad}\alpha}{\sqrt{e}} \sqrt{1 - \frac{W_B}{W}} + \frac{n_0}{\sqrt{W}} \right\} \tag{7-5}$$

where WB=1/2MuB2 is an initial energy at the sheath-plasma boundary.

- **Pre-accelerated ions in the sheath**

At slow fall time, pre-accelerated ions exist in the sheath when pulse-off starts. They do not meet sheath until they are injected to the target thus they are not included in eq. (7.5). Since they are accelerated before pulse-off starts and their flight motion is much faster than variation time of target voltage, they obtain full energy induced from the plateau voltage. Density profile follows the profile that was formed at plateau time. They have mono energy and density can be expressed as below.

$$n_{depletion}(W = V_0) = \frac{1}{s}\int_0^s n(x)dx = \frac{4}{3}\frac{\varepsilon_0}{e}\frac{V_0}{s^2} \tag{7-6}$$

where V_o and s are target voltage and sheath size at plateau time, respectively.

7.3.2 Fast fall time (u_{sh} >> u_{ion})

At fast fall time, fast recovering speed over ion speed exists during the operation. Almost ions in the sheath meets collapsing sheath and do not

accomplish full energy. If it is assumed that recovery speed is infinite, all ions do not gain energy ($\boldsymbol{x_{sheath} = x_{boundary}}$) and the equation is modified as below

$$W_{ion}(t_{target}) = W_{ion}(t_{boundary}) \tag{7-7}$$

All ions maintain its initial energy during the flight.

Ions out of the sheath at plateau time do not gain energy and only diffusion speed is an initial condition. Ions in the former sheath, however, gain energy until pulse-off starts and it takes a role for ion inertia. Therefore ion energy at $\boldsymbol{x=x_0}$ is a sum of Bohm energy and gained ion energy.

$$W_{ion}(t_{target}) = W_B + \Phi(x_0) \tag{7-8}$$

Potential and density profile follow them in the Child-Langmuir sheath.[16]

$$n(x) = \frac{4}{9}\frac{\varepsilon_0}{e}\frac{V_0}{s^2}\left(1-\frac{x}{s}\right)^{-2/3} \tag{7-9}$$

$$\Phi(x) = -V_0\left(1-\frac{x}{s}\right)^{4/3} \tag{7-10}$$

Combining eq. (7.7), (7.8), (7.9), and energy conservation law, ion energy distribution is obtained.

$$n(W) = \frac{4}{9}\frac{\varepsilon_0}{e}\frac{V_0}{s^2}\left(\frac{W-W_B}{eV_0}\right)^{-2/3} \tag{7-11}$$

Ion energy distributions based on the eq. (7.5), (7.6) and (7.11) are shown in Figure 7.4. Particle number is obtained by the assumption that volume is defined as target area multiplied by the grid size in the fluid and

number of pre-accelerated ions is summarized in the sheath at the plateau time. Maximum energy of ions at all cases is same because ions that were gained during the plateau time are remained in front of the target although pulse-off starts. At slow fall time, more ions are energetic because ions at the early time also gain maximum energy. Pre-accelerated ions also have maximum energy and its particle number is much larger than that with same energy it includes all particles in the former sheath. Distribution at slow fall time is uniform particle density comparing with that at fast fall time. At fast fall time, energetic ions consist of remained ions that were accelerated during the plateau time and its density is determined by density profile in the sheath. Since the slope of profile in the sheath is more drastic than that around the bulk, ion energy distribution at fast fall time is more non-uniform. Injection of ions after voltage is floated also enhance the increase of low energy electron (E_{ion} <30eV) where E_{ion} is an ion energy.

7.4 Ion energy distribution with pulse fall time

In this section, ion energy distribution is analyzed and other factors to be considered are discussed.

7.4.1 Ion energy distribution

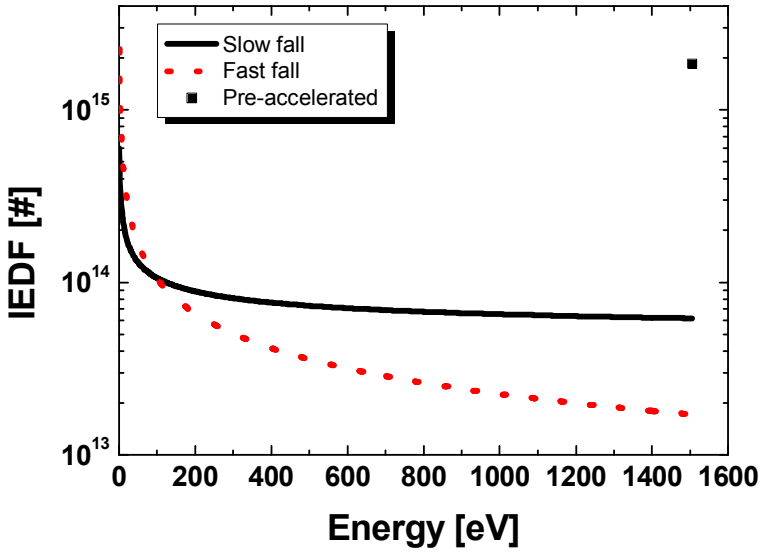

Figure 7.4 Comparison of ion energy distribution at slow fall(solid line) and fast fall(dashed line) of pre-accelerated ions(square dot)

Based on the previous results, ion energy distribution after pulse-off start is calculated as depicted in Figure 7.5. At slow fall time, electric field by target voltage controls the ion energy. All ions gain its full energy during the flight and only decreased target voltage determine the energy as time passes. As fall time becomes short, induced electric field is diminished and quantity of energetic ions over about 100eV decreases. Decreasing at highly energetic ions (E_{ion} > 1.5keV) occurs in the early time of pulse-off then medium energetic ions (100eV < E_{ion} < 1.5keV) follows. Reciprocal proportion of energy and ion counts at slow fall time is reversed as fall time becomes short.

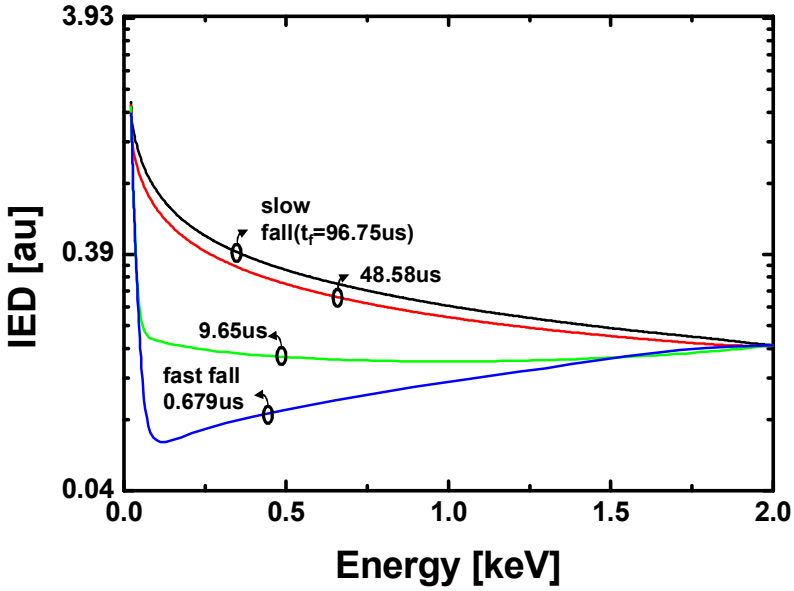

Figure 7.5 Ion energy distribution with pulse fall time period

Gained ion energy with initial position is also varied with sheath recovering speed. Gained energy at the presheath head ($E_{min@sh}$) and the bulk head ($E_{min@pre}$) is displayed at the Figure 7.6. With a supersonic sheath speed, ions at the presheath head do not gain its energy. As the sheath speed decreases under the subsonic, the ions which has Bohm speed enters the recovering sheath and gain full energy. Because ions at the bulk head has its diffusion speed, which is around 0.15 times of Bohm speed, they gain full energy when the sheath speed is under the diffusion speed.

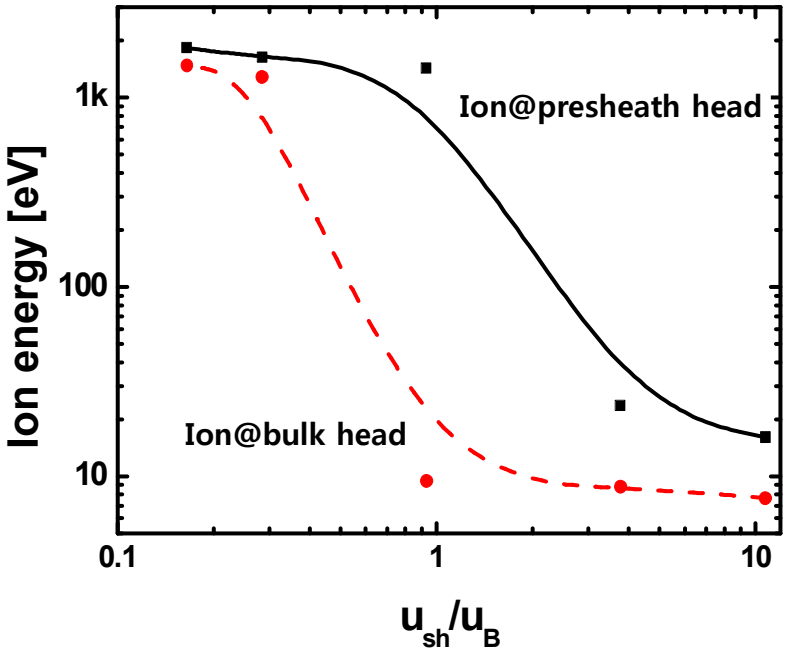

Figure 7.6. Gained ion energy at presheath and bulk head with sheath recovering speed.

Figure 7.7 shows an ion trajectory that is located in the former sheath. Ion motion is similar at the early time and its speed is matched until it is injected to the target. As time passes, ion at slow fall time is accelerated faster than that at fast fall time due to the sustained electric field by the target voltage. Ion at slow fall time flows into the target later with lower energy (slope of the trajectory). It explains the depletion of medium energetic ions as fall time decreases.

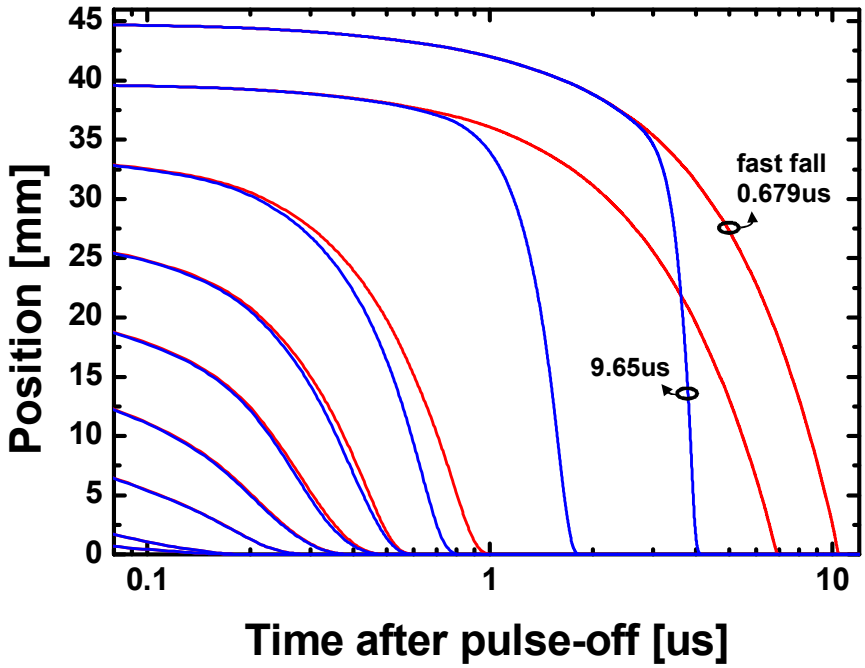

Figure 7.7. Ion trajectory in the former sheath at fast fall time

7.4.2 Acceleration by grad-u and grad-n

Back to the figure 7.4 and 7.5, the simulation and analytic solution at slow fall time have similar shape with ion energy with some slope difference. Low energy ions exists more expected because target voltage decreases as ions fly contrary to the assumption of fixed target voltage. At fast fall time, however, opposite density distribution is shown. More energetic ions are

injected and its quantity decreases as energy decreases and it shows that ions gain an extra energy besides the ion inertia.

Additional energy is explained from flux and momentum conservation equation in Eq. (3.2). Since electric field is removed after pulse-off starts, the momentum conservation equation can be modified as below.

$$\frac{\partial u}{\partial t} = -u\frac{\partial u}{\partial x} + kT_e\frac{\partial n}{\partial x} \tag{7-12}$$

Although external electric field is removed, ambipolar diffusion by pressure gradient and force by spatial difference of speed are an additional energy source to ions. Because high speed gradient that was forced and density gradient that was formed in the sheath at plateau time, more energy is gained at the early time of pulse-off duration. As time passes, speed and density gradient decreases and ion does not gain the additional energy.

Figure 7.8 shows a time varied force profile at fall time of 0.679us. During the pulse fall and sheath recovering rime, ion inertia ($\boldsymbol{u_{init}}$) and induced electric field (***E***) are dominant parameters to organize ion speed. As time passes and sheath is collapsed, density (***grad-n***) and speed gradient (***grad-u***) at the presheath become dominant parameters to compose ion speed and they govern plasma recovery.

7.4.3 Target current

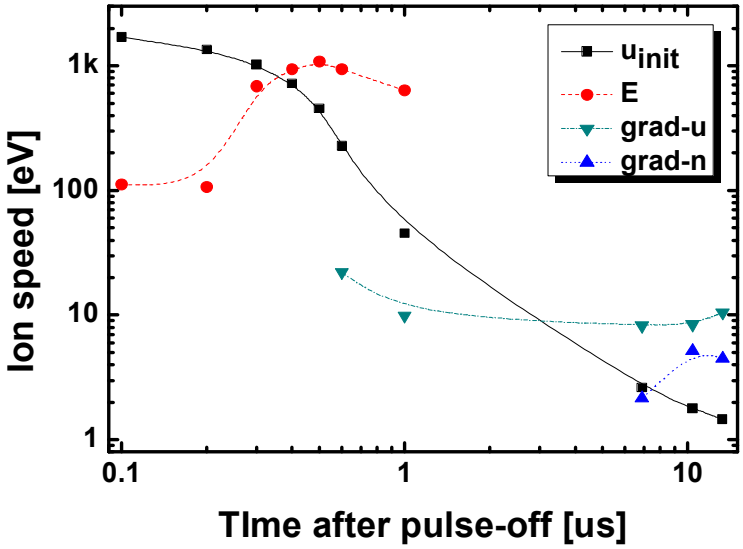

Figure 7.8. Time variation of force profile to organize ion speed at fall time of 0.679us

Target current with the variation of fall time is shown in Figure 7.7. Depletion is shown after high current injection at fast fall time. As fall time increases, the depletion is removed and the current decreases as time passes. Experiments data have similar shape of current with pulse fall time. It is expected that time difference at the depletion region between experiment data and the simulation result is given by inner inductance in the pulse and diagnostic system.

Target current is not an ion current. It consists of ion, secondary electron emission, displacement current by the motion of sheath, and electron current.

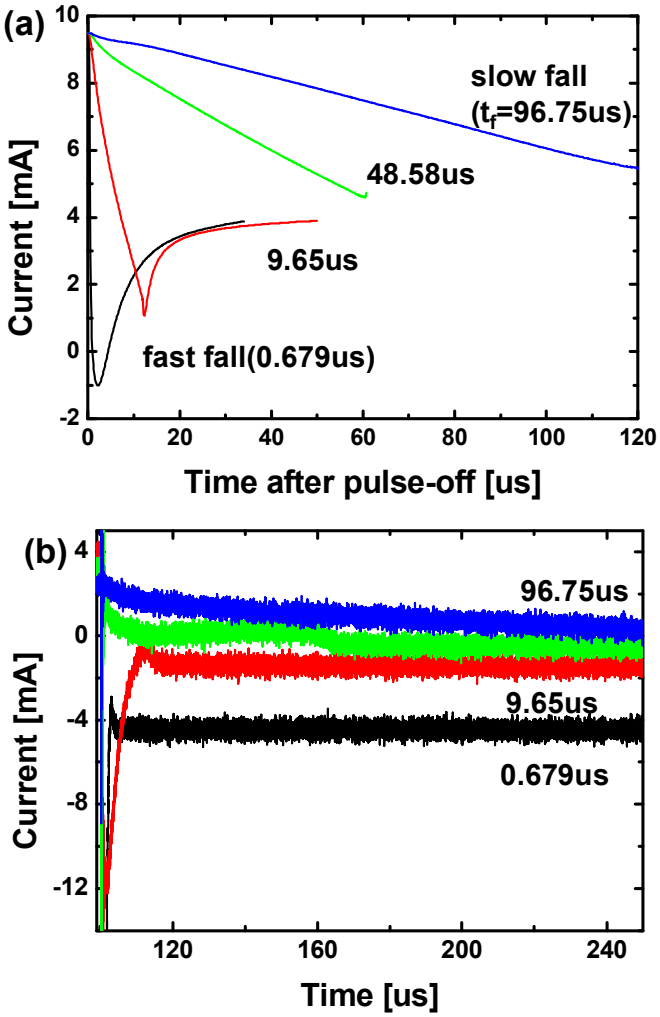

Figure 7.9 (a) Target current with a time and comparison with (b) experimental data

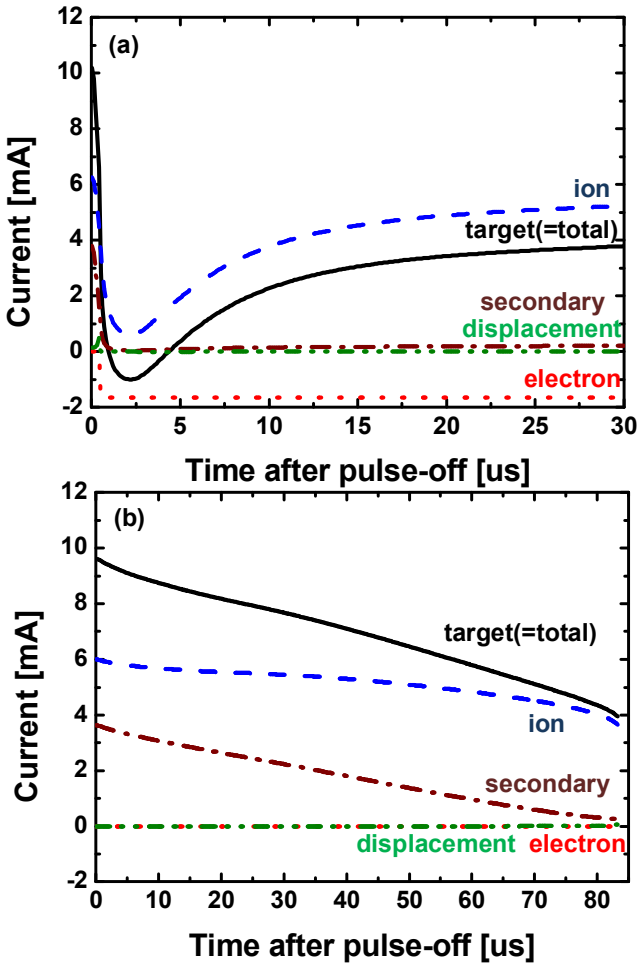

Figure 7.10 Composition of target current at (a) fast and (b) slow fall time.

Figure 7.10 shows variation of those current with time. Ion current take a dominant role to compose target current. Like the total current curve, ion current has a valley at fast fall time due to the non-uniform energy distribution and depletion of ion density at the beginning of pulse-off. At slow fall time the depletion is removed because of the induced electric field by target voltage. Secondary electrons are dominant current as voltage increases but the current is neglected at the fast fall time. Displacement current also is neglected due to stopped motion of sheath at the early time. Instead, electron current is flown to the target and total current increases comparing with ion current.

7.4.4 Contribution ratio of pulse fall time on ion energy distribution

Variation of pulse fall time distorts the injected ion property during the fall time, which affects the overall ion property on pulse-on time. Figure 7.11 shows a ratio of target current and ion energy distribution at pulse fall time comparing those at pulse-on time. It is assumed that pulse plateau time is 100us and pulse rise time is 0.0676us with a plateau voltage of 2kV. Accumulated current and ion quantity are measured until presheath recovers and plasma fills 85% of the depletion volume.

At fast fall time, sheath is collapsed before ions are injected into the sheath and amount of ions on the target at pulse fall time is much lower than those at pulse plateau time. As fall time increases and sheath recovers slower,

more ions are flown to the target through the sheath. In result, target current is proportional with the fall time although plasma-filling volume is same.

Pulse fall time takes on the low energy ions as depicted in Figure 7.11(b). From the figure, most ions which have energy lower than 1.5keV are generated regardless of pulse fall time. With the condition that rise time which is much shorter than the pulse fall time, decreased electric field exist only at pulse fall time regime and it dominates low energy portion of ions. Ratio of high energetic ions which energy is higher than 1.5keV increases with pulse fall time. At this region, ion energy at the fall time is determined from the induced electric field and ions gain more energy as target voltage decreases. Because high energetic ions are also generated at the rise and plateau time, its ratio increases when the electric field is remained as long as possible so that more ions gain energy during the flight.

7.5 Effect of plateau time variation

As mentioned in Chapter 6, variation of plateau time indicates that initial condition of plasma motion is changed. At slow fall time when induced electric field control the ion energy, electric field that is much stronger than the initial speed, is continuously distributed in the sheath. Therefore, variation of initial speed does not change the injected ion energy with the high target voltage condition. Quantity of injected ions can be changed at the early time of pulse-off but it can be negligible comparing to the total amount of injected ions during the fall time.

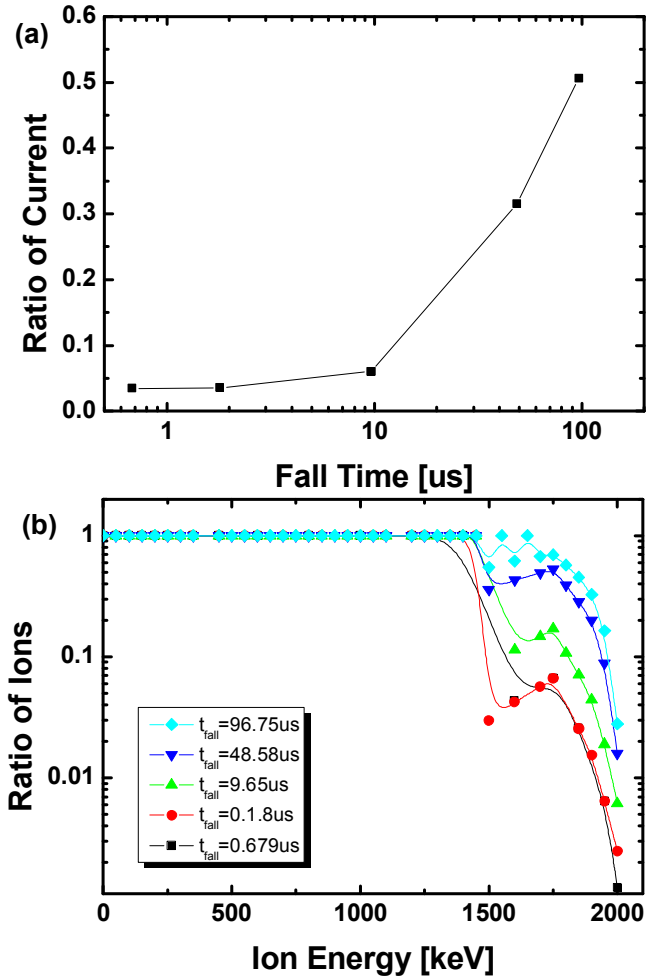

Figure 7.11. Ratio of (a) current and (b) ion energy distribution at pulse fall time comparing with those at pulse-on time.

At fast fall, initial plasma property changes the injected ion motion. Figure 7.12 shows a time-transient energy profile of injected ions to the target. At the plateau time of 2us, ion with energy of 1.89keV is injected when pulse-off starts, which is under the expected maximum energy which is induced from the target voltage at the plateau time. With a short plateau time, ion does not have enough time to gain maximum energy and it causes an insufficient energy band. All energetic ions gain energy from the electric field at the plateau time and energy lack is sustained after pulse-off.

Figure 7.13 show the trajectory of ions from pulse-on starts. Pulse-off start from 2us and the target voltage is zero at 2.848us. In order to gain full energy, ion should be propagated across the stable sheath at plateau voltage. Although ions are injected to the target during the plateau time, ions do not gain maximum energy because sheath is still expanded during the plateau time. Expansion of sheath reduces the distributed electric field and ion does not gain full energy in spited of maximum target voltage. After target voltage is zero, delayed arrival of ions which enter the sheath when the pulse-generated electric field exists due to the ion flight time through the sheath.

Based on the above data, ion energy distribution is presented in Figure 7.14. As mentioned in previous section, quantity of ions is proportional with ion energy. Energetic ions are injected more as plateau time decreases. When plateau time is shorten, ions do not have enough time to be evacuated responding to the target voltage, which increases the amount of injected ions during the fall time. As plateau time increases, ion are evacuated and rearranged in the sheath. In result, small amount of energetic ions recovers.

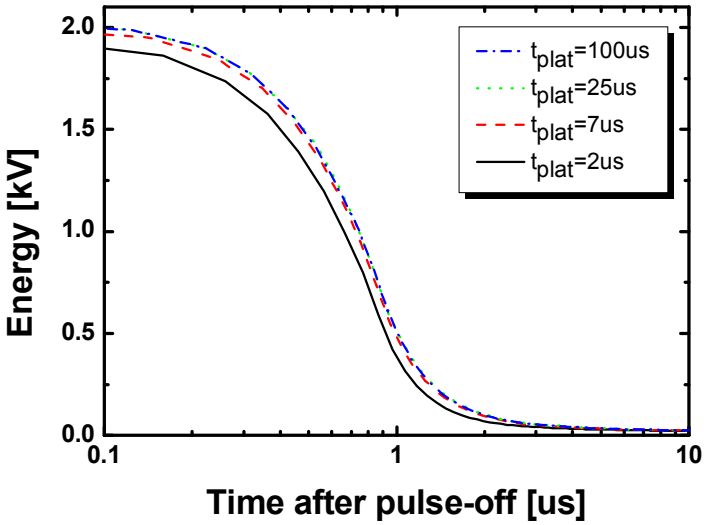

Figure 7.12 Time-transient ion energy with variation of plateau time.

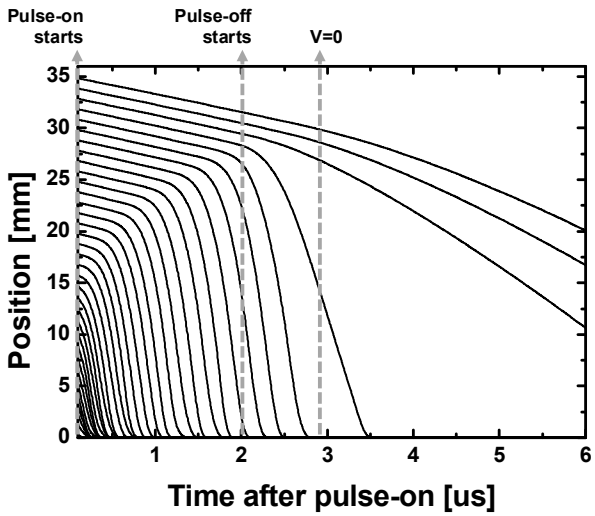

Figure 7.13 Ion trajectory after pulse-on at t_{plat}=2us and t_{fall}=0.679us

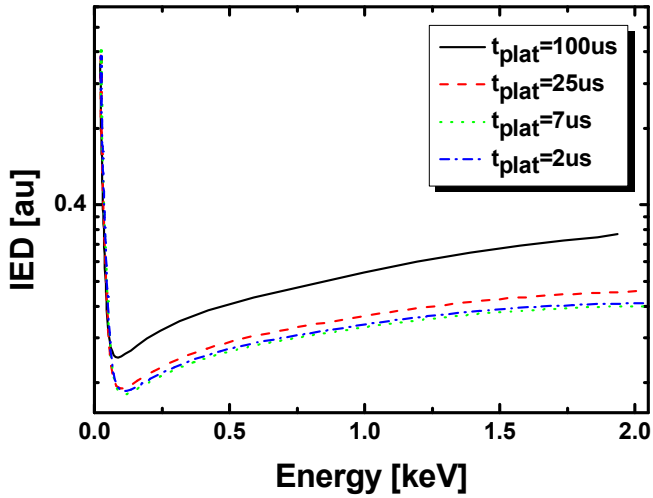

Figure 7.14 Ion energy distribution with variation of plateau time

7.6 Summary

Based on the previous result, ion energy distribution is predicted using the fluid code. Sheath recovery speed and induced electric field comparing with the injected ion speed are dominant factors to determine ion energy distribution.

At slow fall time which causes sheath speed under injected ion speed, induced electric field governs the ion energy. Ions are injected with the energy of potential drop in front of the target and quantity increases due to the diffusion from the bulk plasma. Typical ion energy distribution, where amount

of ions decreases as energy increases, is shown during the fall time.

As fall time decreases and sheath recovering speed increases, ions entering in the sheath decreases and ion inertia and density gradient in the former sheath become dominant role to constitute ion energy distribution. Because ions with inertia mainly is those with maximum energy, which was already gained at the plateau time. Depletion of ions at medium energy level increases as fall time decreases and sheath speed increases. In result, linearity of particle number and energy is reverted.

Fast recovery of sheath also enhances the acceleration of ions by density and velocity gradient. However it is dominated after the time scale of inverse ion plasma frequency because it is based on the motion of ion.

Short plateau time modify the ion energy distribution at fast fall time. Due to the decreased electric field by the expanding sheath, ions do not gain maximum energy during the flight. However, ions, which exist in front of the target before pulse-on, remain containing energy by plateau voltage. In result, quantity of energetic ions is larger than that at long plateau time.

Chapter 8. Conclusion

In this thesis, motion of plasma faced on the target is studied at pulse fall time. By modifying pulse shape, recovery process of sheath and presheath is analyzed and governing parameter is investigated. From the result, it is revealed that key factor in recovery motion is an ion motion responding to both electric field that is induced from the target voltage and plasma property that was formed at the plateau time.

Plasma at pulse fall time has ions with high energy that was gained during the plateau time and an ion distribution with drastic gradient made by the sheath at the plateau time. In addition to the induced electric field in the sheath, recovery motion of sheath and presheath is determined from the balance of those forces.

At fall time larger than ion flight time, electric field induced by target voltage has a governing factor to determine sheath. High electric field with a sheath speed lower than diffusion one forces ions to be rearranged to form Child-Langmuir sheath concurrently. When the electric field removes, the plasma property governs the recovery motion. As fall time becomes faster than the flight time and electric field is diminished before ions respond, ion distribution becomes a control factor to determine sheath. During the fall time, ions maintain its spatial distribution that was formed at the plateau time and sheath recovers following ion matrix sheath.

Sheath speed comparing with the ion inertia at the presheath region

governs recovery motion. Recovery speed at presheath head is proportional with the sheath speed but it has upper limit of Bohm speed, which is ion inertia. Bulk plasma also has a recovery speed which is matched with the sheath speed but it sustains its speed when sheath speed is faster than diffusion speed at the bulk plasma.

Ion inertia with Bohm speed at the presheath can be obtained from the basis that presheath is stably formed during the plateau time. When the plateau time decreases and pulse fall starts before the stable presheath is not distributed, presheath recovers with the diffusion speed of the bulk plasma. It breaks and recovers with Bohm speed as rarefaction wave that was generated at the rise time expands.

Energy variation of injected ions at the fall time is a main factor to cause the broadening of ion energy distribution. Ion energy distribution during the fall time consists of ions with maximum energy, which was already formed at the plateau time and ions with medium energy, which was gained during the fall time. Since the electric field in the sheath is inversely proportional to the pulse fall time, depletion at the medium energy level increases as pulse fall decreases and sheath speed increases but, additional energy is gained by the spatial distribution of speed and plasma density around presheath.

As plateau time decreases, ions do not gain full energy comparing to the plateau voltage because of the decreased electric field by sheath expansion during the plateau time. However, high flux can be archived due to the remained ions which are not evacuated.

Biblography

1. Celler, G.K. and S. Cristoloveanu, *Frontiers of silicon-on-insulator.* Journal of Applied Physics, 2003. **93**(9): p. 4955-4978.
2. Lu, X., et al., *Ion-cut silicon-on-insulator fabrication with plasma immersion ion implantation.* Applied Physics Letters, 1997. **71**(19): p. 2767-2769.
3. Wu, B., A. Kumar, and S. Pamarthy, *High aspect ratio silicon etch: A review.* Journal of Applied Physics, 2010. **108**(5): p. 051101-20.
4. Soloshenko, I.A., *Physics of ion beam plasma and problems of intensive ion beam transportation (invited)^{a)}*. Review of Scientific Instruments, 1996. **67**(4): p. 1646-1652.
5. Hershkowitz, N., *How Langmuir probes work*, in *Plasma Diagnostics*, O. Auciello and D.L. Flamm, Editors. 1989, Academic: New York. p. 113.
6. Cox, W., et al., *Spatial retarding field energy analyzer measurements downstream of a helicon double layer plasma.* Applied Physics Letters, 2008. **93**(7): p. 071505-3.
7. Seiji, S., et al., *The 2012 Plasma Roadmap.* Journal of Physics D: Applied Physics, 2012. **45**(25): p. 253001.
8. Anders, A., *From plasma immersionion implantation to deposition: a historical perspective on principles and trends.* Surf. Coat. Tech., 2002. **156**: p. 3-12.
9. Shin, H., et al., *Ion energy distributions, electron temperatures, and electron densities in Ar, Kr, and Xe pulsed discharges.* Journal of Vacuum Science & Technology A: Vacuum, Surfaces, and Films, 2012. **30**(3): p. 031304-5.
10. Hyungjoo, S., et al., *Control of ion energy distributions using a pulsed plasma with synchronous bias on a boundary electrode.*

Plasma Sources Science and Technology, 2011. **20**(5): p. 055001.

11. Anders, A., *Handbook of Plasma Immersion Ion Implantation and Deposition*. 2000: Wiley.
12. Kyoung-Jae, C., *Sheath dynamics and plasma recovery in plasma source ion implantation*, in *Department of Nuclear Engineering*2007, Seoul national University: Seoul, South Korea.
13. Wang, S.B. and A.E. Wendt, *Control of ion energy distribution at substrates during plasma processing.* Journal of Applied Physics, 2000. **88**(2): p. 643-646.
14. Qin, X.V., Y.H. Ting, and A.E. Wendt, *Tailored ion energy distributions at an rf-biased plasma electrode.* Plasma Sources Science and Technology, 2010. **19**(6): p. 065014.
15. Xu, L., et al., *Extraction of a nearly monoenergetic ion beam using a pulsed plasma.* Applied Physics Letters, 2005. **87**(4): p. 041502-3.
16. Lieberman, M.A. and A.J. Lichtenberg, *Principles of plasma discharges and materials processing*. 2 ed. 2005: Wiley-Interscience.
17. Guthrie, A. and R.K. Wakerling, *The characteristics of electrical discharges in magnetic fields*. National nuclear energy series: Electromagnetic Separation Project. 1949: McGraw-Hill.
18. Oksuz, L. and N. Hershkowitz, *Plasma, presheath, collisional sheath and collisionless sheath potential profiles in weakly ionized, weakly collisional plasma.* Plasma Sources Science and Technology, 2005. **14**(1): p. 201.
19. Oksuz, L. and N. Hershkowitz, *First Experimental Measurements of the Plasma Potential throughout the Presheath and Sheath at a Boundary in a Weakly Collisional Plasma.* Physical Review Letters, 2002. **89**(14): p. 145001.
20. Alexeff, I., et al., *Transient Plasma Sheath---Discovered by Ion-Acoustic Waves.* Physics of Fluids, 1969. **12**(2): p. 345-346.
21. Child, C.D., *Discharge From Hot CaO.* Physical Review (Series I),

1911. **32**(5): p. 492-511.

22. Israel, D., K.-U. Riemann, and L. Tsendin, *Relaxation of a collisionless ion matrix sheath.* Journal of Applied Physics, 2004. **95**(9): p. 4565-4574.
23. Riemann, K.-U. and T. Daube, *Analytical model of the relaxation of a collisionless ion matrix sheath.* Journal of Applied Physics, 1999. **86**(3): p. 1202-1207.
24. Kim, Y.-W., et al., *Measurement of sheath expansion in plasma source ion implantation.* Surface and Coatings Technology, 2001. **136**(1-3): p. 97-101.
25. Bauernfeind, P. and H.G. Lergon, *Evolution of the maximum ion impact energy at an electrode during sheath and presheath formation.* Journal of Physics D: Applied Physics, 2004. **37**(12): p. 1648.
26. Briehl, B. and H.M. Urbassek, *Simulation of sheath and presheath dynamics in PIII.* Surface and Coatings Technology, 2002. **156**(1–3): p. 131-135.
27. Boris, B. and M.U. Herbert, *Presheath dynamics induced by sudden electrode voltage jumps.* Journal of Physics D: Applied Physics, 2000. **33**(23): p. 3066.
28. Mändl, S., R. Günzel, and W. Möller, *Sheath and presheath dynamics in plasma immersion ion implantation.* Journal of Physics D: Applied Physics, 1998. **31**(9): p. 1109.
29. Kyoung-Jae, C., et al., *Dynamic sheath expansion in a non-uniform plasma with ion drift.* Plasma Sources Science and Technology, 2011. **20**(4): p. 045014.
30. Choe, J.-M., et al., *Investigation of current on the conducting target biased with a large negative potential in the non-uniform plasma.* Jpn. J. Appl. Phys., 2006. **45**: p. L686-L689.
31. En, W. and N.W. Cheung, *Analytical modeling of plasma immersion*

ion implantation target current using the SPICE circuit simulator. J. Vac. Sci. Technol. B, 1994. **12**: p. 833-837.

32. Boris, B. and M.U. Herbert, *Plasma recovery in plasma immersion ion implantation: dependence on pulse frequency and duty cycle.* Journal of Physics D: Applied Physics, 2002. **35**(5): p. 462.
33. Chung, K.-J., et al., *Numerical investigation of plasma recovery in plasma source ion implantation.* Thin Solid Films, 2012. **521**(0): p. 197-200.
34. Stewart, R.A. and M.A. Lieberman, *Model of plasma immersion ion implantation for voltage pulses with finite rise and fall times.* Journal of Applied Physics, 1991. **70**(7): p. 3481-3487.
35. Linder, B.P. and N.W. Cheung, *Modeling of energy distributions for plasma implantation.* Surface and Coatings Technology, 2001. **136**(1–3): p. 132-137.
36. Lieberman, M.A., *Model of plasma immersion ion implantation.* Journal of Applied Physics, 1989. **66**(7): p. 2926-2929.
37. Scheuer, J.T., M. Shamim, and J.R. Conrad, *Model of plasma source ion implantation in planar, cylindrical, and spherical geometries.* Journal of Applied Physics, 1990. **67**(3): p. 1241-1245.
38. Widner, M., I. Alexeff, and W.D. Jones, *Plasma Expansion into a Vacuum.* Physics of Fluids, 1971. **14**(4): p. 795-796.
39. Crow, J.E., P.L. Auer, and J.E. Allen, *The expansion of a plasma into a vacuum.* Journal of Plasma Physics, 1975. **14**(01): p. 65-76.
40. Yatsuzuka, M., et al., *Spatial and temporal growth and collapse in a PBII plasma.* Surface and Coatings Technology, 2001. **136**(1-3): p. 93-96.
41. Hongchen, W. and A. André, *Measurements of the asymmetric dynamic sheath around a pulse biased sphere immersed in flowing metal plasma.* Plasma Sources Science and Technology, 2008. **17**(3):

p. 035030.

42. Diaw, A. and P. Mora, *Rarefaction shock in plasma with a bi-Maxwellian electron distribution function.* Physical Review E, 2011. **84**(3): p. 036402.

43. Kar, S., S. Mukherjee, and Y.C. Saxena, *Excitation of ion rarefaction waves in a low pressure plasma by applying a short high negative voltage pulse.* Physics of Plasmas, 2011. **18**(5): p. 053506.

44. Widner, M., et al., *Ion Acoustic Wave Excitation and Ion Sheath Evolution.* Physics of Fluids, 1970. **13**(10): p. 2532-2540.

45. Daube, T., et al., *Relaxation phenomena in pulsed discharges.* Journal of Applied Physics, 2002. **91**(4): p. 1787-1796.

46. Wood, B.P., *Displacement current and multiple pulse effects in plasma source ion implantation.* Journal of Applied Physics, 1993. **73**(10): p. 4770-4778.

47. En, W.G., M.A. Lieberman, and N.W. Cheung, *Comparison of experimental target currents with analytical model results for plasma immersion ion implantation.* IEEE Transactions on Plasma Science, 1995. **23**(3): p. 415-421.

48. Carlos, D.P., *Plasma chemistry in repetitively pulsed discharges in air at low pressures.* Plasma Sources Science and Technology, 2012. **21**(3): p. 035020.

49. Sobolewski, M.A., *Sheath model for radio-frequency-biased, high-density plasmas valid for all ω/ω_{i}.* Physical Review E, 2000. **62**(6): p. 8540-8553.

50. Smith, H.B., et al. *Pulsing a Low Pressure rf Plasma*.

51. Kyu-Sun, C., *Mach probes.* Plasma Sources Science and Technology, 2012. **21**(6): p. 063001.

52. Yukimura, K., E. Kuze, and K. Matsunaga, *Two switch high voltage modulator for plasma-based ion implantation.* Surface and Coatings Technology, 2002. **156**(1-3): p. 66-70.

53. Szapiro, B. and J.J. Rocca, *Electron emission from glow-discharge cathode materials due to neon and argon ion bombardment.* J. Appl. Phys., 1989. **65**(9): p. 3713-3716.

54. Shamim, M.M., et al., *Measurement of electron emission due to energetic ion bombardment in plasma source ion implantation.* Journal of Applied Physics, 1991. **70**(9): p. 4756-4759.

55. Stewart, R.A. and M.A. Lieberman, *Model of plasma immersion ion implantation for voltage pulses with finite rise and fall times.* 1991. **70**(7): p. 3481-3487.

56. Riemann, K.U., *Plasma and sheath.* Plasma Sources Science and Technology, 2009. **18**(1): p. 014006.

57. Emmert, G.A., et al., *Electric sheath and presheath in a collisionless, finite ion temperature plasma.* Physics of Fluids, 1980. **23**(4): p. 803-812.

58. Cipolla, J.W. and M.B. Silevitch, *On the temporal development of a plasma sheath.* Journal of Plasma Physics, 1981. **25**(03): p. 373-389.

초 록

펄스 전압이 인가된 타겟 주위의 플라즈마와 쉬스의 움직임을 연구하였다. 펄스 유지 시간과 내림 시간을 조절하여 펄스 내림 시간 동안 쉬스와 프리쉬스가 어떤 방식으로 회복되는지 분석하고 플라즈마 및 시스템 인자와의 상관성에 대한 연구를 진행하였다. 본 연구는 플라즈마 내 삽입된 타겟에 유지 전압을 0.5~5kV, 펄스 내림 시간을 0.6~500us, 유지 시간을 2~100us로 변화시켜가며 실험을 수행하였고, Langmuir 탐침을 이용하여 대응하는 플라즈마의 움직임을 관찰하였다.

펄스 내림 시간에서의 쉬스의 움직임은 이온이 움직이는 시간(ion flight time)에 의해 결정된다. 펄스 내림시간이 쉬스 내 이온의 비행 시간(ion flight time)보다 큰 경우 이온은 타겟의 전압에 충분히 대응할 시간을 가져 쉬스는 Child-Langmuir 법칙을 만족하며 타겟쪽으로 회복된다. 쉬스 내 이온의 밀도는 Child-Langmuir 쉬스에 의해 인가된 전기장에 의해 시간에 따라 재배열되고 쉬스로 들어오는 이온의 양은 펄스가 인가되지 않을 당시의 플라즈마 밀도를 따른다. 반면, 이온의 비행시간보다 작아 타겟 전압에 이온이 충분히 대응하지 못하는 경우, 전압의 변화는 전자의 운동이 지배하여 ion matrix 쉬스의 형태를 가진다. 타겟의 전압 변화에 대응하지 못하는 이온으로 인하여 쉬스내 이온 분포는 펄스 유지 시간 동안 형성된 분포를 따르며 이온 움직임보다 빠른 쉬스의 회복으로 쉬스 내로 유입되는 이온은 존재하지 않는다.

타겟 주변부의 프리쉬스와 벌크 플라즈마(bulk plasma)의 회복 운동은 쉬스의 회복 속도와 해당 위치에서의 초기 이온의 속도로 결정된다. 펄스 내림 시간은 유지 시간 이후에 진행이 되므로 내림 시간이 시작이 되었을 경우 프리쉬스에서의 이온은 봄 속도(Bohm speed)를 가지고 이후 벌크 플라즈마는 불균일한 밀도 분포에 의한 양극성 확산 속도(ambipolar diffusion speed)를 가진다. 빠른 펄스 전압 내림율을 가져 쉬스의 속도가 봄 속도보다 큰 경우, 프리쉬스 및 벌크 플라즈마에서의 이온은 쉬스내 전기장에 영향을 받지 않아 펄스 내림 시간동안 쉬스의 속도와는 상관없이 자신의 속도를 유지한채 플라즈마는 회복된다. 하지만 전압 내림율이 낮아 느린 쉬스 회복 속도를 가지게 되면, 이온은 자신의 초기 속도와 쉬스의 속도 중 낮은 값을 따르게 되며, 해당 속도로 플라즈마는 회복된다.

프리쉬스의 초기 속도는 펄스 유지 시간 동안의 이온의 속도로 결정된다. 펄스 유지 시간이 이온이 타겟 전압에 충분히 반응할 시간보다 길게 되면($t_{plateau}\omega_{pi}>>1$), 유지 시간 동안 타겟 전압에 의해 Child-Langmuir 쉬스가 형성되어 있으므로 내림시간에서의 프리쉬스의 초기 속도는 봄 속도이다. 하지만 반응시간보다 짧게 되면($t_{plateau}\omega_{pi}<1$) 프리쉬스의 회복 속도는 펄스 인가전 플라즈마 분포에 의한 양극성 확산 속도를 가지며, 시간이 지남에 따라 펄스 오름 시간동안 발생하였던 소밀파(rarefaction wave)에 의해 봄속도에 도달된다.

쉬스와 프리쉬스의 움직임을 토대로 펄스 내림 시간 동안 타겟에 입사되는 이온의 에너지 분포를 시뮬레이션 코드를 사용하여 예상하였다. 이온 에너지 분포는 쉬스의 속도와 유지 시간 동안

미리 가속된 쉬스내 이온의 양에 의해 결정된다. 최상위 에너지를 가진 이온(E_{ion}>0.8$V_{plateau}$)은 유지 시간 동안 미리 가속된 이온에 의해 양이 결정되며 이보다 낮은 에너지를 가진 이온의 양은 내림 시간동안 인가된 쉬스의 전기장에 의해 결정된다. 그러므로, 최상위 에너지를 가진 이온의 양은 유지 시간동안 결정되어 쉬스의 속도에 속관없이 일정한 양이 들어오지만, 이보다 낮은 에너지를 가진 이온은 쉬스의 속도가 빠를수록 양은 감소한다. 유지 시간이 짧아져 플라즈마가 안정화 되지 않을 때 내림 펄스가 시작할 경우 쉬스 내 남아있는 이온의 양은 증가하여 이온 에너지 분포가 전체적으로 증가하지만, 유지 시간 동안 충분히 에너지를 받는 이온의 양은 줄어 에너지 분포상 이온이 가진 최대 에너지는 반비례하여 감소한다.

주요어: 플라즈마, 쉬스, 프리쉬스, 펄스 운전, 봄속도, 펄스 내림 시간

학 번: 2004-23437